

Feasibility Study of Ionospheric Tomography using HF Radar


by

Fred Joe Nambala

A thesis submitted as the dissertation component
in partial fulfilment of the academic
requirements for the degree of
Masters of Science (Physics)
in the School of Physics,
University of KwaZulu-Natal,
Durban.

20/03/2009

As the candidate's Supervisor I have/~~have not~~ approved this thesis for submission

Signed:  Name: JPS RASH Date: 20/03/2009

As the candidate's Co-Supervisor I have/have not approved this thesis for submission

Signed: Name: Date:

Abstract

This thesis gives an outline of the ionosphere and studies that were conducted to investigate whether ionospheric tomography can be performed using a High Frequency (HF) radar. The current theory pertaining to ionospheric tomography is such that satellite technology is implemented to map out a picture of the ionosphere by analysing two radio signals simultaneously propagating at different frequencies from the satellite to the dedicated ground receivers. A description of the SuperDARN HF radar network's recorded parameters is presented. Results obtained from processing and analysing the SuperDARN radar, for Hankasalmi ($62.32^{\circ}N, 26.61^{\circ}E$) and Prince George ($53.98^{\circ}N, 122.59^{\circ}W$), archived data were compared to those produced by simple radio wave ray tracing computer program simulations on a model ionosphere — generated using the International Reference Ionosphere (IRI) Model. Experiments to check the effect on signal propagation by changing the ionosphere, transmitted radar frequency and elevation angle were conducted. A postulate regarding backscatter of radio signals for a static ionosphere and constant transmitted radar frequency was developed. The postulate was tested by processing a month's worth of Saskatoon ($52.16^{\circ}N, 106.53^{\circ}W$) SuperDARN radar data into readable format and then using the IRI to verify the Saskatoon's ionosphere structure after utilising ray tracing. The observed scenario is such that the HF radar can be used to recover the ionosphere's electron density structure — with sections of the E and F layers accurately produced from the SuperDARN HF radar's data. A possible future study to improve the findings is to investigate a way of implementing this knowledge into performing real time tomography using the SuperDARN HF radar.

Keywords: Ionospheric Tomography, Ray Tracing, International Reference Ionosphere.

PREFACE

The experimental work described in this dissertation was carried out at the Hermanus Magnetic Observatory, Hermanus, and in the School of Physics, University of KwaZulu-Natal, Durban, from July 2007 to June 2008 under the supervision of Professor Jon Rash and Mr. Lindsay Magnus.

These studies represent original work by the author and have not otherwise been submitted in any form for any degree or diploma to any tertiary institution. Where use has been made of the work of others it is duly acknowledged in the text.

DECLARATION 1 - PLAGIARISM

I, Fred Joe Nambala, declare that

1. The research reported in this thesis, except where otherwise indicated, is my original research.
2. This thesis has not been submitted for any degree or examination at any other university.
3. This thesis does not contain other persons' data, pictures, graphs or other information, unless specifically acknowledged as being sourced from other persons.
4. This thesis does not contain other persons' writing, unless specifically acknowledged as being sourced from other researchers. Where other written sources have been quoted, then:
 - (a) Their words have been re-written but the general information attributed to them has been referenced
 - (b) Where their exact words have been used, then their writing has been placed in italics and inside quotation marks, and referenced.
5. This thesis does not contain text, graphics or tables copied and pasted from the Internet, unless specifically acknowledged, and the source being detailed in the thesis and in the References sections.

Signed: 

DECLARATION 2 - PUBLICATIONS

DETAILS OF CONTRIBUTION TO PUBLICATIONS that form part and/or include research presented in this thesis (include publications in preparation, submitted, *in press* and published and give details of the contributions of each author to the experimental work and writing of each publication)

Publication 1

Publication 2

Publication 3

etc.

Signed: 

Dedication

"And we know that all things work together for good to them that love God, to them who are the called according to [his] purpose." Roman 8: 28, Holy Bible.

To the good Lord God, our Creator; the whole Nambala Family and all human beings.

Acknowledgements

I would like to thank the National Astrophysics and Space Science Programme (NASSP) for providing the scholarship that has financially supported and also enabled me to pursue this work. Thanks are due to Dr. Lee-Anne McKinnell for her unwavering support, facilitating everything regarding my MSc Project coining and securing a place to carry out my project practical training at the Hermanus Magnetic Observatory (HMO). I would also like to offer a special thank you to my Co-Supervisor Mr. Lindsay Magnus for providing all the necessary insights and guide throughout the project work and Prof. Jon Rash for his role in his capacity as my Supervisor — especially for the effort he personally put in to see to it that all was well for me at the very end. This work also calls for acknowledging the assistance that was rendered to me by Chris Ndiitwani, Jean Uwamahoro, Kenneth Maphaha, Masimba W. Paradza and Patrick Sibanda. Lastly, I am thankful to all the HMO interns especially Candice Arendse and Misheck F. Magatshavha for proof-reading this dissertation work, staff and students who made my stay at the HMO a real life learning and telling social experience.

Contents

1	Introduction	1
1.1	Motivation	2
1.2	Project Aims	3
1.3	Thesis Outline	3
2	The Ionosphere and its Investigation	5
2.1	The Earth's Atmosphere	5
2.2	The Ionosphere	5
2.2.1	The D Layer	8
2.2.2	The E Layer	8
2.2.3	The F Layer	9
2.3	Distinct Ionospheric Features	9
2.3.1	Low-latitude Ionosphere	10
2.3.2	Mid-latitude Ionosphere	10
2.3.3	High-latitude Ionosphere	10
2.4	Ionospheric Variations	11
2.4.1	Diurnal Variation	11
2.4.2	Seasonal Variation	11
2.4.3	Latitudinal Variation	12
2.4.4	Solar Activity Variation	12
2.5	Radio Waves Propagating In The Ionosphere	13
2.6	Investigating the Ionosphere	14
2.6.1	The Ionosonde	15
2.6.2	Refractive Index of the Ionosphere	16

2.7	Ray Tracing	18
2.7.1	Ray Tracing Equations	19
2.8	Backscatter of Radio Signals	21
2.8.1	Coherent Scatter Radar Measurements	23
2.9	The Radar System	25
2.9.1	Backscatter power	31
2.9.2	Doppler Velocity	31
2.9.3	Spectral Width	31
2.9.4	Elevation	31
2.10	Ground Scatter	32
2.11	International Reference Ionosphere Model	32
3	Current Ionospheric Tomography Techniques	34
3.1	Ionospheric Tomography using GPS Satellites	34
3.2	Measurement of Total Electron Content	35
3.3	Radio Tomography	36
4	Processing SuperDARN Radar and IRI Data	39
4.1	Scatter Data	42
4.2	Elevation data from all the Beams and Range-gates	43
4.3	Ground Scatter	47
4.4	Ionospheric Scatter	48
4.5	Other SuperDARN Measured Parameters for the Time Period Under Study	49
4.6	HF Radar Transmitted Frequency change effects	54
4.7	Averaging over One Month	65
5	Discussion	77
5.1	Scatter Analysis	78
5.2	Elevation Scatter from all Beams and Range-gates Analysis	78
5.3	Ground and Ionospheric Scatter Analysis	79
5.4	Other SuperDARN Radar Data Measurements Analysis	80
5.5	Radar Transmitted Frequency Change Effects Analysis	83
5.6	Ray Tracing Analysis	83

<i>CONTENTS</i>	x
6 Conclusion	85
6.1 Possible Future Work	86
6.2 Inference	86
References	87
A IDL Moment Function	91

List of Figures

2.1	The ionospheric layers in pictorial form side by side with the temperature of the Earth's neutral atmosphere (adapted from http://www.astrosurf.com).	8
2.2	Various radio signals of which the "Pedersen ray" path (middle line in the diagram) follows from the "Pedersen ray angle" (from the horizontal line to the Pedersen ray) for the propagating signal. The Pedersen ray is one which just makes it through the ionosphere instead of being reflected back to the Earth's surface.	14
2.3	The plot shows an ionogram for Grahamstown, South Africa, with all the necessary information explained on it (adapted from http://ionosond.ru.ac.za).	15
2.4	Ray Traces using a simple program that uses Snell's law, trigonometry and Pythagoras' theorem for a model ionosphere generated using the IRI 2001 Model. The ray trace in the top panel shows a path for a 20° elevation angle radio signal. Embedded in the figure are 20° elevation angle plots of the distance travelled, phase- and group-velocities against time taken for the signal to move from the radars' transmitter to its propagation ending point.	21
2.5	Reflection from field-aligned ionospheric irregularities along the Earth's magnetic field (thick shaded parallel lines). In component (a), partial reflections of signals from periodic irregularities are indicated. In part (b), directions of coherent backscatter in the ionosphere are shown. The figures are versions of one of the graphs in Walker (2002).	22
2.6	Propagation modes for the SuperDARN HF radar: Ray A shows E-region mode, Ray B indicates F-region mode, Ray C penetrates the ionosphere. Backscatter ensues at the reflection points (Ground and Ionospheric reflections respectively in this figure) as presented. This graphic was adapted from Milan <i>et al.</i> (1997).	23

- 2.7 The picture on the left shows a graphical representation of how HF, VHF and UHF radar signals are scattered in space by high-latitude E- and F-layer ionospheric irregularities. This left-most graph was adapted from Greenwald *et al.* (1985). On the other-hand, the right graph illustrates the HF signal's refraction and backscatter effects more clearly. The right picture was obtained from Rash *et al.* (1991). The refraction of HF radio waves takes place in the E and F layers of the ionosphere when the transmitted radio frequency is less than the plasma frequency. At the point(s) where the transmitted radio frequency is equal to the plasma frequency, reflection of signals occurs and this results in formation of backscatter of the original forward signal. No backscatter takes place when the transmitted radio frequency is greater than the plasma frequency. 24
- 2.8 Half-hop of the full ground range for a radio signal that is reflected by an ionospheric layer through successive refraction in the ionosphere. This figure shows a radio signal of 20° elevation angle path which is backscattered at the point of ray reflection. 25
- 2.9 SuperDARN Radars with their respective fields of view. The left most plot shows the northern hemisphere radars based in the arctic region of the Earth whereas the right one portrays the southern hemisphere radars located in the Antarctica region and its nearby islands (adapted from <http://superdarn.jhuapl.edu>). 26
- 2.10 The primary array 16 log-periodic antennae and the secondary array of 4 antennae in the background (adapted from <http://superdarn.jhuapl.edu>). . 27
- 2.11 SuperDARN archived data plot for 8th March 2004. The transmitted frequency for the whole day's data was 11 – 12 MHz (second degree light blue colour shade in the frequency colour-bar shown clearly in the frequency bar just above the Noise bar in the figure). Thus, the 2004030816.fit data which contains 2 hours data from 16 – 18 hours could be viewed as having been observed for 11 MHz. 28
- 2.12 Field of views of the Prince George SuperDARN radar for the day 2004/04/05 at the times shown on the plots about 02:00 UT archived data (adapted from <http://superdarn.jhuapl.edu>). 30
- 3.1 Geometry of a GPS satellite (S), the ionosonde and a receiver (R). The ionosphere is assumed to be a screen at a height $h = 400$ km above the ground. P represents the intersection of the line of sight and the ionosphere, and χ is the zenith angle (adapted from Ma and Marunyama, 2003). 36

- 3.2 A pictorial representation of the satellite - receiver geometry for ionospheric tomography, with an array of ground receivers receiving signals from several satellites (only one is shown) along numerous paths through the ionosphere (adapted from Tucker, 1998). 37
- 4.1 The Doppler velocity, Doppler spectral width and echo power of beam 8 and range-gate 14 data of the SuperDARN radar is shown. The top-most panel presents a plot of power versus time. The middle panel indicates the Doppler velocity against time graph. The lower-most plot shows the spectral width versus time data. The inscriptions 'N:\SuperDARN\nh\2004\fit3\2004030816f.fit' on the plots provides the source and file of the raw SuperDARN radar data that was processed on the computer. 40
- 4.2 Elevation angle data versus time plot for beam 8 and range-gate 14 of the radars field of view is shown in the top panel of the figure. The elevation is presented in degrees. The lower panel indicates the SuperDARN radar's transmitted signal frequencies for the period of data recordings with the frequency being in kilo-Hertz (kHz). The time is in hours of the Universal Time (UT) standard. The time range span is 2 hours corresponding to one '.fit' file's data. 41
- 4.3 Elevation angle upon filtering out either ground or ionospheric scatter data. The left plot, (a), gives the ground scatter elevation data plot. The right graph, (b), portrays ionospheric scatter elevation data plot. All the data measurements were recorded from 16 : 00 – 18 : 00 hours Universal Time (UT). These two plots are close in features of Figure 4.2's elevation plot above, which gives a full combination of their data. 42
- 4.4 Contour plot of backscattered power versus elevation and range-gate for elevation data, both ground and ionospheric scatter. 43
- 4.5 Ray Traces of a Hankasalmi ionosphere modelled using the IRI 2001 Model for 8th March 2004, around 16 – 18 hours. 45
- 4.6 This graph is similar to Figure 2.11 except that this one shows data from all the 16 Beams of the radar's field of view for a time period from 16 : 00 – 18 : 00 hours. 46
- 4.7 Ground scatter elevation data plot. This graph shows the ground scatter components of the information relayed in Figure 4.4 above. 47
- 4.8 Ionospheric scatter elevation data contour plot. This ionospheric scatter information in this graph is a part of the data presented in Figure 4.4 only that ground scatter has been eliminated in it. 48

- 4.9 Backscatter plots of power, Doppler velocity and Doppler spectral width data from the 2004030816*f.fit* file. The radar's field of view beam that was used is number 8. 49
- 4.10 The plot shows the ground scatter elevation data only from the 2004030816*f.fit* file after filtering out the ionospheric scatter information. Beam 8 of the full field of view data was used to generate the plot. 50
- 4.11 The plot shows the ionosphere scatter elevation data alone from the 2004030816*f.fit* file after filtering out the ground scatter information. The beam that was used is number 8 from the total field of view of the radar. 51
- 4.12 Plot of all scatter from the online archived SuperDARN data generated on using the 'shade ground scatter' effect. The range-gate span is between 10–30. The ground scatter is shown in the gray colour while the ionospheric scatter appears in the any of rainbow colours. 52
- 4.13 Plot of both ground and ionospheric scatter from the online archived SuperDARN data on effecting the 'ignore ground scatter flag' parameter. The range-gates covered are 10 – 30. 53
- 4.14 Plot of ionospheric scatter from the online archived SuperDARN data produced on using the 'exclude ground scatter' effect on the Internet interactive resource. The range-gates covered are from 10 – 30. 54
- 4.15 The plot shows how the radar transmitted frequency change produces different scatter information from the ionosphere. This plot was generated from archived Prince George SuperDARN data on 5th April 2004 from 00 : 00 – 04 : 00 hours UT. 55
- 4.16 The top most panel shows all elevation scatter information plotted in one graph. The middle panel presents ground scatter data plot using the ground scatter flag embedded in the data 'fit' file. The bottom plot indicates the ionospheric scatter data produced by inverting the ground scatter flag and then masking it to the raw elevation data from the SuperDARN archive. The 'fit' file data that was used is 2004040502*b.fit* for Prince George. This implies that the time axis for the figure is from 02 : 00 – 04 : 00 hours UT since one single 'fit' file of the archived dataset harbours recordings for approximately 2 hours. These plots were generated for only Beam 8 of the full radar's field of view. 56

- 4.17 These scatter plots similar in nature to those of the figure just above except that they were generated for all the 16 Beams of radar's field of view. The top most panel shows all elevation scatter information plotted in one graph. The middle panel presents ground scatter data plot using the ground scatter flag embedded in the data 'fit' file. The bottom plot indicates the ionospheric scatter data produced by inverting the ground scatter flag and then masking it to the raw elevation data from the SuperDARN archive. 57
- 4.18 Ray traces through a Prince George ionosphere at about 00 : 30 hours UT with various transmission frequencies. The transmitted frequencies for the plots in Figure 4.15 are: 10 MHz for plot (a), 14 MHz for plot (b), 16 MHz for plot (c) and 18 MHz for plot (d). 58
- 4.19 Ray traces through a Prince George ionosphere at about 01 : 30 hours UT with various transmission frequencies. The transmitted frequencies for the plots in Figure 4.15 are: 10 MHz for plot (a), 14 MHz for plot (b), 16 MHz for plot (c) and 18 MHz for plot (d). 59
- 4.20 Ray traces through a Prince George ionosphere at approximately 02 : 50 hours UT with various transmission frequencies. The transmitted frequencies for the plots in figure 4.15 are: 10 MHz for plot (a), 14 MHz for plot (b), 16 MHz for plot (c) and 18 MHz for plot (d). 60
- 4.21 Ray traces through a Prince George ionosphere at approximately 03 : 30 hours UT with various transmission frequencies. The transmitted frequencies for the plots in Figure 4.15 are: 10 MHz for plot (a), 14 MHz for plot (b), 16 MHz for plot (c) and 18 MHz for plot (d). 61
- 4.22 Ray traces through a Prince George ionosphere at approximately 03 : 50 hours UT with various transmission frequencies. The transmitted frequencies for the plots in Figure 4.15 are: 10 MHz for plot (a), 14 MHz for plot (b), 16 MHz for plot (c) and 18 MHz for plot (d). 62
- 4.23 Ray Tracing of a 17 MHz signal propagating through Prince George IRI Model ionosphere at 00 : 30 hour UT. 64
- 4.24 Scatter elevation and power plots for one full month of December 2004 recorded for 00 : 00 – 02 : 00 hours UT every day. The data used was from the Saskatoon SuperDARN radar. The transmitted frequency for the plots is all of those that the radar used within the range 8 – 20 MHz from which any SuperDARN radar can operate. 66
- 4.25 Both ground and ionospheric scatter plots for 8 – 20 MHz for one months Saskatoon data. The left hand plot shows the ground scatter while the rightmost one portrays the ionospheric scatter information. 67
- 4.26 Ground and ionospheric scatter from higher and lower elevation angles respectively case as portrayed in Figure 4.25. **B** is the Earth's magnetic field. 67

4.27	Ray traces through a Saskatoon IRI ionosphere for December 2004 with the radar transmitted frequency range of 8 – 18 MHz. The angle of elevation used in doing the necessary studies was 25°	68
4.28	SuperDARN radar ray transmitted frequencies every day between 00 : 00 – 02 : 00 hours for the whole month of December 2004 for Saskatoon. 'Point number' is the number for the various 2 hour time length points when the radar transmission frequency at a specific time was recorded for each 2 hour data additively from 1st to the 31st day of the one full month between 00 : 00 – 02 : 00 hours.	69
4.29	The plot was generated from SuperDARN data for a full month of December 2004 between 00 : 00 – 02 : 00 hours UT from the Saskatoon Radar. The most transmitted frequency, of 10.59 MHz, during the observation time was calculated and then only the (elevation and power) data for that particular frequency was plotted.	70
4.30	The plots were produced for the most transmitted frequency, 10.59 MHz. The ground scatter is illustrated in the leftmost plot and ionospheric one in the right placed plot for the Saskatoon radar elevation and power data respectively.	71
4.31	Ray traces at intervals of 1° corresponding to the December 2004 Saskatoon IRI Model ionosphere data that is portrayed in figure 4.29. The transmitted signal frequency was 10.59 MHz. This was calculated from the SuperDARN radar archived data by the ray tracing program as the most transmitted frequency through out the one month's 2 hour fit file data for each day between 00 : 00 – 02 : 00 hours UT.	72
4.32	Ground scatter elevation and power plots for one full month of December 2004 recorded for 00 : 00 – 02 : 00 hours every day. The data used is from the Saskatoon SuperDARN radar. The transmitted frequency for the plots is range from 10.0 – 11.0 MHz.	74
4.33	Ionospheric scatter elevation and power plots for one full month of December 2004 recorded for 00 : 00 – 02 : 00 hours every day. The data used is from the Saskatoon SuperDARN radar. The transmitted frequency for the plots is range from 10.0 – 11.0 MHz.	75
4.34	Ray traces of radar transmitted frequencies ranging from 10.0 – 11.0 MHz on 0.1 increments each successive time. The elevation angle of the signal is 32°	76

List of Tables

4.1	Numbers gleaned from Figure 4.4 regarding the Radio Ray Path distances .	44
4.2	Ray Tracing results for an IRI Model ionosphere at 17 hours (UT) of 2004/03/08	45
4.3	Distances covered by the ground scatter plot backscattered signal	47
4.4	Distances covered by the ionospheric scatter plot backscattered signal . . .	48
4.5	Ray tracing ray path results for selected elevation angles pertaining to both ground and ionospheric scatter	48
4.6	Ionosphere at 00 : 30 UT and elevation with different backscattered ray transmitted frequencies	62
4.7	Constant backscattered ray transmitted at 10 MHz and elevation with dif- ferent ionospheres	63
4.8	Constant backscattered ray transmitted at 14 MHz and elevation with dif- ferent ionospheres	63
4.9	Constant backscattered ray transmitted at 16 MHz and elevation with dif- ferent ionospheres	63
4.10	Constant backscattered ray transmitted at 18 MHz and elevation with dif- ferent ionospheres	63
4.11	Constant rays transmitted at 17 MHz and an ionosphere at 00 : 30 UT with changing angles	64
4.12	December 2004 IRI Saskatoon Ionosphere	68
4.13	Range results from the most-transmitted frequency plots of elevation and echo power	70
4.14	Most transmitted frequency, 10.59 MHz, ray tracing results for the Saska- toon IRI ionosphere.	73
4.15	Ground scatter ray path results for 10 – 11 MHz transmitted frequencies . .	74
4.16	Ionospheric scatter ray path results for 10 – 11 MHz transmitted frequencies	75

4.17 Results for 10.0 – 11.0 MHz transmitted frequencies through a Saskatoon IRI ionosphere	76
--	----

LIST OF ABBREVIATIONS

Elev.	Elevation
Freq.	Frequency
GPS	Global Positioning System
H-H. H.	Half-Hop Height
Iono.	Ionosphere
TEC	Total Electron Content
UT	Universal Time

Chapter 1

Introduction

The term tomography refers to a recording of sections or projections of an object and the associated reconstruction of its morphology using these data (Kunitsyn and Tereshchenko, 2003). Thus, Ionospheric Tomography is a technique for determining the electron density structure of the ionosphere by using radio-wave propagation data which is collected upon sounding radio waves through it. Currently, this technique furnishes us with high resolution images of the electron density distribution in the vertical, meridional plane using only a small number of satellites in space.

In current studies, a satellite transmits phase-locked radio carrier waves concurrently at two frequencies, 150 and 400 MHz respectively, and these signals are measured at a small number of ground stations, e.g. five, along the length of the Earth. Then, the total electron content (TEC) along each ground-satellite path is calculated. TEC is the number of electrons in a column with one square meter cross section that extend along a ray path from a satellite to a ground receiver (Tate and Essex, 2001). In other words, TEC can be defined as the total number of electrons in a column of unit cross-section from a transmitter system on board a satellite to a ground based receiver system. It can be expressed mathematically as:

$$I = \int_T^R N(r, \theta, \phi, t) ds \quad (1.1)$$

where I represents TEC in TEC units (TECU) of 10^{16} electrons per square metre, N (normally written as N_e) is the electron density, r is the radial distance from the Earth's centre, ϕ is the latitude, θ is the longitude, t is the time, s is the satellite-to-receiver path length, R stands for Receiver and T is the Transmitter (Mitchell and Spencer, 2003). Using the recorded TEC measurements, a special algorithm is then implemented to reconstruct an image of the ionospheric electron density distribution.

The material in this thesis aims at presenting the work that was carried out in an effort to

investigate whether Ionospheric Tomography could be done using a High Frequency (HF) Radar. An HF radar is a powerful instrument that is used to study the behaviour of the Earth's ionosphere. There are many types of such radars. Among them are Ionosondes, a type of Radar which vertically sound into the ionosphere to determine its vertical electron density profile, and the Over-the-Horizon radar. There are also radars which perform oblique sounding of the ionosphere where radio wave energy is directed into the space at any angle relative to the horizontal ground of the location that may not necessarily be vertical to the ground.

In this study, oblique HF radar sounders which form part of the Super Dual Auroral Radar Network (SuperDARN) are used to observe ionospheric irregularities, i.e., regions of slightly different densities compared to the surrounding plasma (Greenwald *et al.*, 1995), in the Arctic and Antarctic (high latitude) regions. SuperDARN is a network of coherent scatter HF radars which observe backscatter emanating from 10 m scale field-aligned ionospheric irregularities (see Chisham and Pinnock, 2002 and Chisham *et al.*, 2007). The irregularities form due to different plasma instabilities and drift with the background plasma flow (Baker *et al.*, 1989). Irregularities in the ionosphere are simply bunches of electrons, forming an inhomogeneous sea of electrons, caused by a break up of ionisation which distorts the regular distribution of ionisation in an ionospheric layer (McNamara, 1991). Walker (2002) indicated that irregularities can be regarded as fluctuations in the refractive index of a medium. These irregularities become stretched along the lines of force shortly after being formed since electrons move freely up and down along the Earth's magnetic field, turning into what is commonly known as field-aligned irregularities. Villain *et al.* (1984) pointed out that ionospheric irregularities are, thus, electron density irregularities of approximately 1 – 100 m scale sizes elongated in the direction of the Earth's magnetic field (field-aligned) in the E and F layers of the ionosphere. It is envisioned that knowledge of the positions of the Ionospheric Irregularities in the ionosphere will aid in performing a reconstruction of the ionospheric morphology.

1.1 Motivation

The SuperDARN radars are HF radar systems which utilise ionospheric refraction to achieve the orthogonality condition with the Earth's magnetic field in both the E and F layers of the high latitude regions (Greenwald *et al.*, 1995). Unlike Very High Frequency (VHF) and Ultra High Frequency (UHF) radio signals, HF rays are susceptible to refractive effects varying from weak to strong in strength so much that the resultant propagation paths can be highly dependent on the ionospheric electron density distribution. Villain *et al.* (1984) indicated that HF sounders operated in the oblique mode have observed backscatter from the F layer of the polar ionosphere which implies that ionospheric irregularity structures are a common feature in those regions. This backscatter can be studied to create a picture of the structure of the ionosphere. As a matter of fact, backscatter

signals contain useful information pertaining to the state of the ionosphere at the time and over the propagation paths of the returned rays (Norman *et al.*, 2004). The SuperDARN radars provide measurement of elevation angle of the returned radio signals which is used to determine the propagation modes of the echo rays as a function of range together with the height of the scatterers, i.e., irregularities (Greenwald *et al.*, 1995). The radars have the capability to measure echoes from 10 m scale magnetic field aligned ionospheric irregularities and the Earth's surface backscatter (Norman *et al.*, 2004). To this end, a new way of performing Ionospheric Tomography is sought since current studies used in this area of study implement VHF and/or UHF radio waves, i.e., the GPS utilised method, to do the reconstructions of the ionosphere. Therefore the above-mentioned refractive effects that are encountered at HF frequencies to achieve magnetic orthogonality in the high latitude regions will be utilised to study backscattering of rays.

1.2 Project Aims

The main objective of this work is to outline a feasibility study into the use of an HF radar to extract information about the behaviour of the lower and bottomside parts of the polar region ionosphere which range from about 50 – 350 km vertically upwards into space from the ground — the Earth's surface. Thus more emphasis is placed on analysing and processing the recorded raw SuperDARN radar data into a suitable format which can be used to glean some useful information on the behaviour and structure of the ionosphere at specified times of the day.

Also, a thorough understanding of oblique sounding of the ionosphere is sought so as to perform ray tracing. The ray tracing results will provide a way of checking on the harmony of the information that will be recovered from the SuperDARN archived data. This is in an effort to study whether the scatter observed by the radar is indicative of ionospheric scatter by irregularities encountered along an oblique ray path or ground scatter from the Earth's surface.

Finally, the results from the above-mentioned two aims will be compared to provide the Ionospheric Tomography patterns.

1.3 Thesis Outline

The background theory regarding this study is presented in Chapter 2. The definitions of the various terminologies used herein are given. The general structure of the ionosphere is discussed in terms of ionospheric layers and the processes that cause their build up. Since this work focuses on using the information that can be recovered from the polar regions' ionosphere, the high latitude ionosphere is described in great detail therein. Also, the radar system used to study the ionosphere is discussed.

In Chapter 3, the current methods used to do Ionospheric Tomography are described. A case for our choice to use the HF radar is also discussed.

An overview of the methods that were used and results obtained in this work is presented in Chapter 4. Various sections present the procedures and their attendant information that was obtained upon performing them (i.e., the methods).

The overall discussion of the project results is provided in Chapter 5. It encompasses the reasoning used in the processing of the data and the way it was done and what was ultimately learnt from the plots that were generated and sourced from the archived online SuperDARN community.

The conclusions regarding the work is given in Chapter 6. Some possible future work is described in relation to what may be done to accomplish better results.

Chapter 2

The Ionosphere and its Investigation

This Chapter is devoted to providing necessary theoretical background regarding the ionosphere, techniques used to study it and the radar system whose recorded data will be used to carry out the experimental part of this thesis.

2.1 The Earth's Atmosphere

The Earth's atmosphere is a layer of gases that engulf the planet Earth (McKinnell, 2006). It is held together by the Earth's gravity. The gases consist of about 78% Nitrogen, 21% Oxygen and other trace elements of which the combined mixed is called air. This layer acts as a protective cushion to life on Earth as it absorbs harmful radiation from the Sun. The extent of this layer can not be clearly quantified although it merges up with the extra-terrestrial environment somewhere in space. The atmosphere is divided up into regions which are primarily temperature dependent since temperature varies with altitude. The temperature variation with altitude is shown in Figure 2.1(a).

With respect to this study, the main focus falls in the ionosphere, a region which ranges from about 50 km to roughly 2000 km of the Earth's atmosphere. This layer is of key interest since radiation from the Sun ionises particles within the layer which causes radio waves sent into space from either the ground or far space to be reflected back or refracted as they propagate through it depending on the prevailing conditions regarding the signal transmission.

2.2 The Ionosphere

The name ionosphere was coined by Watson-Watt and it came into use in about 1932. The ionosphere is a thick shell of free moving electrons and ions within the upper atmosphere

of the Earth that is an ionised plasma (Nambala, 2006). A plasma is a quasi-neutral gas of charged and neutral particles which portrays a collective behaviour (Chen, 1983). The ionisation of the atmospheric constituents is mainly due to solar radiation in a processes known as photoionisation. It is represented by



where M is a neutral atom or molecule, hv is the solar radiation energy, M^+ is the resultant positively charged ion and e^- is the free negatively charged electron. The free electrons in the ionosphere cause HF radio signals to be refracted and eventually be reflected back to the Earth or space through successive refractions of the waves (IPS Radio and Space Services, <http://www.ips.gov.au/Educational/>) "Introduction to HF Radio Propagation", 2008).

The solar ultraviolet radiation which causes the ionisation is absorbed as it penetrates through the atmosphere. The rate of ionisation is proportional to the gas density (which increases downwards) and the intensity of radiation (which decreases downwards because of absorption). This results in a peak of ionisation at a certain height. The basic theory was developed by Chapman (1939) and the basic "production layer" of electrons produced by photoionisation is known as the Chapman layer. Electrons are lost by recombination resulting in a steady-state "layer" of enhanced electron density. A combination of such layers for a range of ultraviolet wavelengths and gas species yields the typical electron density versus height profile shown in Figure 2.2(b), and which is described in more detail below (Ratcliffe, 1972).

It is multi-layered, a consequence of the complexity of the plasma at each altitude, and has a dispersive nature (Norman *et al.*, 2004). It is divided into three notable layers: namely the D, E and F layers. During daytime there may be four regions namely the D, E, F1 and F2 while in the night only the F2 layer will exist owing to the fact that the rest will have been depleted. The depletion of these layers occurs due to recombination processes known as radiative and dissociative recombination. Radiative recombination is an ion-atom exchange process while dissociative recombination is one where ions and electrons recombine to form neutral particles. The combined chain processes of both recombination mechanisms provides a faster way of total loss of free electrons. These processes are highlighted in equation form below as:



and



There is also movement of ionisation in the F2 layer which is governed by diffusion, neutral winds and vertical electromagnetic drift. Diffusion is the most important form here: in a process called Ambipolar Diffusion where an electron-ion behaves like a particle (Chen, 1983).

Therefore, it is imperative to make mention that the ionosphere is highly non-linear (McKinnell, 2006). Yau K.S.B (<http://hdl.handle.net/2440/35226> "Fading of high frequency radio signals propagating in the ionosphere - results from the jindalee radar experiment", 2006) indicated that the ionosphere is an ever-changing medium. It varies with day, season and solar activity due to the intensity of solar radiation at a particular time. Also, notable variation due to geographic and/or geomagnetic location, and magnetic activity has been attributed to the ionosphere (McNamara, 1991). Most of the above-mentioned variation behaviour is clearly portrayed by Nambala *et al.* (2008) in a study of ionospheric parameters.

The E, F1 and F2 regions are the only ones that can refract HF radio signals while the D layer is important because it absorbs them especially lower frequency ones and those with greater obliquity.

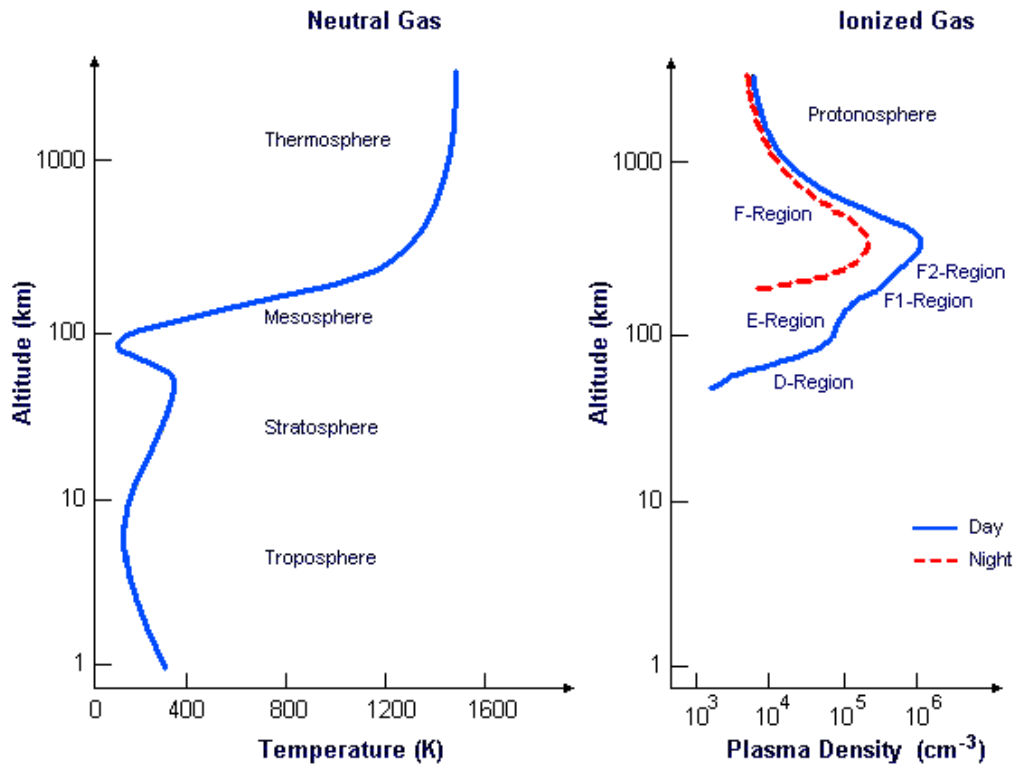


Figure 2.1: The ionospheric layers in pictorial form side by side with the temperature of the Earth's neutral atmosphere (adapted from <http://www.astrosurf.com>).

The ionosphere is also sub-divided into three components called the lower-, bottomside- and topside-ionosphere. The lower-ionosphere is largely composed of the D layer. The E and F layers form the bottomside-ionosphere starting at an altitude of about 90 km to the height of maximum electron density. From the maximum electron density height up to about 2000 km is the topside-ionosphere, a region of low and reducing particle density. Figure 2.1 shows a fair representation of the ionosphere side-by-side with an atmosphere picture.

2.2.1 The D Layer

The D layer is nearest to the Earth's surface and ranges from about 50 – 90 km. Ionisation in this layer takes place due to hard X-rays with wavelength ≤ 1 nm from the Sun. The ionised particles found in this layer are nitrogen (N) and oxygen (O). It does not play a key role in Ionospheric Tomography because it constitutes lower electron densities, contributing negligibly to TEC, compared to the other layers of the ionosphere (Katamzi, 2007).

2.2.2 The E Layer

This layer lies just above the D layer at altitudes ranging from about 90 – 120 km. Ionisation of molecular oxygen is caused by soft X-rays (1 – 10 nm) and far ultraviolet (UV)

solar radiation. It can reflect radio signals with frequencies of about 10 MHz and below.

Sporadic E Layer

This is an unpredictable region which forms into very high electron density in the E layer. It may form at any instance of day- or night-time at altitudes of 90 – 130 km in the ionosphere (McNamara, 1991) although it can stretch up to 140 km sometimes. Interestingly, its electron densities are comparable to those of the F Layer. Consequently, it can reflect high frequency waves which normally are supposed to be reflected by the F Layer. While it totally obscures the F layer mostly, it sometimes becomes transparent allowing most radio waves to pass through it. The short form of representing sporadic E is E_S.

2.2.3 The F Layer

The F layer ranges from about 120 – 400 km above the Earth's surface. Atomic oxygen is ionised by Extreme Ultraviolet (EUV) solar radiation (10 – 100 nm) forming this layer. This is arguably the most cardinal layer of the ionosphere with regard to HF communication or signal propagation. It divides into two conspicuous portions, the F1 and F2 regions, during daylight due to solar radiation and reverts back into forming one F layer at night as it retains most of its ionisation even after the source of ionisation — the Sun — disappears.

Spread F

This phenomenon which occurs in the F layer is caused by irregularities and the F layer becomes diffuse resulting in scattering of the radio wave signal. Its main effect is that of causing the received signal at the receiver to be a superposition of a number of waves that are reflected from different heights and locations in the ionosphere at different times. Consequently, multiple traces appear on an ionogram (see Figure 2.3) so that the F trace is observed as a 'spread'.

2.3 Distinct Ionospheric Features

The terrestrial ionosphere presents interesting features at different latitudes. It is thus divided into 3 regions that exhibit different properties according to their geomagnetic latitude. These regions are the low- (or equatorial-)latitude, mid-latitude and the high-latitude (polar) ionospheres (Hunsucker and Hargreaves, 2003). Most of the information that follows in this Section below can be found explained in greater detail in the work by Hunsucker and Hargreaves (2003).

2.3.1 Low-latitude Ionosphere

This ionosphere spans 20 – 30 degrees on either side of the magnetic equator. It is mainly influenced by electromagnetic (e-m) forces arising because the geomagnetic field runs horizontally over the magnetic equator. Consequently, the electrical conductivity is abnormally large over the equator.

A strong electric current, called an electrojet, flows in the E layer causing the F layer to electrostatically lift resulting in a "fountain effect" that distorts the general pattern of the ionosphere in that zone.

2.3.2 Mid-latitude Ionosphere

The mid-latitude ionosphere falls roughly in the range of about 30 – 60 degrees on either side of the geomagnetic equator. In this region, ionisation of the ionosphere is produced almost entirely by energetic ultra-violet and X-ray emissions from the Sun. It is removed by chemical recombination processes which involve the neutral atmosphere together with ionised species. The movement of ions combined with balance of production and loss of ions are affected by winds in the neutral air.

The processes that take place in this ionosphere also manifest themselves in both high- and low-latitude ionospheres except that additional processes ensue in the last two.

A cardinal feature about this ionosphere is that it is connected to the inner magnetosphere which co-rotates with the Earth.

2.3.3 High-latitude Ionosphere

Notably, an opposite situation to that which occurs in the low-latitude ionosphere takes place here. In this region, the geomagnetic field is nearly vertical to the Earth's surface. The magnetic field lines connect the ionosphere to the outer part of the magnetosphere which is driven by the solar wind from the Sun. Thus, the ionosphere is dynamic in this region owing to the fact that it circulates in a pattern controlled by the solar wind which is variable.

It is also exposed to energetic particle emissions that produce excess ionisation. Also, the dayside ionosphere is directly accessible to material from the solar wind on a limited range of latitudes. The auroral zones have phenomena including electrojets and sub-storms which occur within the magnetosphere, and which have associated with them enhanced ionisation in the ionosphere due to auroral electron precipitation. A trough of lesser ionisation may be formed between the auroral and mid-latitude ionospheres caused by the difference in circulation patterns between the inner and outer parts of the magnetosphere.

It is also worthwhile to mention that the polar ionosphere alternates between two states depending on the alignment of the interplanetary magnetic field (IMF) either northward

or southward (Carlson, 1994). The IMF is the magnetic field "frozen" into the solar wind which is very variable in time. For the southward IMF, the IMF field lines merge and reconnect with the Earth's field lines at the "front", i.e., sunward side, of the magnetosphere, and this is associated with more direct influence of the magnetosphere, and the more likely triggering of substorms. For the northward IMF, any such merging of field lines can only take place in the magnetospheric "tail" and the magnetosphere is less directly influenced (Ratcliffe, 1972).

The aurora occurs near the boundary between open and closed field lines. Open field lines are field lines of the Earth which are connected directly to IMF field lines, while the closed field lines are those which connect to the opposite hemisphere. Particle "bounce" backwards and forwards along the closed field lines between conjugate points (Baker *et al.*, 1989, 1990).

2.4 Ionospheric Variations

It has already been highlighted that the ionosphere varies with height in terms of electron density distributions because different ionised species are dominant over certain ranges of altitude. In looking at the theory that the ionosphere is mainly created by the Sun, it follows that the ionosphere varies with time of the day, season and position of a particular area of the Earth's surface. The electron density of the ionosphere is greatest at midday, in the summer and near the Earth's equator. During winter, the values of the electron density are thus lower in comparison to those in summer. Also, as the amount of EUV radiation from the Sun increases or reduces following the solar cycle, appreciable variation in the ionosphere is noted.

2.4.1 Diurnal Variation

This type of ionospheric variation ensues as a consequence of the Earth's rotation about its axis. Therefore, solar radiation causes production of free electrons and ions differently depending on the time of the day. For a particular location above the Earth's surface, the intensity of solar radiation reaching different altitudes of the atmosphere from sunrise through midday to sunset and night causes ionisation to increase and decrease correspondingly. During morning hours, photo-ionisation becomes more and more prominent until midday. After that, recombination and other-electron loss mechanisms dominate until sunset causing only the F2 layer to survive through the nighttime.

2.4.2 Seasonal Variation

This variation emanates from the fact that the Earth revolves around the Sun, the source of solar radiation, causing different seasons on the Earth's environment as it completes

one full revolution. Greater ionisation takes place in summer while a lower one is observed during winter months for the D, E and F1 layers whereas the F2 layer presents a more complicated situation. In both the northern and southern hemispheres, the F2 noon electron density generally peaks around the equinoxes i.e March 21 and September 22.

Around the solar minimum (see 2.4.4 below), the summer electron densities are normally greater than those in winter. Winter electron densities tend to be greater though near the solar maximum (2.4.4): a scenario known as seasonal anomaly. At both solar minimum and maximum, electron densities are greater around the equinoxes than those in summer or winter.

2.4.3 Latitudinal Variation

This also portrays part of the ionospheric variation due to position of the Earth's surface. The variation is due to the solar zenith angle (McNamara, 1991). Solar radiation strikes the atmosphere more obliquely causing the daily production of free electrons to decrease with increasing latitude (Chapman, 1939; Ratcliffe, 1972). Beyond the Tropics of Capricorn and Cancer, the solar zenith angle can never reach zero degrees in magnitude. The maximum zenith angle increases as latitude extends from the tropics towards the poles (see Section 2.3).

The F2 layer latitude variation continues throughout the night due to atmospheric wind currents from the day-lit to the night-side-hemispheres. The daytime F2 electron densities peak at about $15^\circ - 20^\circ$ north and south of the geomagnetic equator, a phenomenon referred to as the equatorial anomaly.

2.4.4 Solar Activity Variation

This variation is associated with the 11 year solar cycle in which the number of sunspots, active regions, on the Sun's surface play a key role. The solar cycle is simply a periodic rise and fall in the activity of the Sun which varies from 9 – 14 years (Hathaway *et al.*, 1994). When the solar cycle is at its peak of activity called the solar maximum, showing highest number of sunspots, the electron densities in the various layers of the ionosphere are greater. The opposite is true for the solar minimum when the Sun's activity is relatively much lower showing the smallest number of sunspots on observing the surface of the Sun.

At solar maximum and round about that period of time, a large number of solar flares takes place at the Sun's surface. These are huge explosions which emit radiation that ionises the D layer. This in turn causes increased absorption of HF radio waves in the ionosphere — the D layer — during daytime. Magnetic storms are more frequent around solar maximum, and for large magnetic storms the auroral oval moves large distances equatorwards.

2.5 Radio Waves Propagating In The Ionosphere

There are two ways in which radio signals can propagate between a transmitter and receiver, at least one of which is on the Earth's surface. These are ground and sky wave propagation. Ground waves propagate along the curvature of the Earth while sky waves move to-and-from or through the ionosphere from either radars on the ground or on-board a satellite system.

In a case of sky waves propagating from a ground transmitter, the radio signal first encounters the D layer of the ionosphere where the electric field component of the ray forces the free electrons into oscillations at its same frequency. The charged particles then vibrate and collide with one another in-turn passing their energy to other particles in the process. Consequently, attenuation of the original signal from the radar takes place. The attenuation of the signal is inversely proportional to the radio wave's frequency squared. Hence, the transmitted lower frequency radio signals are more attenuated than their higher frequency counterparts.

The amount of signal loss is directly proportional to the number of particles present in the layer and its level of ionisation.

Therefore, only HF signals and those of higher frequency are able to propagate beyond the D layer. However, in both the E and F layers, HF signals show small attenuation in magnitude and significant refraction due to higher electron density concentrations. At some point in the ionosphere, this refraction becomes sufficient to send back the signals to the Earth's surface — giving the impression that the rays have been reflected.

This reflection of signals depends on both the transmission frequency and incidence angle of the original ray. As the transmission frequency increases for a given angle of incidence, there comes a point where the maximum plasma frequency is exceeded and the signal propagates through the ionosphere into space. The angle at which the HF signals start making it through the ionosphere into further space without being refracted is called the Pedersen ray angle (Villain *et al.*, 1984).

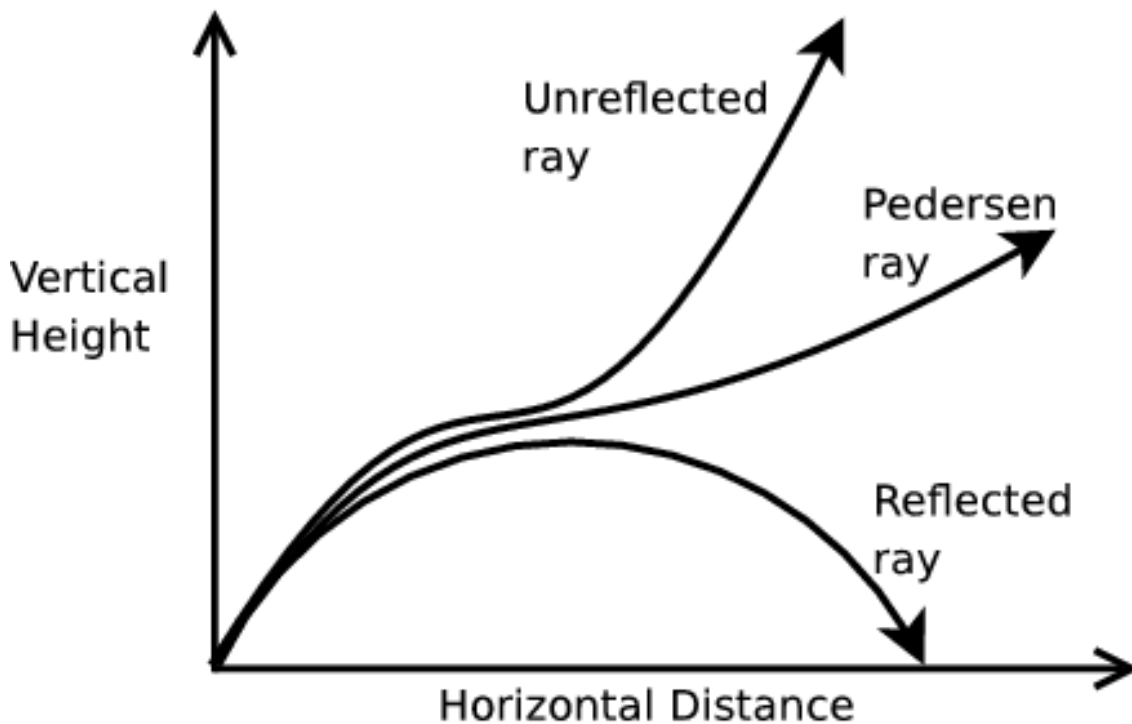


Figure 2.2: Various radio signals of which the "Pedersen ray" path (middle line in the diagram) follows from the "Pedersen ray angle" (from the horizontal line to the Pedersen ray) for the propagating signal. The Pedersen ray is one which just makes it through the ionosphere instead of being reflected back to the Earth's surface.

The above mentioned information is carefully and further described in report under the Umea University, http://www.tp.umu.se/space/Proj_06/Mukumu.E.pdf "Radio Waves in the Ionosphere" (2006).

2.6 Investigating the Ionosphere

Ionospheric measurements are conducted using various instruments. A ground based equipment known as Incoherent Scatter can be used to probe the lower ionosphere. Other types of radar, such as HF, to be described later (Section 2.9), are also used. Also, experimental equipment on-board rockets and sometimes balloons are used to carry out the measurements. The bottom-side ionosphere is studied using the vertical sounding radar known as an ionosonde. This probe can be ground based like the incoherent scatter radar or satellite borne for topside ionosphere measurements. Satellite systems like the Global Positioning System (GPS) are also used to study the ionosphere from the topside all the way to the lower ionosphere (see Chapter 3).

2.6.1 The Ionosonde

The ionosonde is an HF radar that is used to send radio energy pulses vertically into the ionosphere. The ionosonde radiates a modulated radio wave which is measured and analysed if or when it is reflected by the ionosphere (Kunitsyn and Tereshchenko, 2003). The receiver measures the time lag of the signal that is reflected from the ionosphere as a function of ray transmission frequency. Its output in simple terms is a graph of the time-of-flight of the signal against the transmitted frequency. The reflection height is calculated under the assumption that the signal propagates at the speed of light c . In fact, the effective reflection height of the signal depends on the transmission frequency and the frequency-height plot is called an ionogram. An example ionogram is shown in Figure 2.3 below.

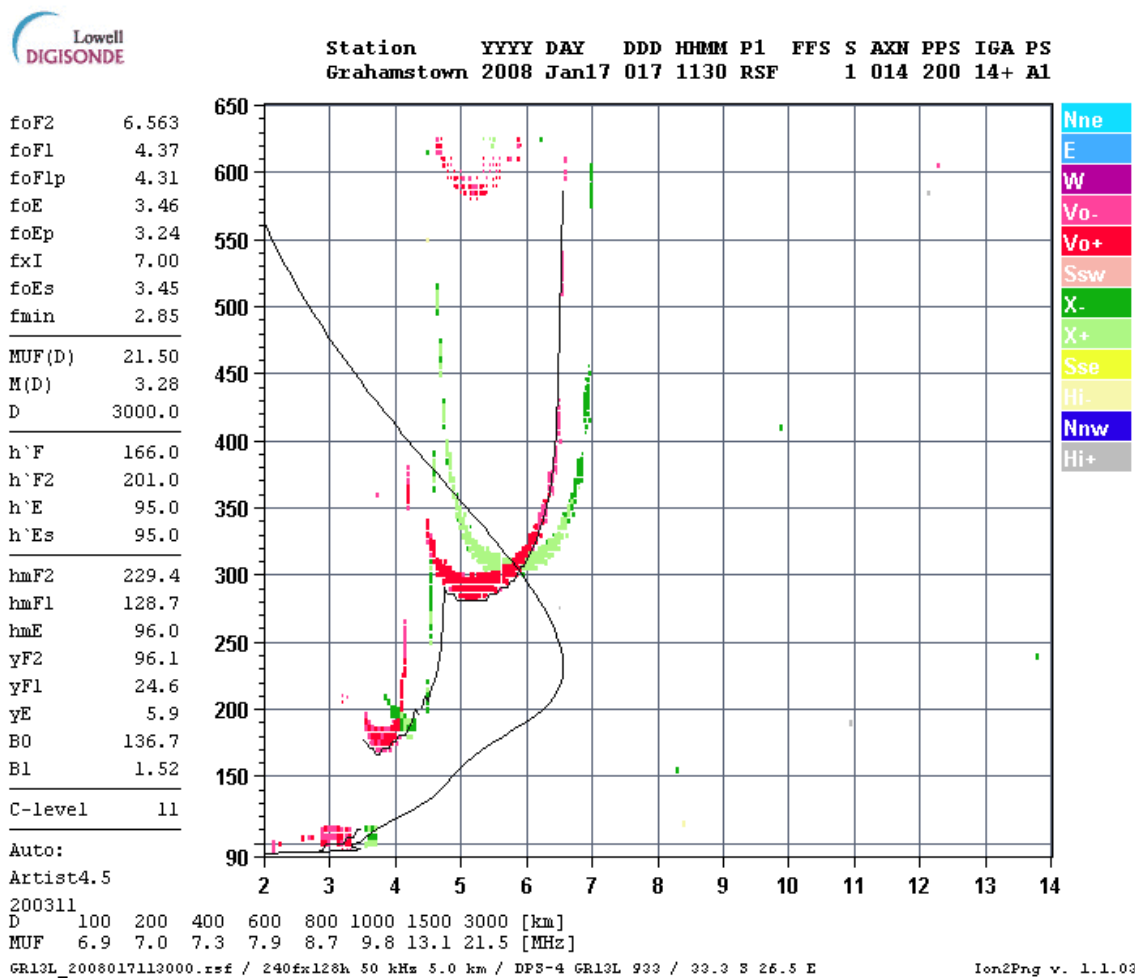


Figure 2.3: The plot shows an ionogram for Grahamstown, South Africa, with all the necessary information explained on it (adapted from <http://ionosond.ru.ac.za>).

The various ionospheric layers appear as approximate smooth curves separated by asymptotes at each layer's critical frequency. The layer's critical frequency and virtual heights are scaled from the asymptotes and lowest points on each curve respectively. The layer

sections curve upwardly from their starting points due to the slowing down of the transmitted radio wave by the ionisation with plasma frequency which is close to although not equal to the transmitted one. The red-like and green-like markings on the ionogram represents ordinary and extra-ordinary components of the radio wave propagating in the ionosphere. These two traces represent the virtual heights of the reflection points in relation to the plasma frequency of the constituent particles at each height or equivalently the transmitted frequency of the the radio waves from the ionosonde.

The consistent black line starting from about 90 km curving all the way to approximately 560 km shows the electron density as a function of height, or "electron density profile", scaled from the ionogram (McKinnell, 2006). The black traced out line along the bottom part of the ordinary wave result is generated when the Artist4.5 Software is scaling the ionogram. Scaling the ionogram is done automatically by the Artist4.5 Software producing the real heights trace in the process.

An ionogram can be very complicated at times when there are activities such as Sporadic E, multiple hops of signals, D layer absorption, Spread F and Lacuna (gaps in the reflected radio signals ionosonde trace when turbulence occurs as a consequence of large electric fields causing the stratified nature of the ionosphere to be complicated).

2.6.2 Refractive Index of the Ionosphere

Radio wave propagation in the ionosphere, and space in general, is described by the Appleton-Hartree equation. If we neglect collisions in the plasma, the Appleton-Hartree equation is given by

$$\mu^2 = 1 - \frac{X(1-X)}{(1-X) - \frac{1}{2}Y_T^2 \pm [\frac{1}{4}Y_T^4 + (1-X)^2Y_L^2]^{\frac{1}{2}}} \quad (2.4)$$

$$X = \frac{\omega_{pe}^2}{\omega^2} \quad (2.5)$$

$$Y = \frac{\omega_{ce}}{\omega} \quad (2.6)$$

$$Y_L = Y \cos \theta \quad (2.7)$$

$$Y_T = Y \sin \theta \quad (2.8)$$

$$\omega_{ce} = \frac{Be}{m_e} \quad (2.9)$$

$$\omega_{pe}^2 = \frac{n(e)e^2}{m_e \epsilon_0} \quad (2.10)$$

where

1. μ is the refractive index
2. ω_{ce} is the angular electron gyro-frequency
3. ω_{pe} is the angular electron plasma frequency and it can be written also as $2\pi f_{pe}$ with f_{pe} being the plasma frequency
4. ω is the instrument's probing angular frequency of the radio waves, i.e., $\omega = 2\pi f$ with f being the radio frequency
5. θ is the angle between the direction of the propagation of radio waves and the Earth's magnetic field
6. B is the geomagnetic field strength
7. e is the electron charge
8. ϵ_0 is the permittivity of free space
9. $n(e)$ is the electron density
10. m_e is the electron mass

The plus sign in the denominator part of the equation caters for the full equation of the "ordinary wave" while the negative one is for the "extra-ordinary wave".

The basic principle of sounding the ionosphere is that HF radio signals of frequency f are reflected at the cutoff points where $X = 1$ for an ordinary wave and $X = 1 - Y$ for the extraordinary one.

If the magnetic field strength is ignored, then $Y = 0$ together with both Y_L and Y_T become 0 thereby rendering the equation to be reduced to

$$\mu^2 = 1 - X \quad (2.11)$$

or

$$\mu = (1 - X)^{\frac{1}{2}}. \quad (2.12)$$

In the studies conducted here we may be justified in omitting the magnetic field, i.e., neglecting the Y terms, because the frequency used in the HF radar is typically 12 – 13 MHz, while the plasma frequency in the region of interest (e.g. Prince George, see Chapter 4) is typically just over 1 MHz. This means that Y is roughly 0.1 and it is reasonable to neglect it to a first approximation.

2.7 Ray Tracing

Ray tracing is an essential method of studying the propagation of radio signals in the ionosphere (Vastberg, 1994), using electron density profiles and performing step-by-step integration. The techniques used are similar to those in other branches of wave propagation in the anisotropic and dispersive medium (Davies, 1990).

Ray Tracing can be performed taking into account the full magnetoionic nature of the ionospheric medium (Terry, 1971). The original set of equations to perform this analysis was developed by Haselgrove (1955). Several numerical and analytical techniques have been used to trace radio rays through the ionosphere under various conditions, and there are some commonly used computer programs to perform the task. Recent progress in ray tracing has been reviewed by Bennett *et al.* (2004).

However, neglecting the magnetic field, as we have done (see previous section), one can perform useful ray tracing using Snell's law, as in optics. Snell's law is mathematically given as:

$$\mu_i \times \sin \varphi_i = \mu_{i+1} \times \sin \varphi_{i+1} \quad (2.13)$$

$$i = 0, 1, 2, \dots, n.$$

where μ_i is the refractive index of an ionospheric layer i which ranges from an initial ground level height $i = 0$ to a maximum height $i = n$ and φ_i is the elevation angle of the

radio signal relative to the ground level. It requires that the horizontal component of the refractive index vector is constant while the vertical one may change in the ionosphere (Walker *et al.*, 1987).

It is understood that the ray theory is valid for the range of frequencies in the HF spectrum and above it, although in geometric optics this is only true when the scales of the inhomogeneities are large in comparison to the wavelength and Fresnel zone size (see Vastberg, 1994 and references there-in). Thus ray tracing is a powerful tool for calculating the propagation effects due to large scale inhomogeneities and irregularities of the ionosphere.

2.7.1 Ray Tracing Equations

As already mentioned above, Snell's law suffices to perform simple ray tracing of radio wave propagation. To perform the ray tracing, a simple algorithm was followed for this particular thesis work. Snell's law in equation 2.13, trigonometry and Pythagoras' theorem are employed to produce position results of the ray trace. The phase refractive index (equation 2.11) is used to calculate the phase and group velocities and hence the time of flight of the ray. From equation 2.11, the phase refractive index can be re-written as

$$\mu_i = 1 - \left(\frac{f_{pe}}{f_t} \right)^2 \quad (2.14)$$

where a signal can propagate if $f_t < f_{pe}$ with f_t being the radar transmit frequency. Thus, μ_i must be between 0 and 1 in order for a signal to propagate from one layer through to the next one.

From e.q. (2.10) the plasma frequency of each layer is given by

$$f_{pe} = \frac{e}{2\pi\sqrt{m_e\epsilon_0}}\sqrt{n(e)} \quad (2.15)$$

which gives numerically

$$f_{pe} = 8.98\sqrt{n(e)} \quad (2.16)$$

for f_{pe} in MHz and $n(e)$ in units of 10^6 cm^{-3} , where $n(e)$ is the electron density for a layer. The trigonometric equation used to advance the new horizontal range on each iteration is

$$h_{i+1} = h_i + (v_{i+1} - v_i) \tan(\Phi_i) \quad (2.17)$$

where the subscript $i = 0, 1, 2, \dots$ represents horizontal layers of the ionosphere from the ground at $i = 0$ upwards to the maximum height; h is the horizontal distance moved by the ray; v is the vertical height of the signal position and lastly Φ is the angle of elevation calculated from the initial angle at the radar and increments through Snell's law.

From this information, the ray paths are calculated giving a decent picture of how signals propagate in the ionosphere in particular and space in general.

Since the group refractive index is the reciprocal of the phase one, i.e., equation 2.11, the group and phase velocity of the signal are given by

$$v_{phase} = \frac{c}{\mu_i} \quad (2.18)$$

$$v_{group} = c \times \mu_i \quad (2.19)$$

where c is the speed of light (see Appendix B in Walker *et al.* (1987)).

Pythagoras' theorem gives the ray path distance for each iteration as follows:

$$Ray\ path = \sqrt{(v_{i+1} - v_i)^2 + (h_{i+1} - h_i)^2} \quad (2.20)$$

where h and v take the same meaning as given above. The time of flight is calculated from the ray path distance as

$$Time\ of\ Flight = \frac{Ray\ path}{v_{group}}, \quad (2.21)$$

Caution is taken to accumulate the necessary parameters at each iteration as well as to update the arrays that store information for the ray's propagation. Figure 2.4 indicates a result that is obtained from the above description.

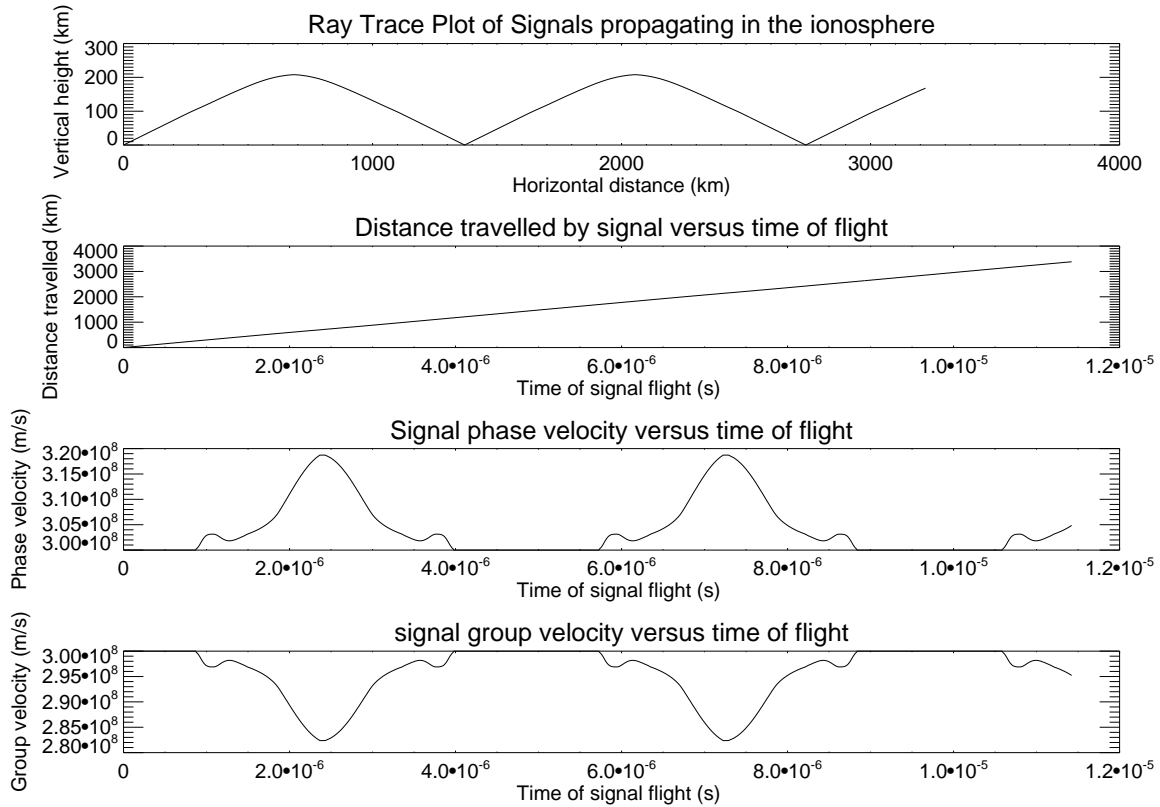


Figure 2.4: Ray Traces using a simple program that uses Snell's law, trigonometry and Pythagoras' theorem for a model ionosphere generated using the IRI 2001 Model. The ray trace in the top panel shows a path for a 20° elevation angle radio signal. Embedded in the figure are 20° elevation angle plots of the distance travelled, phase- and group-velocities against time taken for the signal to move from the radars' transmitter to its propagation ending point.

2.8 Backscatter of Radio Signals

As HF radio waves propagate from one layer to another through the ionosphere, or space in general, they encounter areas of increased or decreased refractive index in the vertical direction from the ground where they get partially reflected and transmitted. Walker (2002) highlighted that most of the wave is transmitted with small reflection if the change in the refractive index is small.

In looking at radio waves propagating through periodic ionospheric irregularities structure of refractive index alterations, an incident signal on these is partially reflected. If the spacing of the irregularities is equal to half the signal wavelength, it follows that all the reflected wave's parts move in phase on any plane AB (Figure 2.5) that is normal to the ray propagation direction causing constructive interference between the reflected signal components. Therefore significant energy is reflected and if the incident ray is normal to the irregularities, the reflected energy moves back along the same path — a phenomenon similar to Bragg scatter in crystals. Since the morphology of ionospheric irregularities is random and not periodic, the structure can be Fourier analysed in space. Thus, the

reflection condition for an incident ray will produce significant reflection if the spatial Fourier component has a periodic component of significant amplitude in the resultant angular spectrum — a scenario known as coherent backscatter. The above-mentioned effect is well explained in detail in Walker (2002).

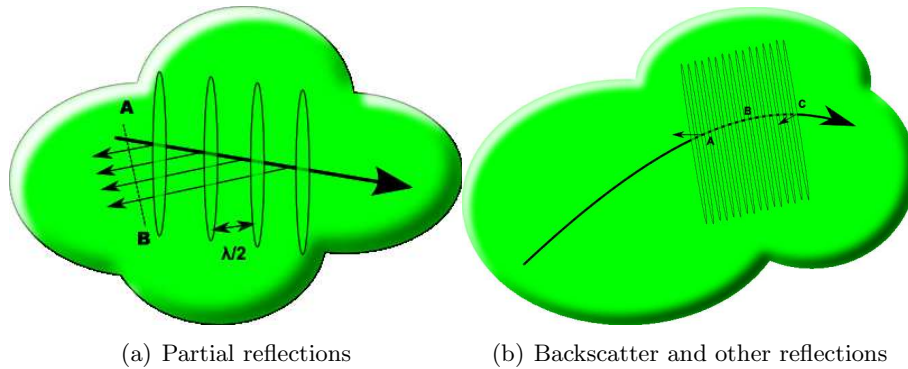


Figure 2.5: Reflection from field-aligned ionospheric irregularities along the Earth's magnetic field (thick shaded parallel lines). In component (a), partial reflections of signals from periodic irregularities are indicated. In part (b), directions of coherent backscatter in the ionosphere are shown. The figures are versions of one of the graphs in Walker (2002).

Although the description thus far is focused on ionospheric scatter, it is worthy to make mention that backscatter also manifests itself in terms of ground backscatter at the surface of the Earth. Actually, this behaviour can be extended to sea scatter and so on. More information on ground scatter is discussed later on in section 2.10.

Schematic diagrams illustrating various typical propagation modes of the SuperDARN HF radar signals backscattered from the Earth's surface and ionospheric irregularities are shown in Figure 2.6 below.

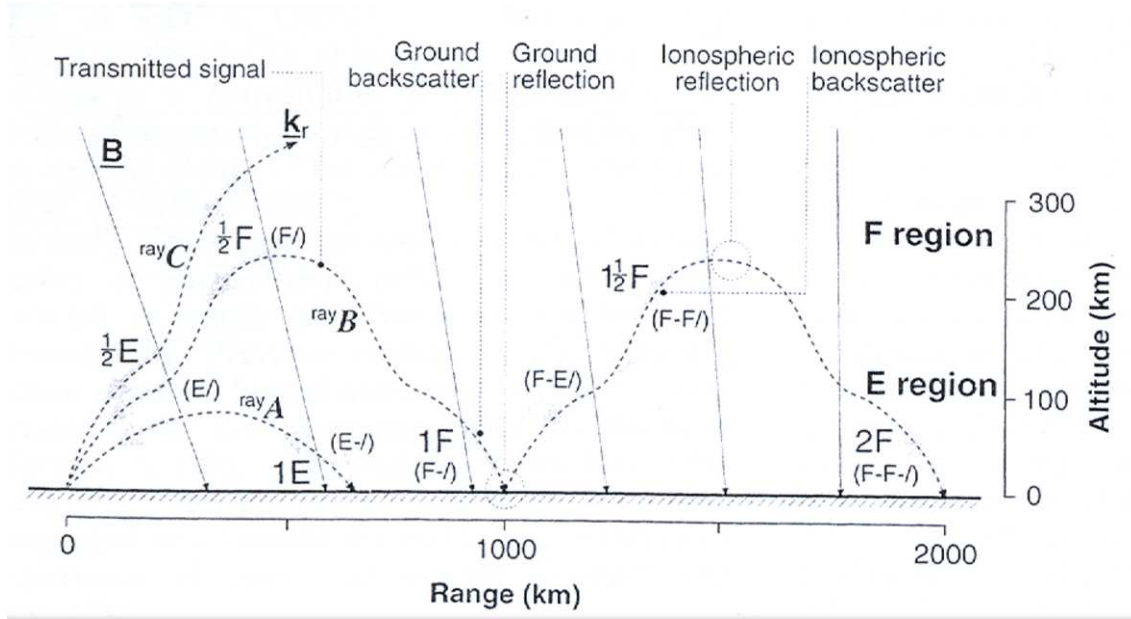


Figure 2.6: Propagation modes for the SuperDARN HF radar: Ray A shows E-region mode, Ray B indicates F-region mode, Ray C penetrates the ionosphere. Backscatter ensues at the reflection points (Ground and Ionospheric reflections respectively in this figure) as presented. This graphic was adapted from Milan *et al.* (1997).

2.8.1 Coherent Scatter Radar Measurements

Coherent-scatter radars are sensitive to the Bragg scattering phenomenon that emanates from electron density irregularities in the ionosphere (Greenwald *et al.*, 1995). A radar is sensitive to irregularities that have one-half wavelength of the radar's signal wavelength. In the ionosphere, irregularities are identified by their field-aligned structure — whereby their wave-number vector is directed almost orthogonal to the magnetic field at a specific point. Thus, for backscatter — i.e., the scattered radio signal to return back to the radar — to occur, the incident radar signal must be nearly orthogonal to the magnetic field as well. This is so because significant backscatter occurs only when the transmitted ray is normal to the magnetic field for irregularities that are elongated along it (Walker *et al.*, 1987).

Radar operations have been done at HF (3 – 30 MHz), VHF (30 – 300 MHz) and UHF (300 – 3000 MHz) frequencies, enabling research of irregularity wavelengths ranging from about 20 cm through 3 m to approximately 19 m.

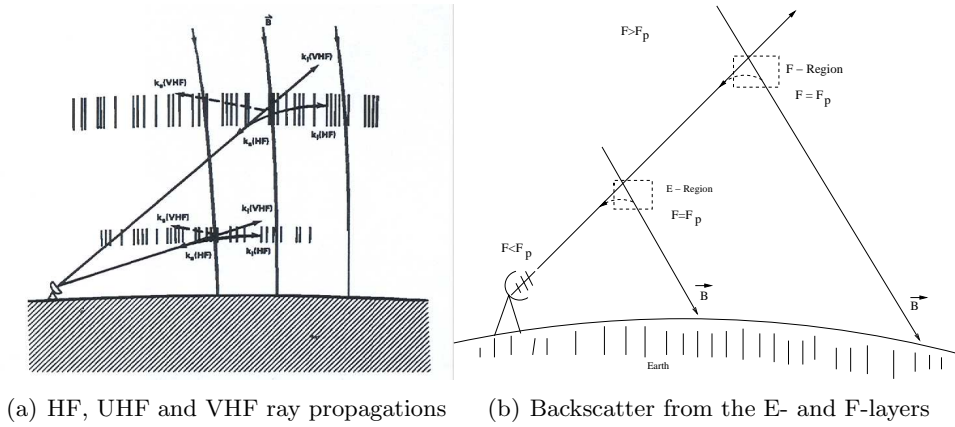


Figure 2.7: The picture on the left shows a graphical representation of how HF, VHF and UHF radar signals are scattered in space by high-latitude E- and F-layer ionospheric irregularities. This left-most graph was adapted from Greenwald *et al.* (1985). On the other-hand, the right graph illustrates the HF signal's refraction and backscatter effects more clearly. The right picture was obtained from Rash *et al.* (1991). The refraction of HF radio waves takes place in the E and F layers of the ionosphere when the transmitted radio frequency is less than the plasma frequency. At the point(s) where the transmitted radio frequency is equal to the plasma frequency, reflection of signals occurs and this results in formation of backscatter of the original forward signal. No backscatter takes place when the transmitted radio frequency is greater than the plasma frequency.

Figure 2.7 illustrates how different transmitted frequency ranges (HF, VHF, UHF) propagate in the high-latitude ionosphere. Clearly, it is notable that ionospheric refraction is negligible at VHF and UHF frequencies showing straight-line propagation paths throughout the ionosphere. Signals at VHF can backscatter from irregularities and have been used in radars to study the E region. However, HF frequencies are affected by ionospheric refraction, bending downwards in the process and forming a curved path. There is normally scatter from the irregularities along the HF curved path, but backscatter takes place only at the point where the incident ray is perpendicular (at right angles) to the magnetic field.

At high latitudes, the magnetic field lines are nearly vertical to the Earth's surface resulting in the orthogonality condition for backscatter being easily satisfied. Ionospheric density structure is produced by plasma instability processes, e.g. the cross-field two stream and gradient drift instability in the E layer. In the F layer, ionospheric irregularities are also produced by plasma instabilities, particle precipitation and magnetospheric turbulence. The Rayleigh-Taylor, Kelvin-Helmholtz and Current Convective Instabilities also contribute to irregularity production.

Most of the above-mentioned can be used for studies in the low- and mid-latitude regions using the VHF and UHF radars in which the wavelength range is shorter than 3 m. Hence, HF radars are used to study the orthogonality condition in both the E and F layers of the ionosphere using the concept of radio wave ionospheric refraction.

In looking at the theory of backscatter in relation to ray tracing, it is imperative to make mention that knowing the signal propagation information — ray path distance — from

the radar transmitter up to the point of backscatter is sufficient to describe ionospheric and ground scatter. This is so because the ground range is simply twice the half-hop range. Hence the distance of a ray path of a radio signal into the ionosphere for half-hop is effectively half of the ray path distance for a full one-hop ground signal in magnitude. Thus, half-hop, one hop, one-and-half hop and so on ranges can be taken as multiples of the half-hop distance which is indicated in Figure 2.8 below relative to Figure 2.4 above.

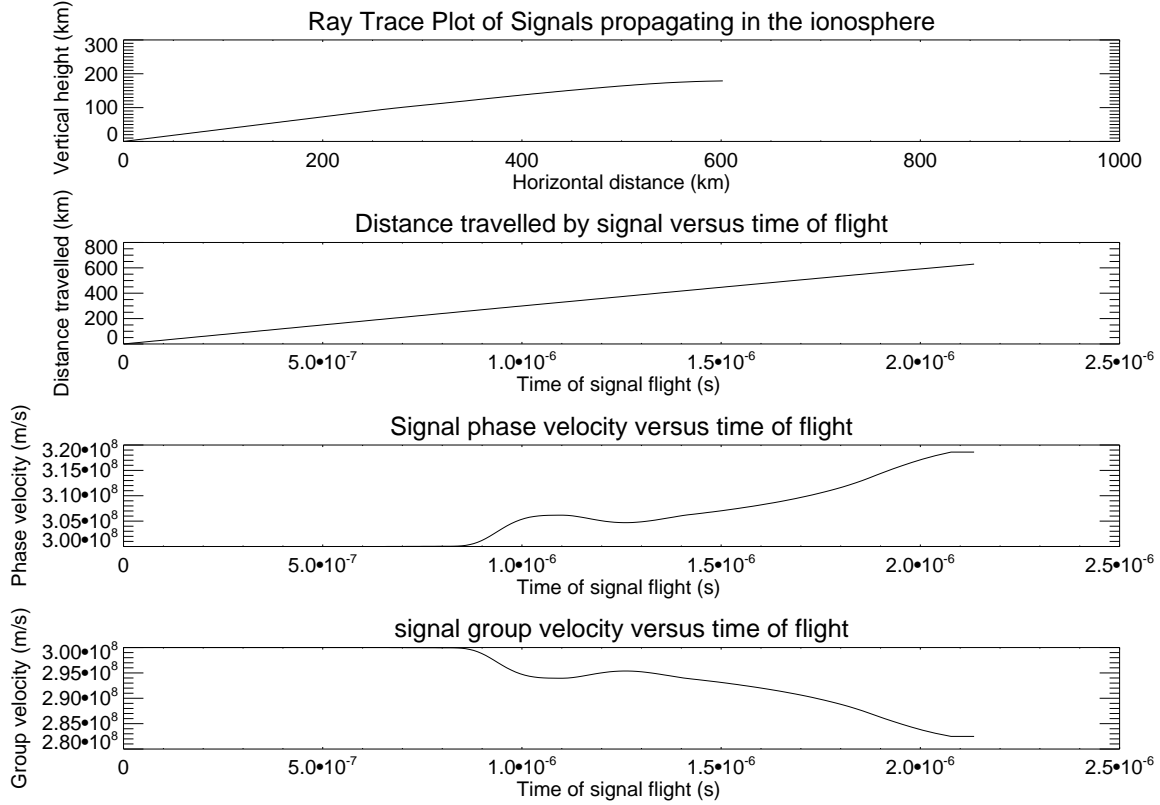


Figure 2.8: Half-hop of the full ground range for a radio signal that is reflected by an ionospheric layer through successive refraction in the ionosphere. This figure shows a radio signal of 20° elevation angle path which is backscattered at the point of ray reflection.

The computer program that was used to produce Figures 2.4 and 2.8 is used for all subsequent ray tracing results presented in the remainder of this thesis.

2.9 The Radar System

Coherent scatter HF radar systems give a powerful experimental technique used to investigate the magnetospheric storm of which the SuperDARN radar network (which looks into the northern and southern hemispheres space) is an example. The SuperDARN utilises a concept where the HF radars operate in pairs with common field of view areas so that the backscatter Doppler information is combined to yield two-dimensional vectors, and data from the entire network in each hemisphere can be combined to produce maps of

high-latitude ionospheric convection (Chisham *et al.*, 2007).

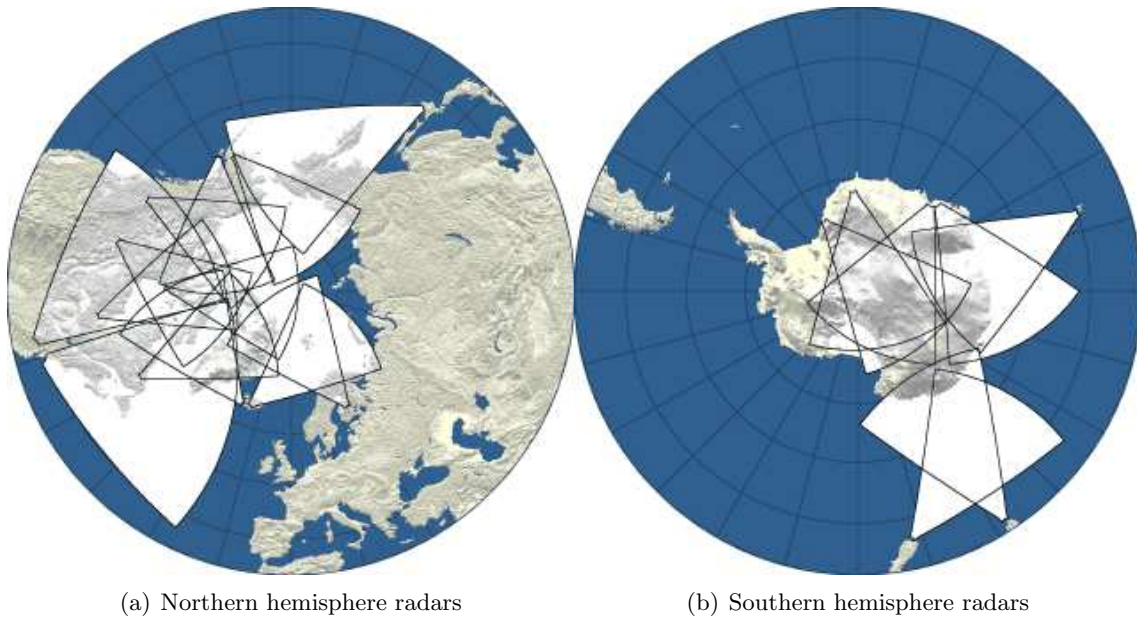


Figure 2.9: SuperDARN Radars with their respective fields of view. The left most plot shows the northern hemisphere radars based in the arctic region of the Earth whereas the right one portrays the southern hemisphere radars located in the Antarctica region and its nearby islands (adapted from <http://superdarn.jhuapl.edu>).

Each SuperDARN radar comprises of a main array of 16 log-periodic antennae (Greenwald *et al.*, 1995). These both transmit and receive HF signals and provide echo location in the horizontal plane (Chisham and Pinnock, 2002). Some of these radars have an interferometer array of 4 antennae which receive signals only, but are dedicated to evaluate the vertical angle of echo arrival. This second array is located 100 m in front of or behind the 16 log-periodic array (Greenwald *et al.*, 1995).



Figure 2.10: The primary array 16 log-periodic antennae and the secondary array of 4 antennae in the background (adapted from <http://superdarn.jhuapl.edu>).

The radars are electrically steerable, narrow-beam, use phase arrays and are operated at a specific frequency each time which falls in the range of 8 – 20 MHz band (Walker, 2002). Each radar operates on a fixed ray transmission frequency in the above mentioned range and is sensitive to ionospheric irregularities (Munsami *et al.*, 2002). The radar detects coherent backscatter radio waves produced by ionospheric density E and F layers' irregularities that have a spatial periodicity of the magnitude of half the radar signal wavelength (Baker *et al.*, 1990). This allows for the calculation of signal backscatter power, line-of-sight Doppler velocity, spectral width and elevation angle data in the radar field of view (see (Chisham and Pinnock, 2002)) once conditions of backscatter are fulfilled as the signal propagates in the ionosphere (see Figure 2.11). These parameters are mainly used to identify events (Walker, 2002).

Station:Hankasalmi (han)
Operated by:University of Leicester

Beam 08

08, March 2004 (20040308)
Program IDs:-6401,153

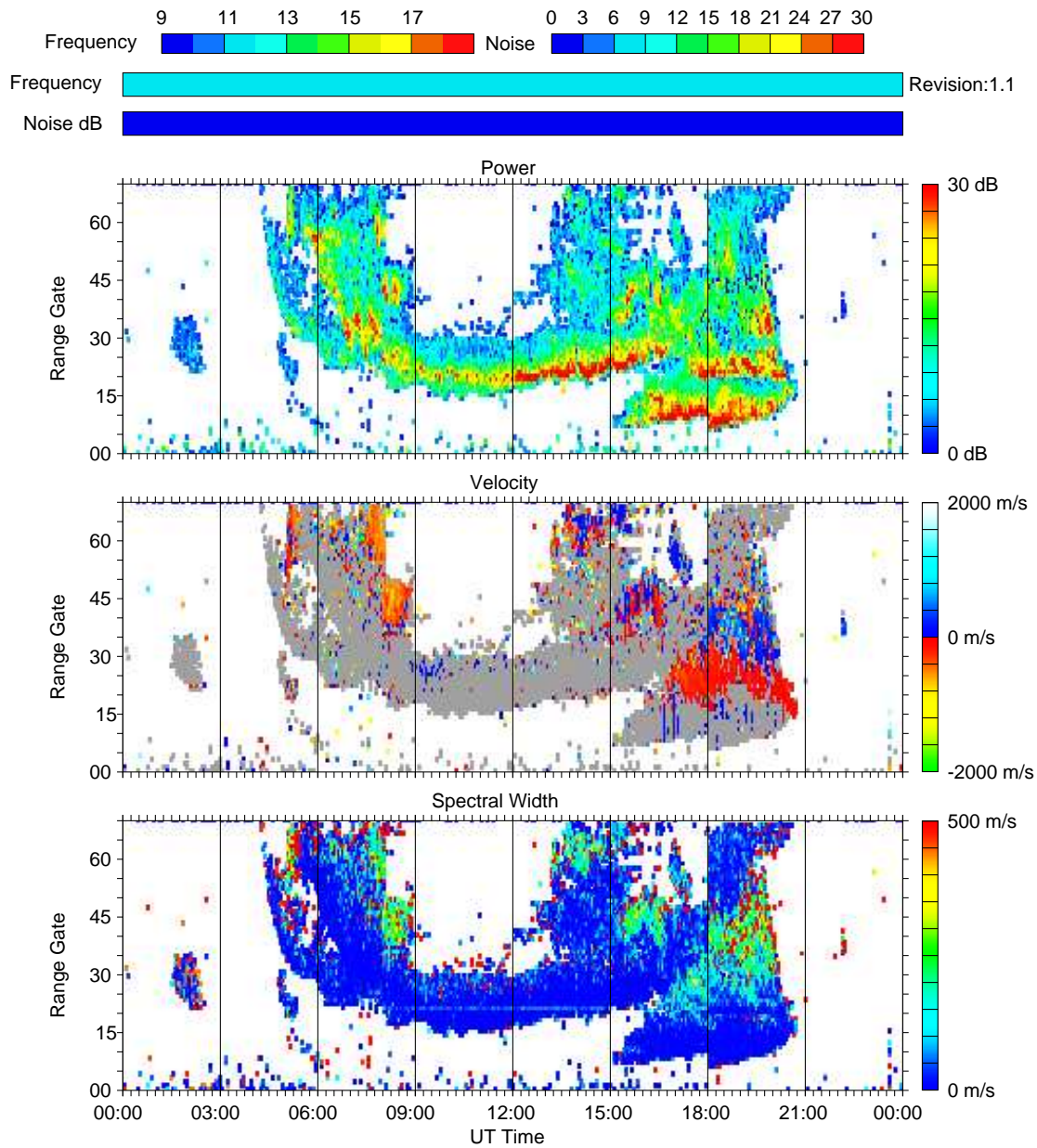


Figure 2.11: SuperDARN archived data plot for 8th March 2004. The transmitted frequency for the whole day's data was 11 – 12 MHz (second degree light blue colour shade in the frequency colour-bar shown clearly in the frequency bar just above the Noise bar in the figure). Thus, the 2004030816.fit data which contains 2 hours data from 16 – 18 hours could be viewed as having been observed for 11 MHz.

The radars' field of view is measured over 16 beam directions covering an area of about $3 \times 10^6 \text{ km}^2$ Munsami *et al.* (2002). The SuperDARN radars operate in oblique sounding mode and form 16 beams of azimuthal separation 3.24° each (Gauld *et al.*, 2002). Each beam is divided into 75 range gates of length 45 km each although there is an initial range distance for measuring backscatter of 180 km from the radar. Mathematically, the

distance is given by:

$$Distance\ (km) = 180 + (range - gate \times 45) \quad (2.22)$$

When the radars are used in standard mode, the dwell time for each beam is about 7 s. This gives a full 16 beam sweep that covers 52° (see Figure 2.12) in azimuth and about 3500 km in the horizontal direction of ground distance every 2 minutes. When operating in non-standard mode, the integration time of each beam can be as low as 2 s and consequently this lowers the signal-to-noise ratio, essentially power, accordingly. Another notable result is that the data coverage is reduced following the loss of low returned powers. However, this has little resultant effect on the data coverage in high latitude auroral regions where powerful HF scatter is normally observed.

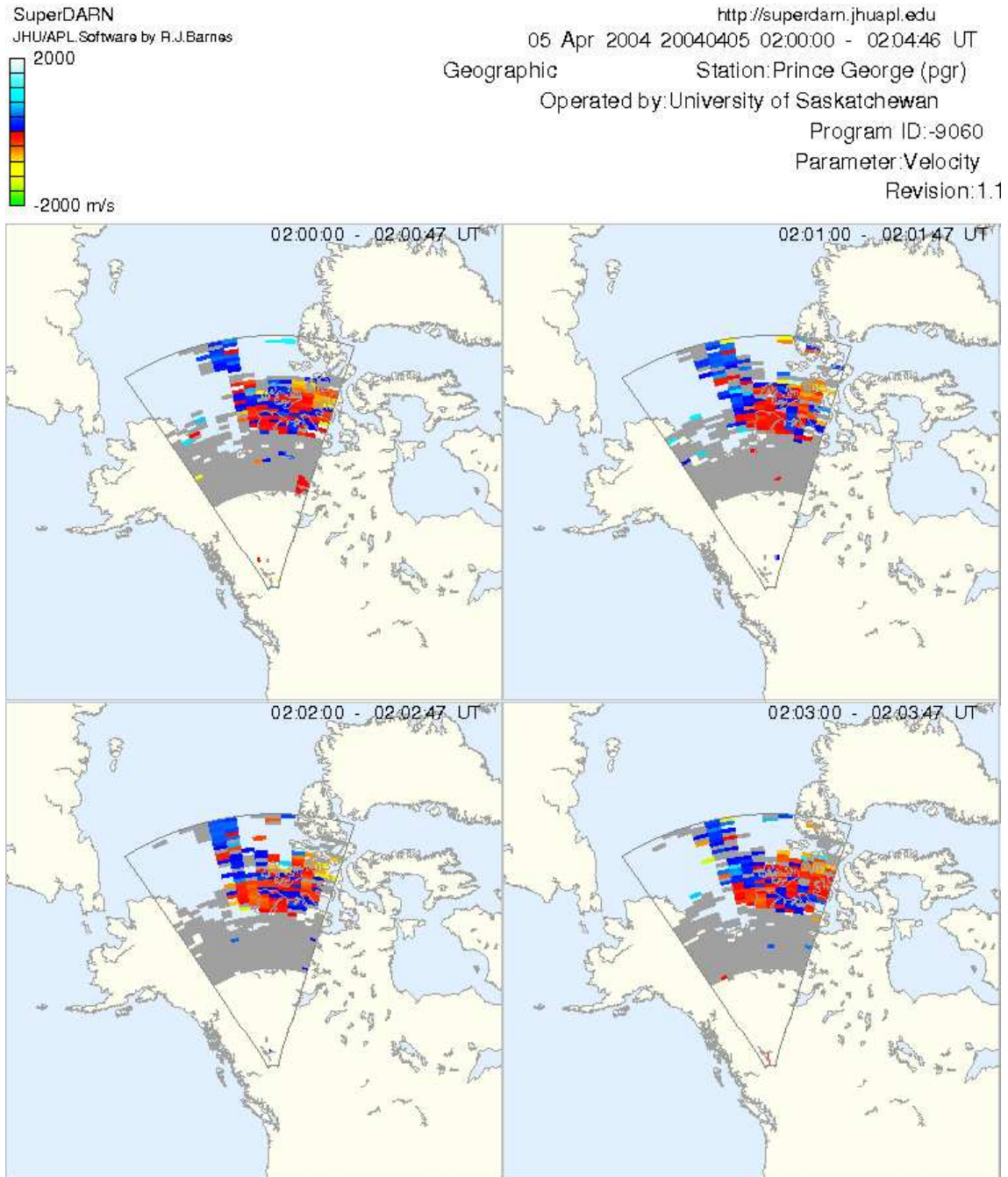


Figure 2.12: Field of views of the Prince George SuperDARN radar for the day 2004/04/05 at the times shown on the plots about 02:00 UT archived data (adapted from <http://superdarn.jhuapl.edu>).

Gauld *et al.* (2002) indicated that the usual anticlockwise sequence sweep through beams 15, 14, 13, ..., 0 can be altered to suit the desired enhanced temporal resolution in addition to the provision of very high time resolution data along a single look direction. It has been established that the extensive field of view of the HF coherent scatter radars makes them suitable and powerful tools for measuring large scale spatial and temporal development of the ionospheric electric fields.

2.9.1 Backscatter power

This SuperDARN radar measured component indicates the strength of the backscattered signal. Echo power is recorded in dB — the logarithmic units of the signal-to-noise ratio. If the irregularities are large in expanse, the strength of the backscattered power is great in magnitude. The reverse is also true for small in size irregularity structures. The top most panel in Figure 2.11 shows the power relative to a threshold in decibels on a colour bar.

2.9.2 Doppler Velocity

This parameter is the line-of-sight Doppler velocity, v_{los} , of the irregularities as they move in the ionosphere. Its units are the m.s^{-1} . In Figure 2.11, the middle panel illustrates the Doppler velocity with a colour coded bar such that the colours on the red side represent irregularities motion away from the radar while the blue side corresponds to motion towards the radar. Zero Doppler velocity is usually indicative of ground scatter.

2.9.3 Spectral Width

The width of the spectrum, Δv , is a measure of how broad or narrow the velocity spectrum is. It tells of how turbulent the target (say irregularities) is. The units of spectral width are m.s^{-1} . The lower most panel in Figure 2.11 portrays this spectral width information. The plot expresses the irregularities velocity spread. A narrow spectral width indicates that the irregularities are more or less stationary while a broad one represents a situation where they are in appreciable motion.

A careful study of the Auto-Correlation Functions (ACF), which are implemented to perform the needed measurements by the radar system, reveals the following interesting information. The principle behind the ACF is that things that correlate grow and vice versa. The narrower the width, the smaller the velocity distribution of the targets, i.e., irregularities. In fact, a narrow spectral width indicates that there is a dominant velocity in the targets. On the other-hand, a broad spectral width has a connotation that there is much distribution of velocities in the target. Hence, a broader spectral width represents a broad range of Doppler velocities.

2.9.4 Elevation

This is a relatively new measured parameter in the SuperDARN radar systems in comparison to the above mentioned three, i.e., echo power, Doppler velocity and spectral width and is only measured at some stations. It is the vertical angle of arrival of the backscattered signal that is calculated from the phase matrix by determining the relative phases of the signals arriving at two radar antenna array systems, i.e., the main and secondary

interferometer antennae (Senior *et al.*, 2006). The elevation angle is used to determine the propagation modes of the returning signals as a function of range and altitude of scatter according to Mthembu (2006).

2.10 Ground Scatter

Narrow spectral width illustrates the fact that there is one dominant velocity in the target. This means all the Doppler velocities are close to zero or some other constant value. Two competing results follow from this, i.e., ground scatter and closed field lines.

Closed field lines move and hence have a velocity associated with them. On the other hand, ground scatter is therefore recognised as that which shows zero Doppler velocity and narrow spectral width of the targets e.g. Earth's surface. It is normally reflected in the plots of Figure 2.11's nature in terms of the gray colour shade.

Thus, any target shown as having a constant or zero velocity and indicating broad spectral width will not be representing ground scatter — with the broad width of the spectra clearly confirming that the target is in motion and not stationary. Milan *et al.* (1997) indicated that ground backscatter has a near-zero velocity and low spectral width. This criteria and the above description are used to generate the 'ground scatter flag' measured parameter of the radar's data observables which is assumed to contain only ground scatter data and nothing else. $|v_{los}| < 50$ m/s and $\Delta v < 20$ m/s are used to distinguish between ground and ionospheric backscatter although this criterion can be ambiguous in certain cases (Milan *et al.*, 1997). According to Chisham and Pinnock (2002), flagging of the measured SuperDARN raw data as ground scatter (i.e., non-ionospheric backscatter) is done when both $|v_{los}| < 30$ m/s and $\Delta v < 35$ m/s. Thus, it is clear that there are limits where the Doppler velocity and its attendant spectral width values for the data provide for ground or non-ground scatter (ionospheric scatter) which is recorded in the ground scatter flag measured parameter of the SuperDARN radar.

The ground scatter flag data consists of either ones (1) and/or any other values depending on the criterion mentioned above. For cases where both $|v_{los}| < 30$ m/s and $\Delta v < 35$ m/s are used, the ground scatter flag is assigned a one (1) while the non-zero values are recorded for any other combinations of the line-of-sight Doppler velocity data and its attendant spectral width data.

However, it appears like this may not necessarily represent ground scatter and thus such data is only treated as suspected ground scatter data.

2.11 International Reference Ionosphere Model

The ionosphere can be modelled using dedicated simulation methods of which the International Reference Ionosphere (IRI) is one. This is an empirical model that provides

specifications of the ionosphere in terms of electron density, electron and ion temperature, and ion composition for a given geographic location, time, date, altitude range say the maximum possible one 60 – 2000 km and TEC. It is sponsored by the Committee on Space Research (COSPAR) and the International Union of Radio Science (URSI). A special COSPAR general assembly carries out updates to existing IRI versions yearly.

The values it provides for magnetically quiet conditions of the non-auroral ionospheres are monthly averages. It operates on existing data resource recordings from ground, in situ and topside space based instruments (Katamzi, 2007).

The model used in this work is the 2001 edition found on the Internet as the International Reference Ionospheric Model (<http://nssdc.gsfc.nasa.gov/models/iri.html> "International Reference Ionosphere - IRI-2001 at SPDF", 2001). It is imperative to make mention that all electron density simulated data used in thesis for ray tracing activities were obtained from the above-mentioned model.

Chapter 3

Current Ionospheric Tomography Techniques

This Chapter looks at the various methods which are currently available in performing ionospheric tomography. It touches on the underlying procedures that use mathematical analysis to achieve the goal of reconstructing the electron density.

3.1 Ionospheric Tomography using GPS Satellites

The GPS is a part of the Global Navigation Satellite System (GNSS) that was developed by the United States Department of Defence for instantaneous position determination. It consists of about 24 active satellites at a time although there is a small number of standby ones in case of failure in one of the 24. These satellites transmit two separate signals simultaneously at 1.58 and 1.23 GHz frequencies called L1 and L2 respectively.

Because the ionosphere is a dispersive medium, as specified by the Appleton-Hartree equation (see Section 2.6.2), the two different frequencies experience different group delays and phase changes when they propagate along the same path through the ionosphere to a ground receiver. The technique described in the next section may be used to find the TEC along this path from the difference in group delay (or equivalently 'pseudo-range' which is group delay multiplied by c), or, more reliably, from the difference in phase for the two frequencies. The results of such TEC measurements for a network of ground stations may then be combined using the tomographic techniques described in Section 3.3 to generate two-, three- or four-dimensional 'images' (the fourth dimension being time) of the electron density in the ionosphere, in a similar way to 'CAT scans' in medicine.

3.2 Measurement of Total Electron Content

The total electron content (TEC) was defined in Chapter 1. From the Appleton-Hartree Equation (Section 2.6.2), the ionospheric refractive index is $\mu = (1 - X)^{\frac{1}{2}}$ (eq. 2.12), where $X = \frac{f_{pe}^2}{f^2}$ (eq. 2.5), f_{pe} is the plasma frequency (f_{pe}^2 is proportional to $n(e)$ (eq. 2.15)) and f is the radio wave frequency. Since the group delay is the integral of $(1 - \mu)$ along the path, one can see how the group delay is proportional to and inversely proportional to $n(e)$ and inversely proportional to f^2 . Using these arguments, Blewitt (1990) showed how to obtain the TEC along the 'slant path' from the satellite to the receiver:

$$TEC_p = 2(f_1 f_2)^2 \frac{(P_2 - P_1)}{k(f_1^2 - f_2^2)} \quad (3.1)$$

$$TEC_l = 2(f_1 f_2)^2 \frac{(L_1 \lambda_1 - L_2 \lambda_2)}{k(f_1^2 - f_2^2)} \quad (3.2)$$

where f_1 and f_2 are the frequencies L1 and L2 (referred to in Section 3.1) respectively, P_1 and P_2 are the 'pseudo-ranges', L_1 and L_2 are the phases at these frequencies, and k , from the proportionality, related to the ionospheric refraction is $80.6 \text{ m}^3/\text{s}^2$.

The two measurements are often combined because of the 2π ambiguity in the phase measurement, but its greater accuracy, and there are the so-called 'baseline' techniques for doing this (Blewitt, 1990). The slant path TEC may be converted to a vertical TEC above the receiver by multiplying by the cosine of the zenith angle χ of the satellite at the ionosphere, which is usually taken to be at an altitude of about 400 km. Figure 3.1 shows the geometry.

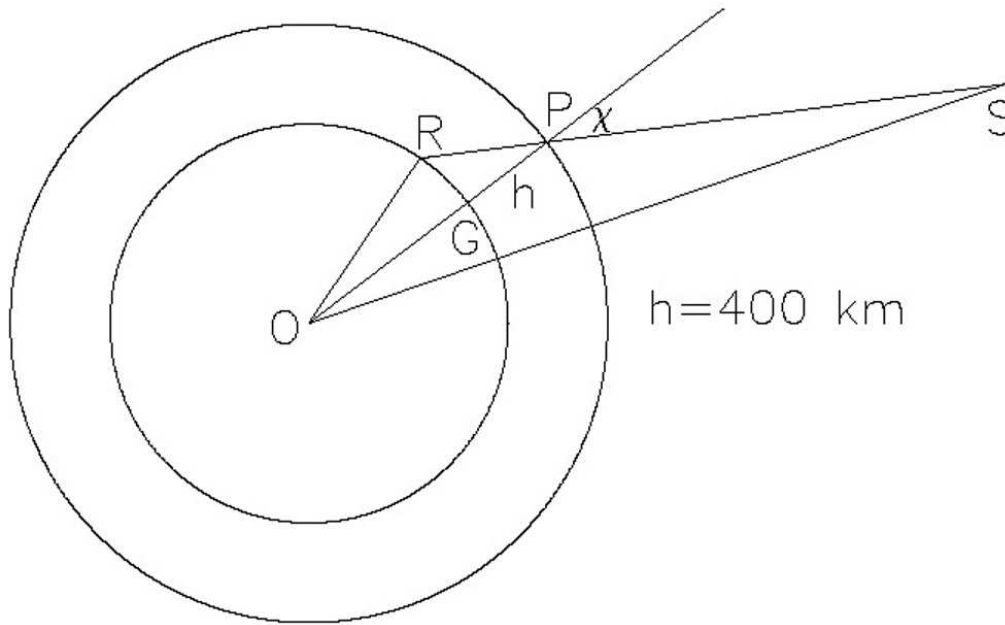


Figure 3.1: Geometry of a GPS satellite (S), the ionosonde and a receiver (R). The ionosphere is assumed to be a screen at a height $h = 400$ km above the ground. P represents the intersection of the line of sight and the ionosphere, and χ is the zenith angle (adapted from Ma and Marunyama, 2003).

The TECs derived from GPS satellites during periods when they are near the vertical above a ground receiver have been compared to those derived from ionosondes at the same location by McKinnell *et al.* (2007) in South Africa and others.

3.3 Radio Tomography

According to Kunitsyn and Tereshchenko (2003), the problem of ray radio tomography is to recover the structure of some ionospheric region from linear integrals measured along rays intersecting a particular region. Ray radio tomography is done for known relations of phases and amplitudes of the radio waves as in the geometric optics approximation where the pair of equations 3.1 and 3.2 provide measurements of TEC along numerous paths to numerous receivers, obtained from the two signal frequencies of the satellite system.

A pictorial representation of the geometry is shown in Figure 3.2 below.

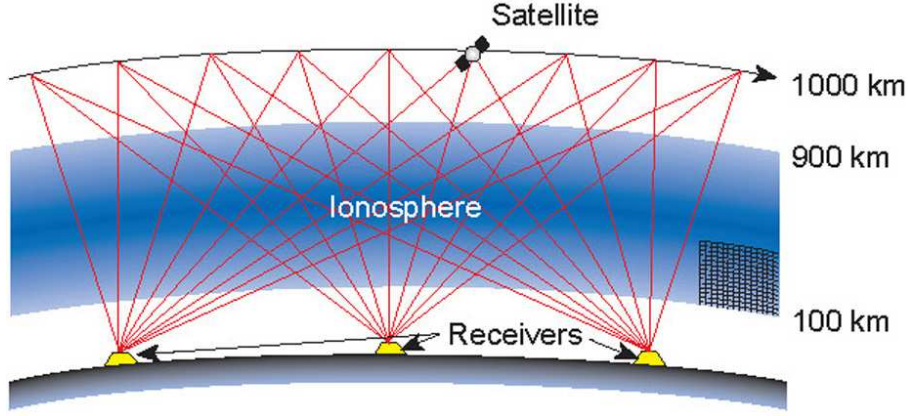


Figure 3.2: A pictorial representation of the satellite - receiver geometry for ionospheric tomography, with an array of ground receivers receiving signals from several satellites (only one is shown) along numerous paths through the ionosphere (adapted from Tucker, 1998).

Most tomographic problems are solved using a system of linear equations. Thus, there is a need to choose a proper method or algorithm for solving the equations in a specific problem which will provide the best results. The following are some of the available methods used to find the solution: Algebraic Reconstruction Technique (ART), ART with relaxation for the inequality systems (ART2), Multiplicative ART (MART) (see Liu *et al.* (2000)), Simultaneous Iteration Reconstruction Technique (SIRT), etc.

The ray Radio Tomography problem hence reduces to a system of linear equations which are written in terms of a projection operator P mapping \mathbf{x} a continuous 2D distribution (electron density) into a set of phase differences or logarithmic relative amplitudes \mathbf{m} :

$$P\mathbf{x} = \mathbf{m} \quad (3.3)$$

More formal details about this ionospheric tomography technique are presented clearly by Kunitsyn and Tereshchenko (2003).

In the Bayesian approach, the system of linear equations (3.3) can be written

$$\sum_i^N A_{ij} \mathbf{x}_i = \mathbf{m}_j \quad (3.4)$$

where $i = 1, \dots, L$.

Rearranging the measured results into a column-vector \mathbf{m} , and then putting the unknown values of electron density at grid points of interest into column vector \mathbf{x} together with constants to be determined, the ionospheric tomography problem can then be re-written as

$$\mathbf{m} = \hat{A}\mathbf{x} + \varepsilon \quad (3.5)$$

where \hat{A} is an $m \times n$ matrix of linear coefficients and ε is a column-vector of measurement errors of \mathbf{m} — considered as random variables.

The probability density and subsequent regularisation calculations then lead to the control of an ionospheric layer. The regularisation procedure can be modified using the fact that the electron density is zero at very low and very high altitudes. This allows for the electron density reconstruction through the grid points.

The technique of Mitchell and Spencer (2003) is used by a number of groups, including the Hermanus Magnetic Observatory, to perform computerised ionospheric tomography, yielding three-dimensional, time-dependent images of the electron density distribution in the ionosphere.

In the next chapter we will investigate whether the information provided by HF radars can possibly be used to provide a similar view of the ionosphere.

Chapter 4

Processing SuperDARN Radar and IRI Data

The SuperDARN radar records its data in various forms. One of them is the 'fit' format. This format has a time axis which spans a range of approximately two (2) hours. It also harbours the actual measured data of interest like the radio signals backscatter 'elevation' (if the radar has an interferometer antenna) as well as echo power, Doppler velocity and spectral width of the Doppler velocity parameters. An example of how the recorded echo power, Doppler velocity and spectral width data for one particular beam and range-gate values of 8 and 14 respectively for the Hankasalmi radar is shown in Figure 4.1. Also, Figure 4.2 shows the elevation and ray transmitted frequency data for above-mentioned beam 8 and range-gate 14 again. These results indicate the basics of the scatter plots that follow in the rest of this chapter.

A brief description of the information from these figures, figures 4.1 and 4.2 below, is presented in the Chapter 5.

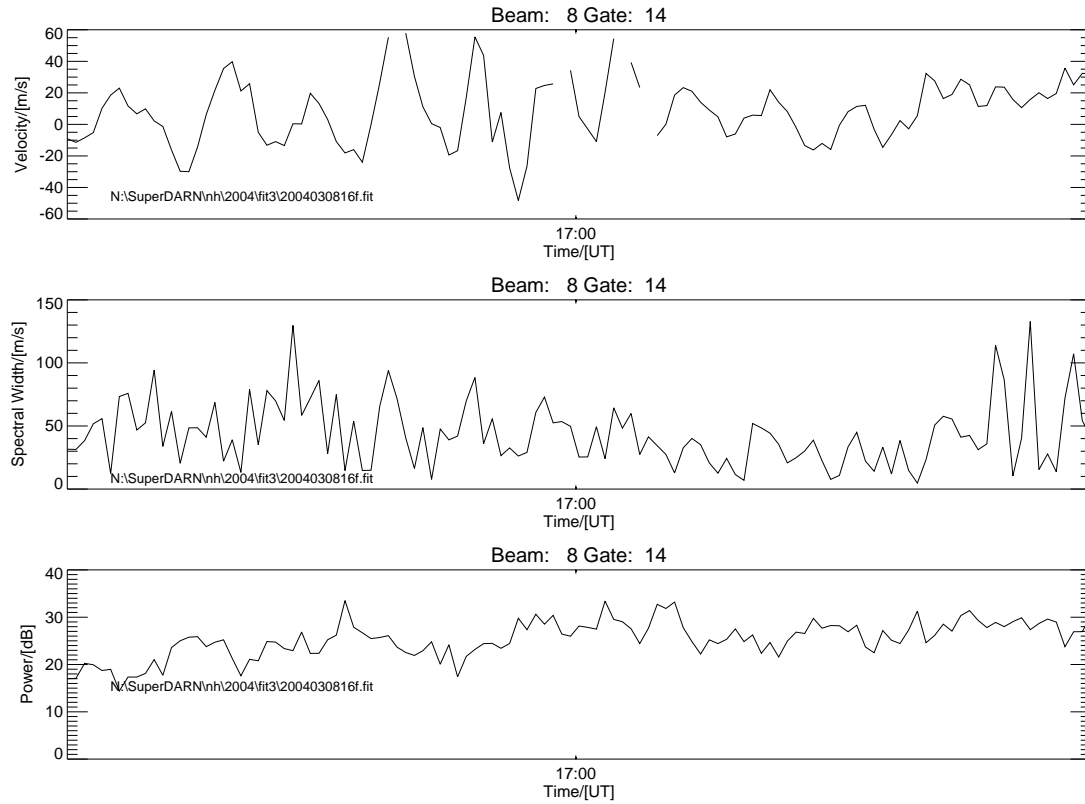


Figure 4.1: The Doppler velocity, Doppler spectral width and echo power of beam 8 and range-gate 14 data of the SuperDARN radar is shown. The top-most panel presents a plot of power versus time. The middle panel indicates the Doppler velocity against time graph. The lower-most plot shows the spectral width versus time data. The inscriptions 'N:\SuperDARN\neh\2004\fit3\2004030816f.fit' on the plots provides the source and file of the raw SuperDARN radar data that was processed on the computer.

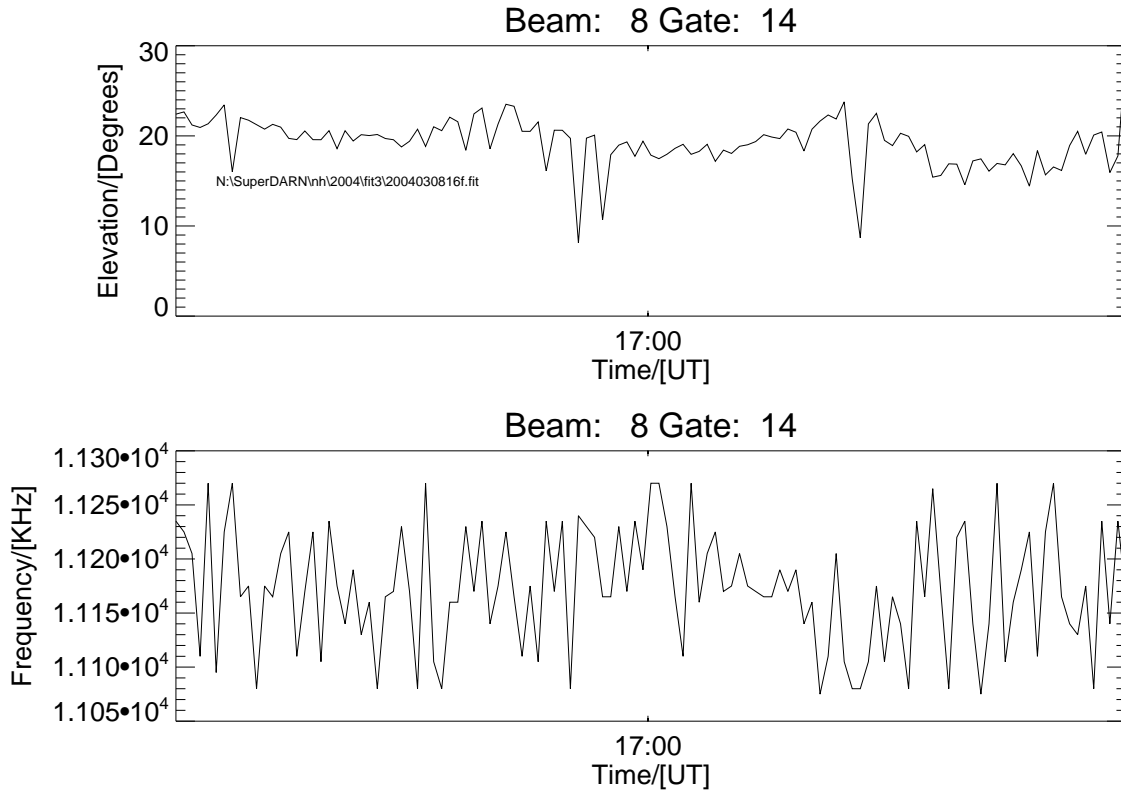


Figure 4.2: Elevation angle data versus time plot for beam 8 and range-gate 14 of the radars field of view is shown in the top panel of the figure. The elevation is presented in degrees. The lower panel indicates the SuperDARN radar's transmitted signal frequencies for the period of data recordings with the frequency being in kilo-Hertz (kHz). The time is in hours of the Universal Time (UT) standard. The time range span is 2 hours corresponding to one '.fit' file's data.

However, it is cardinal to make mention at this point that the frequency plot in Figure 4.2 shows how the radar changes or maintains its signal transmission frequency over the 2 hours period of measuring the rest of the SuperDARN radar parameters' data. The changes in the radio wave's transmitted frequency has a relation to the other data parameters as will be presented later on in this chapter.

In this Chapter, backscatter elevation data is looked at in terms of how it is split into both ground and ionospheric scatter results for a particular cell e.g. beam 8 and range-gate 14 on the radar's field of view beam-pattern. Also, a picture of how the elevation data from all the 16 Beams and 75 Range-gates appears is explored.

The scatter results are then compared with ray tracings generated by simulating radio wave propagation through an IRI 2001 Numerical Model ionosphere.

After this, a presentation of both ground and ionospheric scatter data individually for all Beams and Range-gates is given. Then other SuperDARN measured parameters of ground or ionospheric individual scatter elevation data are explored to help in understanding the results from the various processings that are mentioned above. In order to verify the operation of the (own-written) project computer programs, the other parameters of

raw data plots are then compared with the ones that are archived at the SuperDARN community online resource.

Then the effect of changing the radar transmitted frequency on whether the signal is backscattered from the ground or the ionosphere is investigated.

The testing of consistency our many findings in a large dataset is described by processing one full month's worthy of data. This marks the end of the case for ionospheric tomography studies that were performed in this dissertation work.

4.1 Scatter Data

The SuperDARN radar system records some useful parameters as mentioned in Chapter 2 above. Elevation data is one such parameter. To kick-start the work in our project, elevation data was plotted for a single cell — beam 8 and range-gate 14 — on the radar's field of view grid as shown in figures 4.2 above and 4.3 below. In Figure 4.2, some form of a wobbled line stretches across the whole of the 2 hour time period of measured data. The clearly shown ripples indicate how the take off angle of radio signals varies over the specified data recordings time period. This shows how the radar picks out backscattered signals that originate from ionospheric irregularities positioned at certain elevation angles relative to the radar's location.

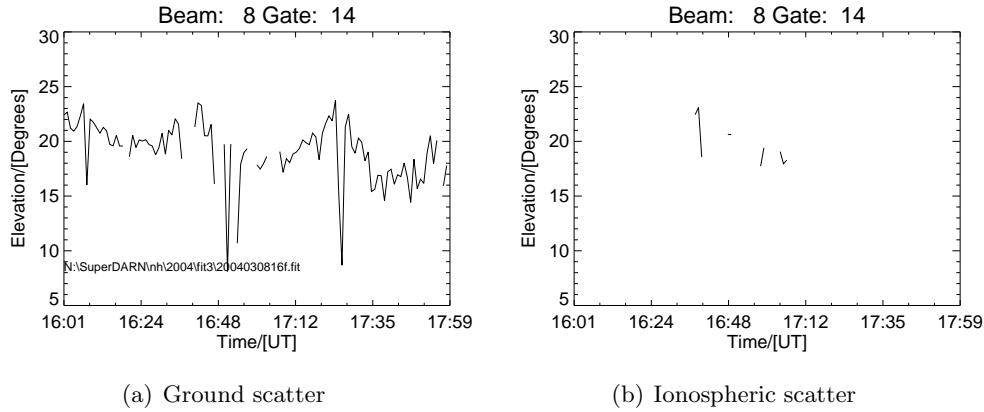


Figure 4.3: Elevation angle upon filtering out either ground or ionospheric scatter data. The left plot, (a), gives the ground scatter elevation data plot. The right graph, (b), portrays ionospheric scatter elevation data plot. All the data measurements were recorded from 16 : 00 – 18 : 00 hours Universal Time (UT). These two plots are close in features of Figure 4.2's elevation plot above, which gives a full combination of their data.

Figure 4.3 was then produced to show the effect of processing both ground and ionospheric scatter data separately. This was accomplished by using the 'ground scatter flag' parameter of the measured SuperDARN radar data. Figure 4.3 (a) was generated by masking the 'ground scatter flag' data to the elevation data consequently forming a new data-set with only pure ground scatter data. Similarly, Figure 4.3 (b) was produced by inverting the

'ground scatter flag' data so that only the ionospheric scatter flagged data was produced. This generated 'ionospheric scatter flagged' data was then masked to the elevation data so that only ionospheric scatter elevation data was produced.

4.2 Elevation data from all the Beams and Range-gates

Having processed the SuperDARN radar measured elevation data in the manner of Figure 4.2 (top panel), a more representative picture of the scatter data from all the 16 Beams and 75 Range-gates was sought. The results of this are presented in Figure 4.4 which indicates data from all 16 Beams and 75 Range-gates of the radar's field of view. From this figure, some information (see Table 4.1) regarding the distances that the radio signal travelled into the ionosphere or even back and forth through successive reflections are recovered. In looking at Table 4.1, some interesting puzzles to critically look at and seek solutions from arise. Firstly signals travelling at elevation angle of 28° , 29° and 30° cannot possibly penetrate through the polar ionosphere to vertical heights of round about 790 – 1637 km. This behaviour is indicative of radio signals' half hop, full hop and/or many more propagation modes' travel upon reflections from both the ground and ionosphere surfaces respectively.

Contour plot of Elevation versus Range gate for all scatter

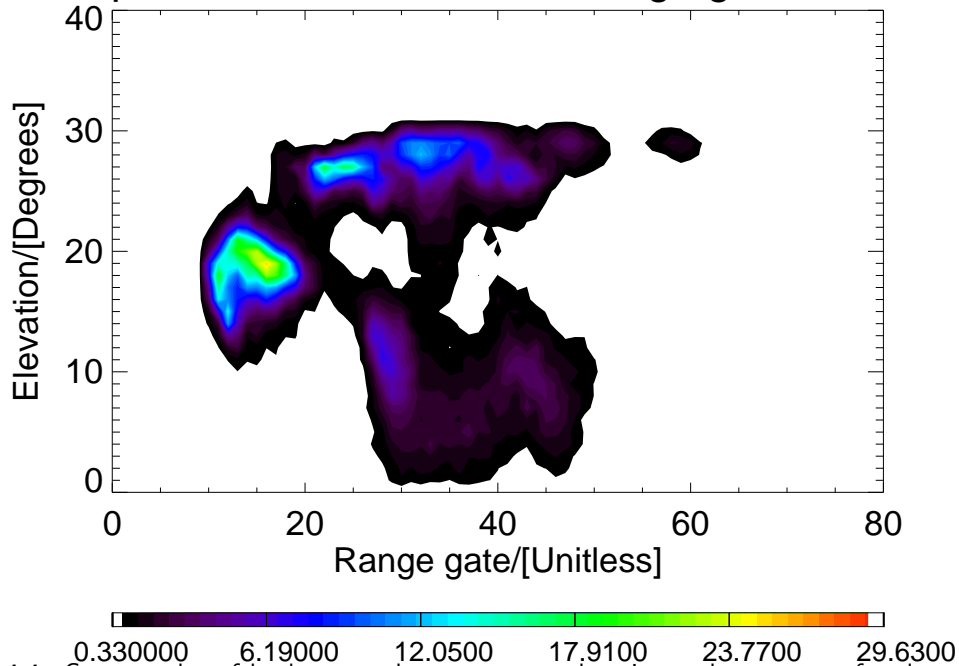


Figure 4.4: Contour plot of backscattered power versus elevation and range-gate for elevation data, both ground and ionospheric scatter.

Table 4.1: Numbers gleaned from Figure 4.4 regarding the Radio Ray Path distances

Range Gate	Elev. ($^{\circ}$)	Ground Range (km)	Vertical Height (km)	Ray Path (km)
17	19	945	325	999
23	10	1215	214	1234
29	28	1485	790	1682
33	29	1665	923	1904
43	8	2115	297	2136
59	30	2835	1637	3274

Upon carefully analysing the obtained intrinsic numbers in Table 4.1 above, a run through the elevation data was thus redone, this time sifting out either ionospheric or ground scatter in the data processing at a particular instance to remain with either ground or ionospheric scatter information only at each time respectively. Having processed elevation data and produced plots for a specific 2 hour "fit" file (2004030816f.fit) for a particular one day, i.e., from 16 – 18 hours UT of 8th March 2004 for the Hankasalmi radar, the results gleaned (Table 4.1) were compared with an output from the ray tracing program (see Table 4.2 below) to establish what was obtaining in the ionosphere and/or on the ground for the randomly selected rays indicated in the table and Figure 4.5 below. The ray traces at intervals of 1° for an IRI 2001 Model ionosphere with the matching date and time of the processed 'fit' file data in question were generated as shown in the figure (Figure 4.5 below).

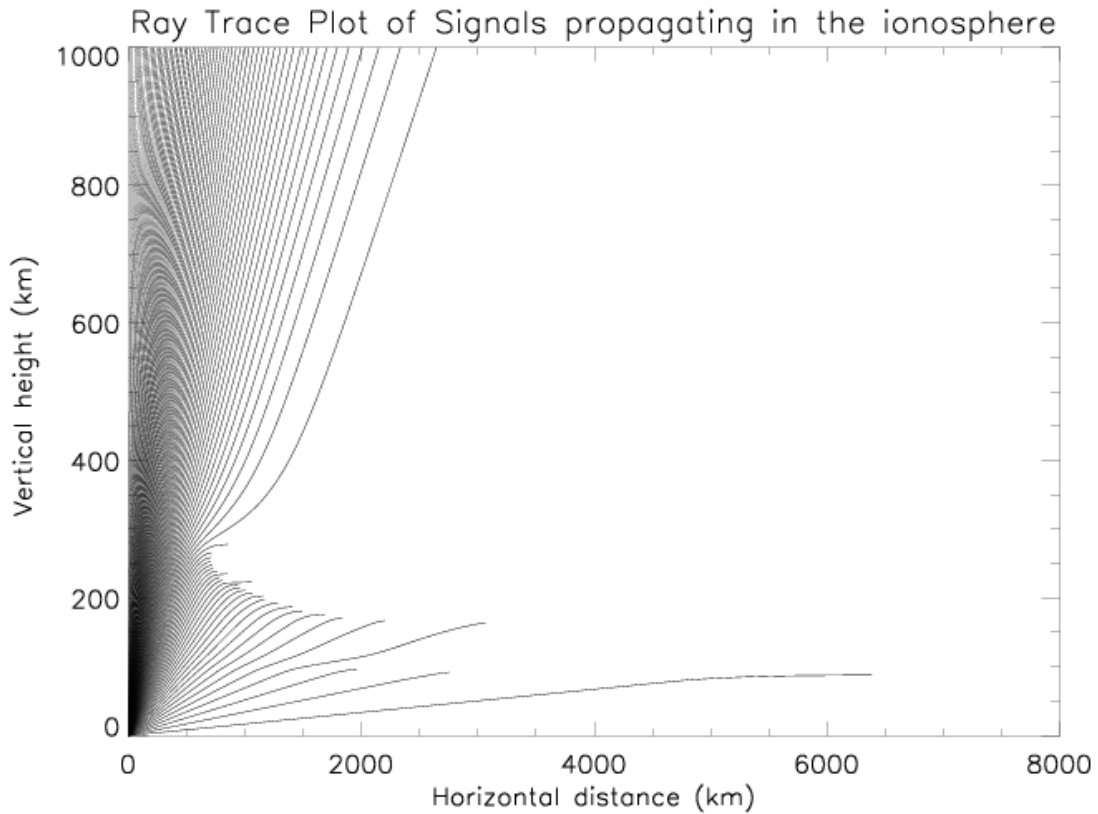


Figure 4.5: Ray Traces of a Hankasalmi ionosphere modelled using the IRI 2001 Model for 8th March 2004, around 16 – 18 hours.

Table 4.2: Ray Tracing results for an IRI Model ionosphere at 17 hours (UT) of 2004/03/08

Freq. (MHz)	Elev. ($^{\circ}$)	Ray Path (km)	H-H H (km)
11	19	815	230
11	10	1295	193
11	28	2853	N/A
11	29	2556	N/A
11	8	1500	181
11	30	2382	N/A

The frequency value of 11 MHz was obtained from Figure 2.11 (light blue colour in one of the colour-bar) which corresponds to the 'fit' file data used in generating Figure 4.4. It is worthy noting that the data in Figure 2.11 is for beam number 8 only while that in Figure 4.6 is for all the 16 Beams which correspond to Figure 4.4 as already described about its production. While the information presented in beam 8 is enough for knowing the necessary information about the radar transmitted frequency of the desired time and day, a plot showing data from all the 16 Beams was generated so that a comparison of the results of Figure 4.4 with those of Figure 4.6 for all the Beams' data could be performed.

Station:Hankasalmi (han)
 Operated by:University of Leicester

Beam:All

08, March 2004 (20040308)
 Program IDs:-26007,153

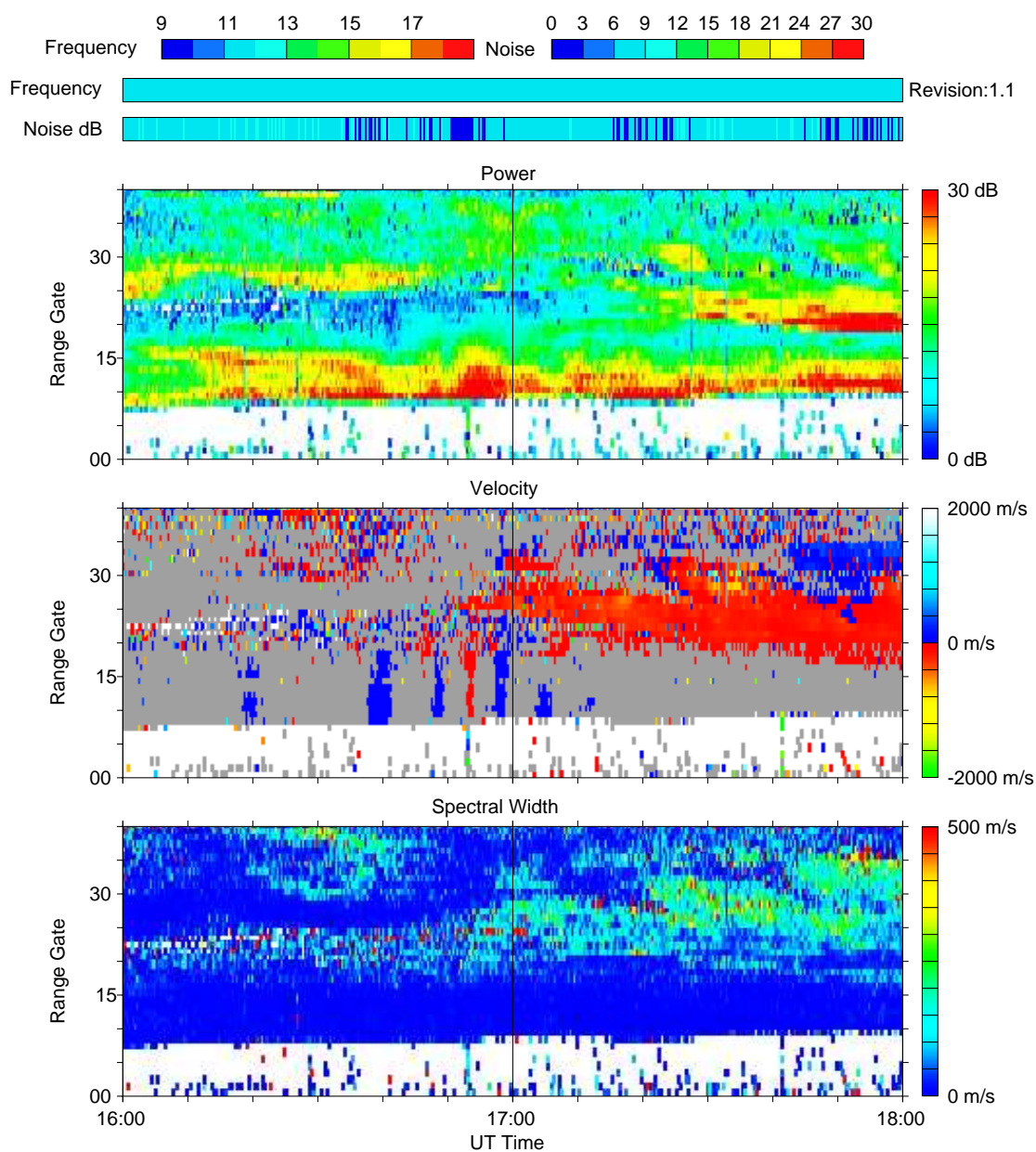


Figure 4.6: This graph is similar to Figure 2.11 except that this one shows data from all the 16 Beams of the radar's field of view for a time period from 16 : 00 – 18 : 00 hours.

4.3 Ground Scatter

Contour plot of Elevation versus Range gate for ground scatter

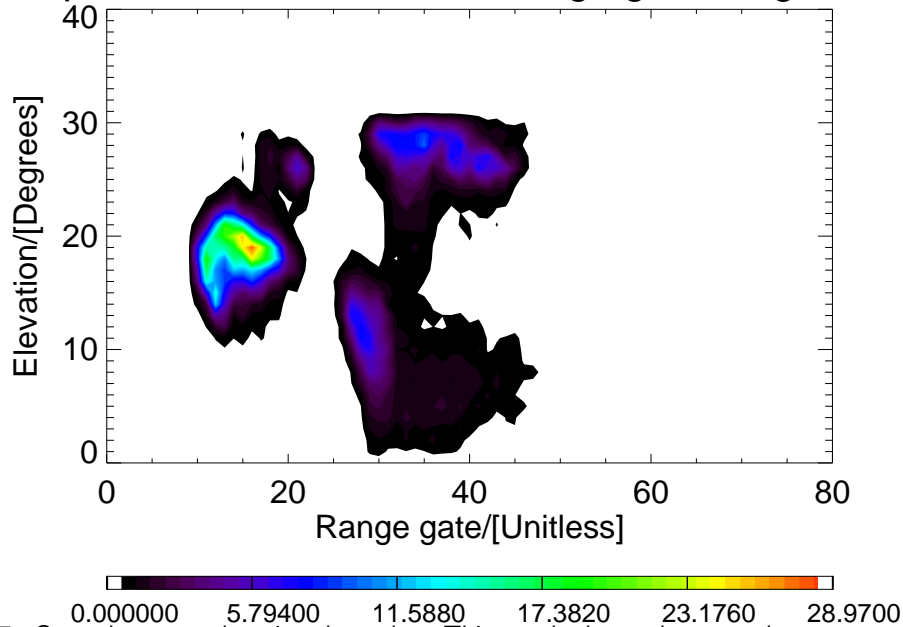


Figure 4.7: Ground scatter elevation data plot. This graph shows the ground scatter components of the information relayed in Figure 4.4 above.

Figure 4.7 is a ground scatter contour plot that was produced on filtering out ionospheric scattered data by obtaining the ground scatter flag data, which is always embedded in any roughly 2 hour fit data, and then masking it to the elevation data thereby eliminating the ionospheric elevation data. Table 4.3 below shows the elevation angle of signals and their associated distances calculated from the area having the most ground scatter data in Figure 4.7 above.

Table 4.3: Distances covered by the ground scatter plot backscattered signal

Range Gate	Elev. ($^{\circ}$)	Ground range (km)	Vertical height (km)	Ray Path (km)
16	17	900	275	941
16	18	900	292	946
17	17	945	289	988
17	18	945	307	994

4.4 Ionospheric Scatter

Contour plot of Elevation versus Range gate for ionospheric scatter

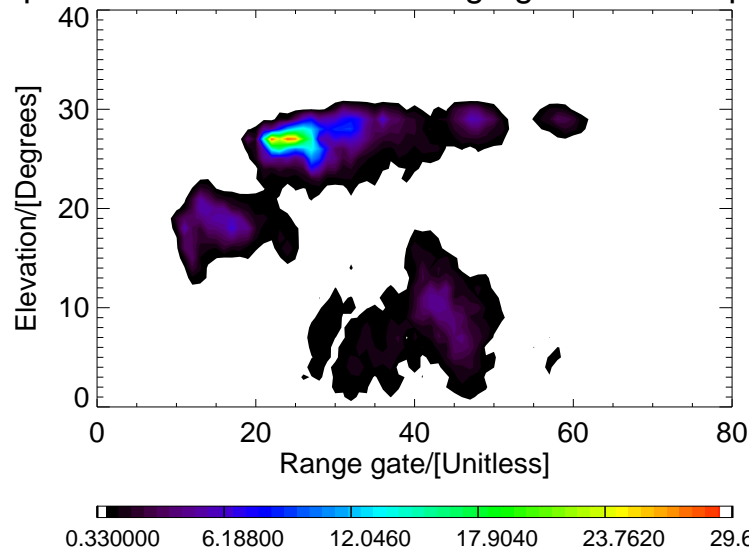


Figure 4.8: Ionospheric scatter elevation data contour plot. This ionospheric scatter information in this graph is a part of the data presented in Figure 4.4 only that ground scatter has been eliminated in it.

As regards the plotting of Figure 4.8, the ground scatter flag data was inverted in-turn producing an ionospheric scatter flag dataset. This obtained ionospheric flag data was then masked to the elevation data to produce ionospheric elevation data only. The data for the most scatter information in Figure 4.8 above were then extracted into Table 4.4 results below. The generated plots in figures 4.7 and 4.8 are clearly subsets of Figure 4.4.

Table 4.4: Distances covered by the ionospheric scatter plot backscattered signal

Range Gate	Elev. ($^{\circ}$)	Ground range (km)	Vertical height (km)	Ray Path (km)
22	26	1170	571	1302
22	27	1170	596	1313
24	26	1260	615	1402
24	27	1260	642	1414

More ray tracing results corresponding to data presented in Tables 4.3 and 4.4 are given in Table 4.5 below. This was done to make sure a one-on-one elevation angle analysis is done for both ground and ionospheric scatter information in relation to ray tracing results.

Table 4.5: Ray tracing ray path results for selected elevation angles pertaining to both ground and ionospheric scatter

Freq. (MHz)	Elev. (km)	Ray Path (km)	H-H H (km)
11	17	1088	223
11	18	840	226
11	26	766	266
11	27	910	278

4.5 Other SuperDARN Measured Parameters for the Time Period Under Study

Since Doppler characteristics of backscattered signals are used to determine whether echoes come back from the ground or ionosphere; the echo power, Doppler velocity and Doppler spectral width plots were generated for the same 'fit' file data under study. Figures 4.9, 4.10 and 4.11 below illustrate the resultant data. This was done in order to establish whether the results in tables 4.3 and 4.4 related to the figures that were mentioned as being associated to them (tables) were indeed showing ground or ionospheric scatter respectively.

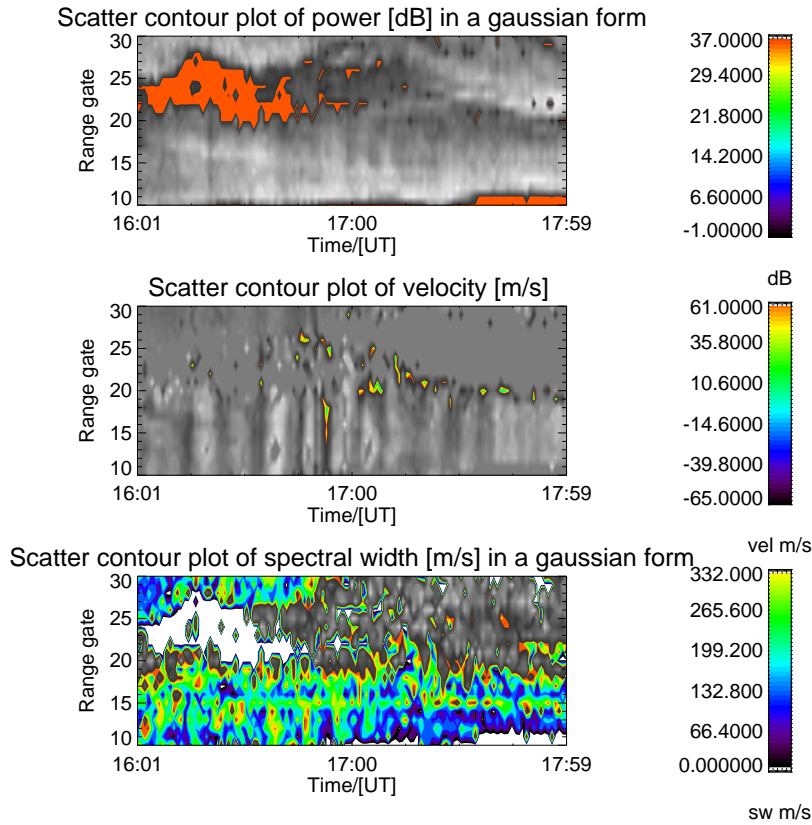


Figure 4.9: Backscatter plots of power, Doppler velocity and Doppler spectral width data from the 2004030816f.fit file. The radar's field of view beam that was used is number 8.

Figure 4.9 shows echo power, Doppler velocity and spectral width data for the Hankasalmi radar for the 2004030816f.fit file corresponding to Figure 4.4. Likewise figures 4.10 and 4.11 correspond to 4.7 and 4.8 above respectively. The Range-gates window of 10 – 30 was specially chosen to match up to the scenario portrayed in tables 4.3 and 4.4, for the most scatter positions of figures 4.7 and 4.8 respectively.

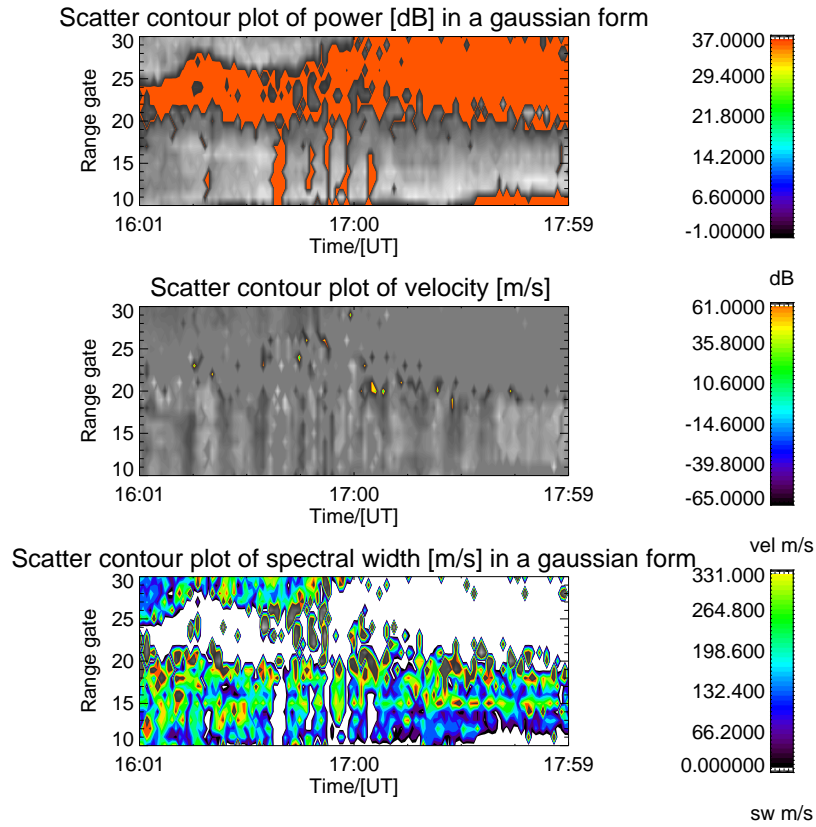


Figure 4.10: The plot shows the ground scatter elevation data only from the 2004030816*f.fit* file after filtering out the ionospheric scatter information. Beam 8 of the full field of view data was used to generate the plot.

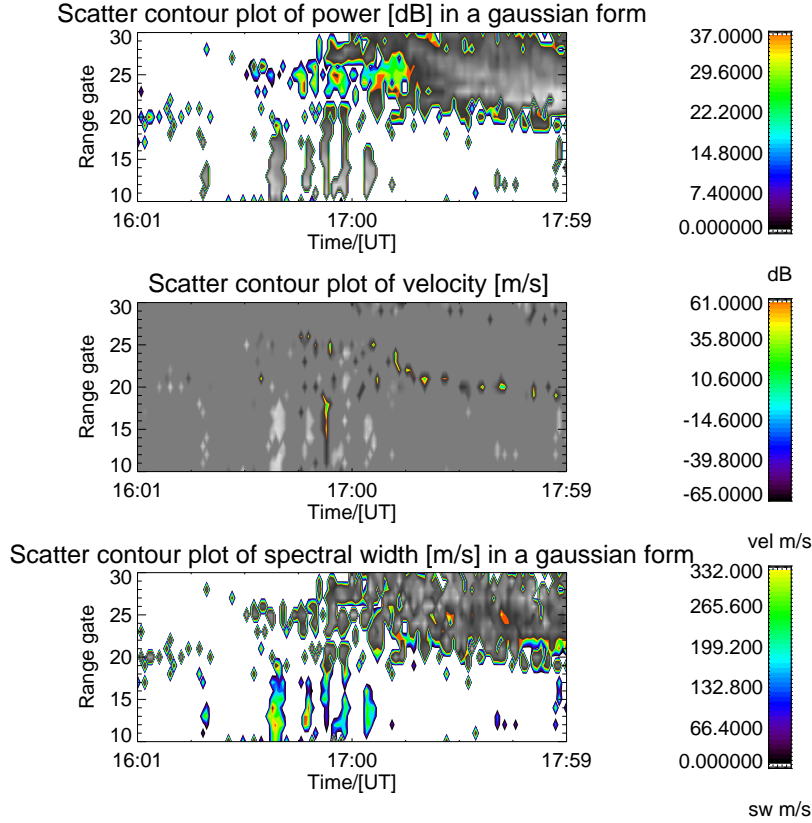


Figure 4.11: The plot shows the ionosphere scatter elevation data alone from the 2004030816*f.fit* file after filtering out the ground scatter information. The beam that was used is number 8 from the total field of view of the radar.

These plots were compared with those generated using the Internet archive resource by the SuperDARN community (from <http://superdarn.jhuapl.edu>) for the validation of the performance of the computer programs that were written. It is imperative to make mention here that the archive resource plots were then generated for the exact time-scale and range gate window so as to take stock of any differences that might show up in the results.

To compare the all scatter information in Figure 4.9 to the online resource's one, Figure 4.12 was produced with ground scatter being included in it by selecting the 'shade ground scatter' effect on the archive interactive plotting resource. The ground scatter colour shade is gray in the figure's panel plot. Figure 4.13 was then produced to show ground scatter with their actual colour values instead of the gray colour together with the ionospheric scatter ones. This was achieved by using the 'ignore ground scatter flag' option on processing the plot from all the selected archived scatter data.

Station:Hankasalmi (han)

Beam 08

08, March 2004 (20040308)

Operated by:University of Leicester

Program ID:153

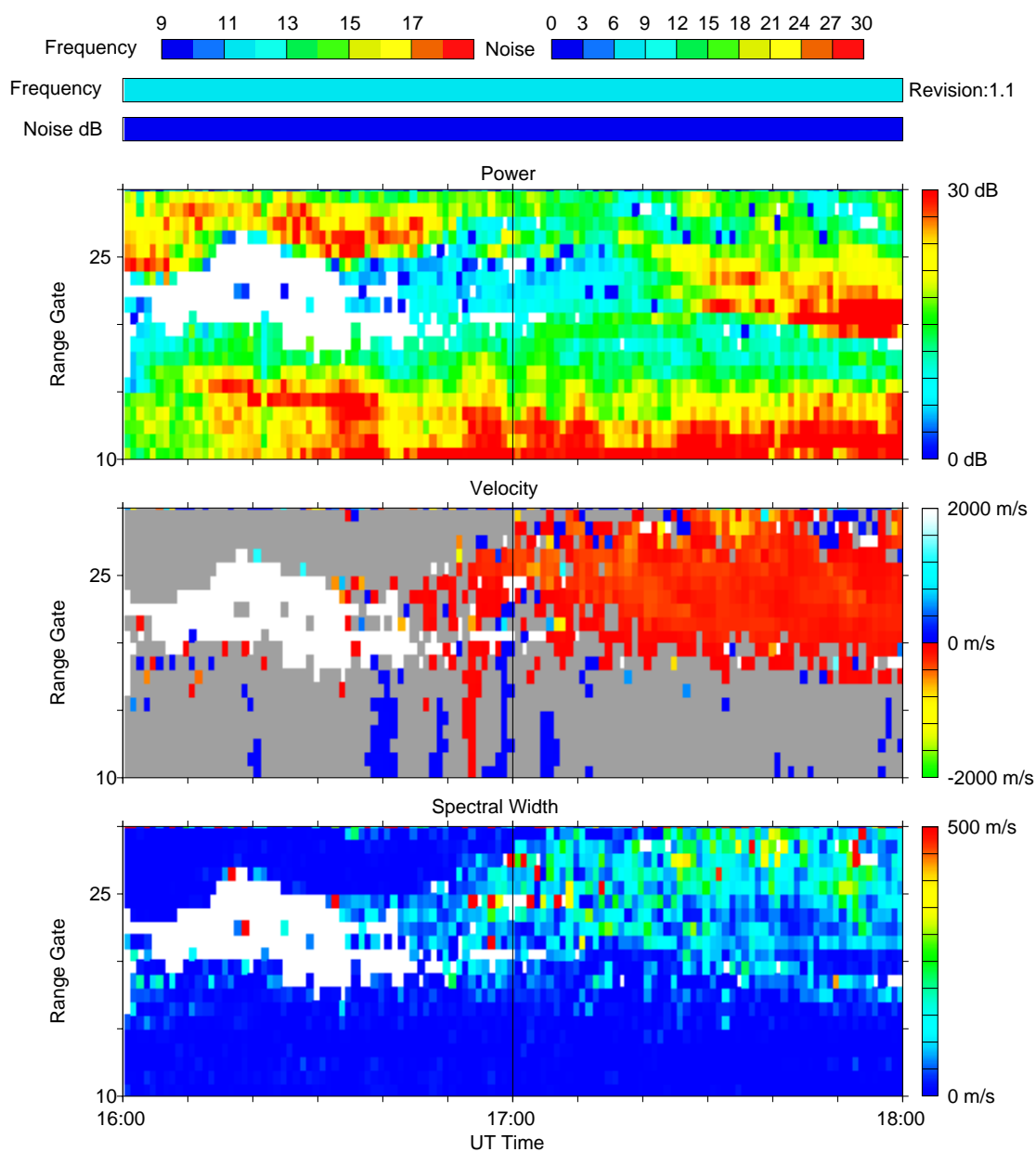


Figure 4.12: Plot of all scatter from the online archived SuperDARN data generated on using the 'shade ground scatter' effect. The range-gate span is between 10 – 30. The ground scatter is shown in the gray colour while the ionospheric scatter appears in the any of rainbow colours.

Station:Hankasalmi (han)
 Operated by:University of Leicester

Beam 08

08, March 2004 (20040308)
 Program ID:153

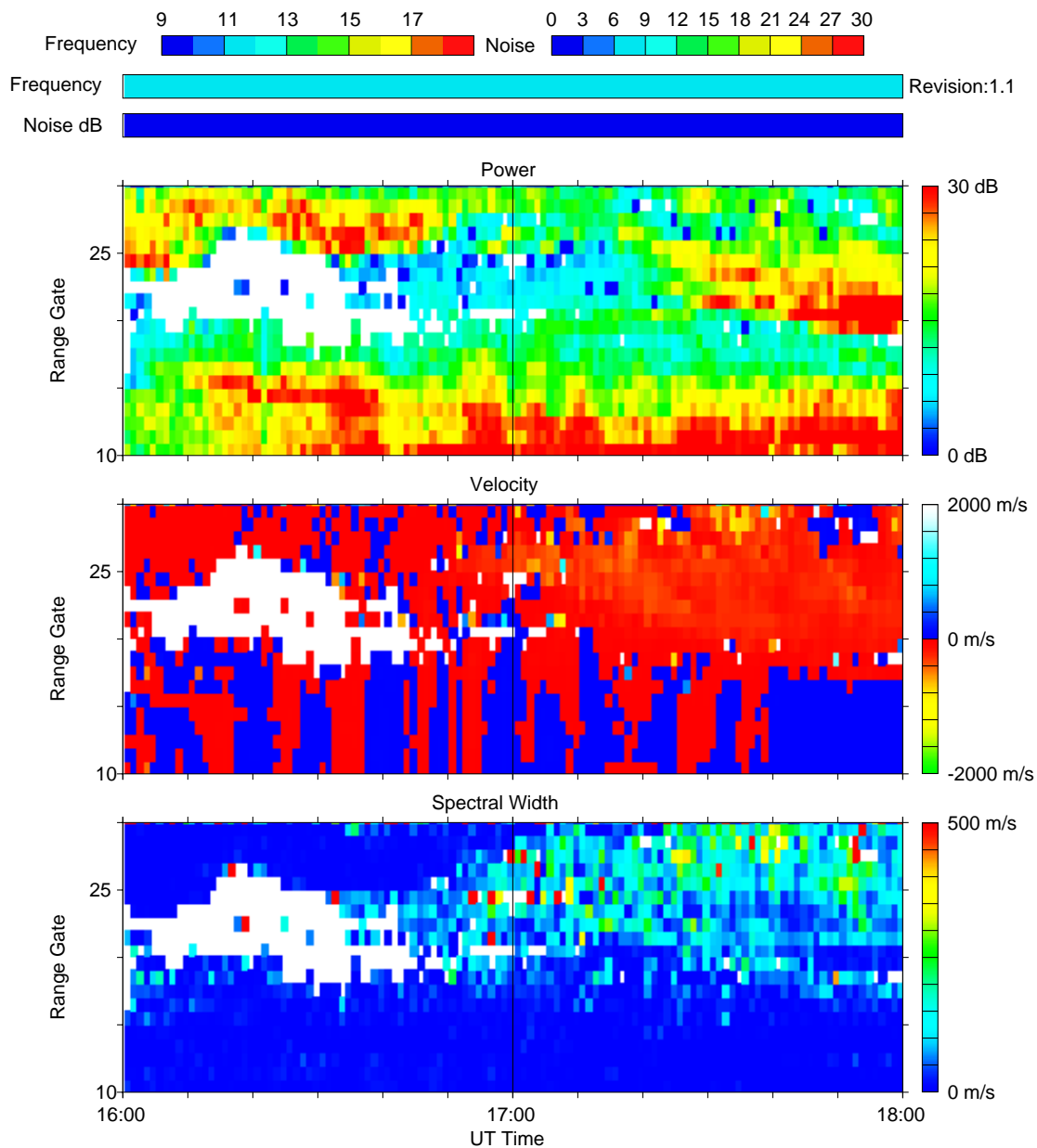


Figure 4.13: Plot of both ground and ionospheric scatter from the online archived SuperDARN data on effecting the 'ignore ground scatter flag' parameter. The range-gates covered are 10 – 30.

After this data processing, the 'exclude ground scatter' effect option was implemented to produce Figure 4.14 in an effort to illustrate the scatter plot for only the ionospheric echo. This plot presents only ionospheric scatter information since ground scatter data is excluded from the total data used for processing the figure.

The analysis of the information gathered from the plots that were produced by the (own) IDL written computer programs and the Internet archive are presented in Chapter 5.

Station:Hankasalmi (han)
 Operated by:University of Leicester

Beam 08

08, March 2004 (20040308)
 Program ID:153

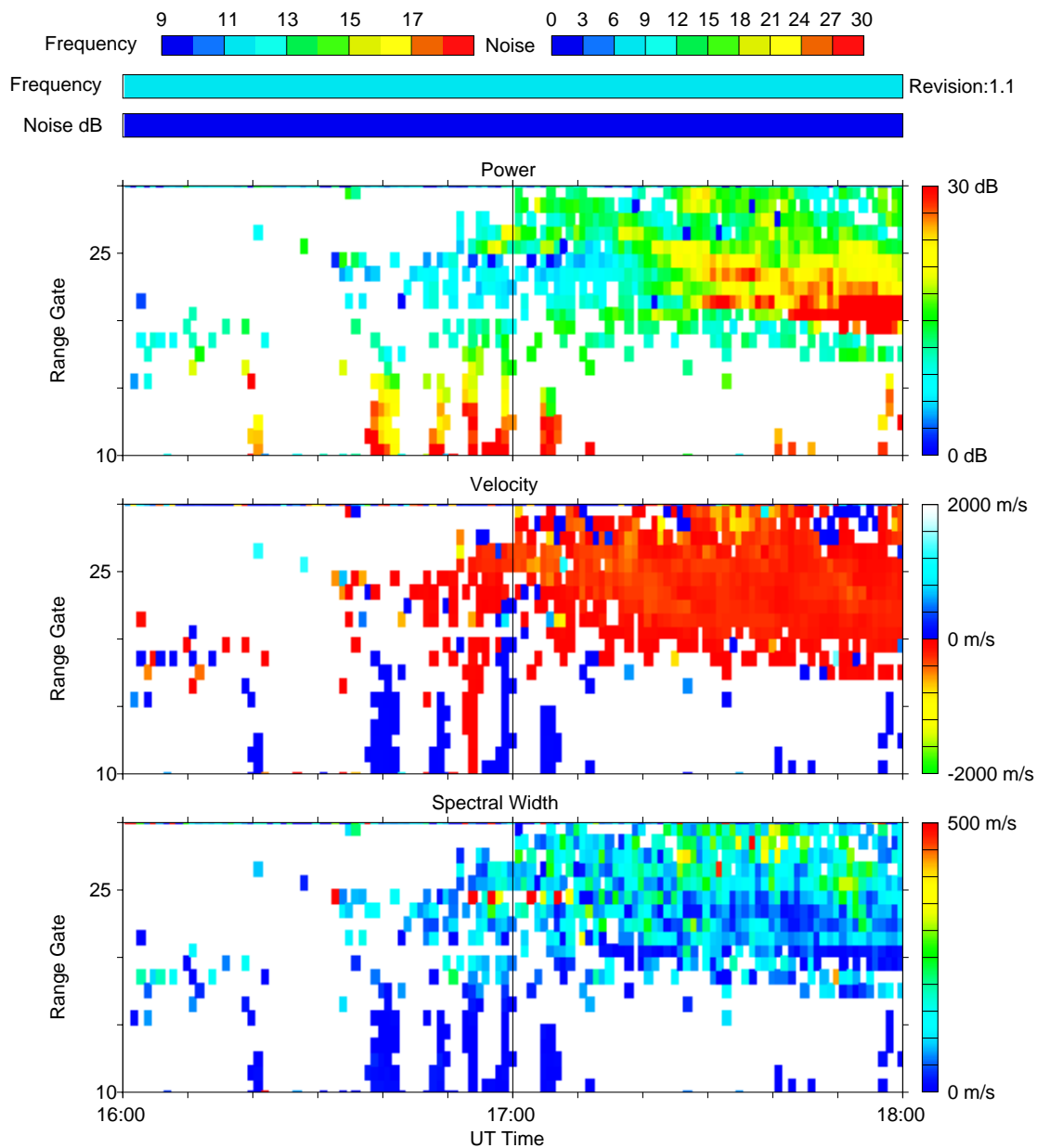


Figure 4.14: Plot of ionospheric scatter from the online archived SuperDARN data produced on using the 'exclude ground scatter' effect on the Internet interactive resource. The range-gates covered are from 10 – 30.

4.6 HF Radar Transmitted Frequency change effects

Following through on the introduction part of this Chapter, the radar's signal transmitted frequency change provides information about how the ionosphere changes with time. This behaviour is clearly illustrated in Figure 4.15 below. The backscatter information shows that positions of scatter follow the ray transmitted frequency change faithfully. Another

fundamental point to note is that the velocity panel plot portrays most ground scatter (gray colour) information at Range-gates below 45, but 15 between 00 : 00 – 03 : 00 UT as also evidenced by the low values of the spectral width for the same period of time. On the other-hand, ionospheric scatter information, shown in the colours for the actual values and high spectral width values, is mostly above the Range-gates 45 to about 70.

Station:Prince George (pgr) Beam 08 05, April 2004 (20040405)
 Operated by:University of Saskatchewan Program ID:-9060

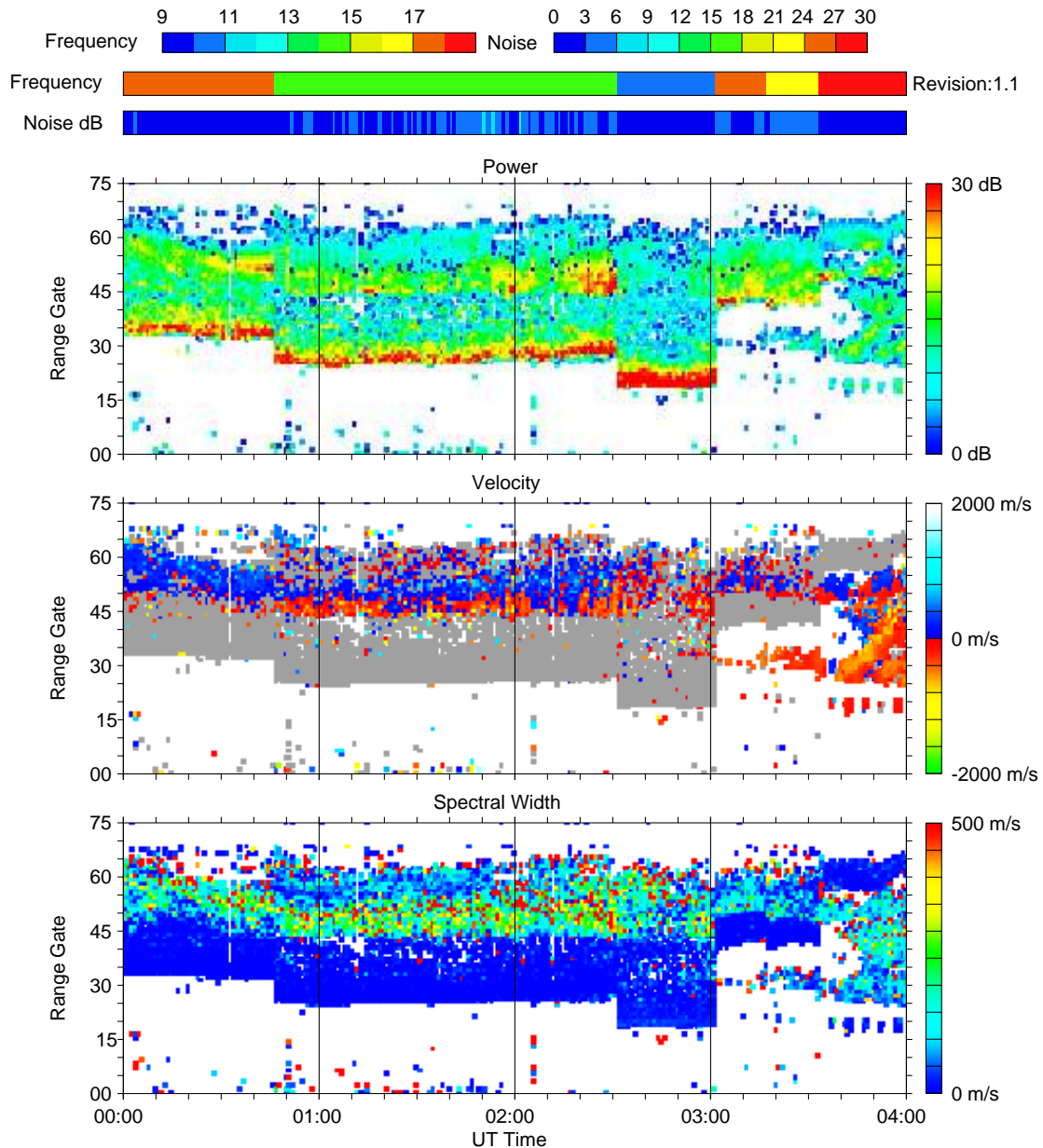


Figure 4.15: The plot shows how the radar transmitted frequency change produces different scatter information from the ionosphere. This plot was generated from archived Prince George SuperDARN data on 5th April 2004 from 00 : 00 – 04 : 00 hours UT.

Just to complete the picture of the full SuperDARN radar observable parameters for this

particular dataset, a code was written to also plot (raw) elevation data for all the scatter information and their two separate backscattered data — as in ground-scatter as well as ionospheric-scatter information. This is shown in Figure 4.16 below.

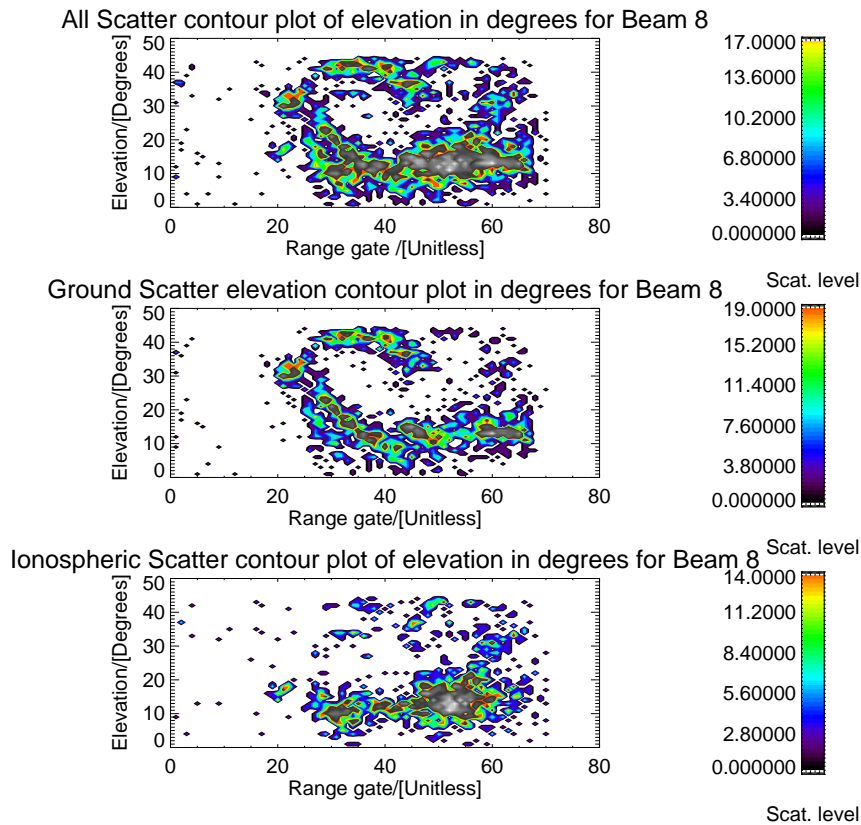


Figure 4.16: The top most panel shows all elevation scatter information plotted in one graph. The middle panel presents ground scatter data plot using the ground scatter flag embedded in the data 'fit' file. The bottom plot indicates the ionospheric scatter data produced by inverting the ground scatter flag and then masking it to the raw elevation data from the SuperDARN archive. The 'fit' file data that was used is *2004040502b.fit* for Prince George. This implies that the time axis for the figure is from 02 : 00 – 04 : 00 hours UT since one single 'fit' file of the archived dataset harbours recordings for approximately 2 hours. These plots were generated for only Beam 8 of the full radar's field of view.

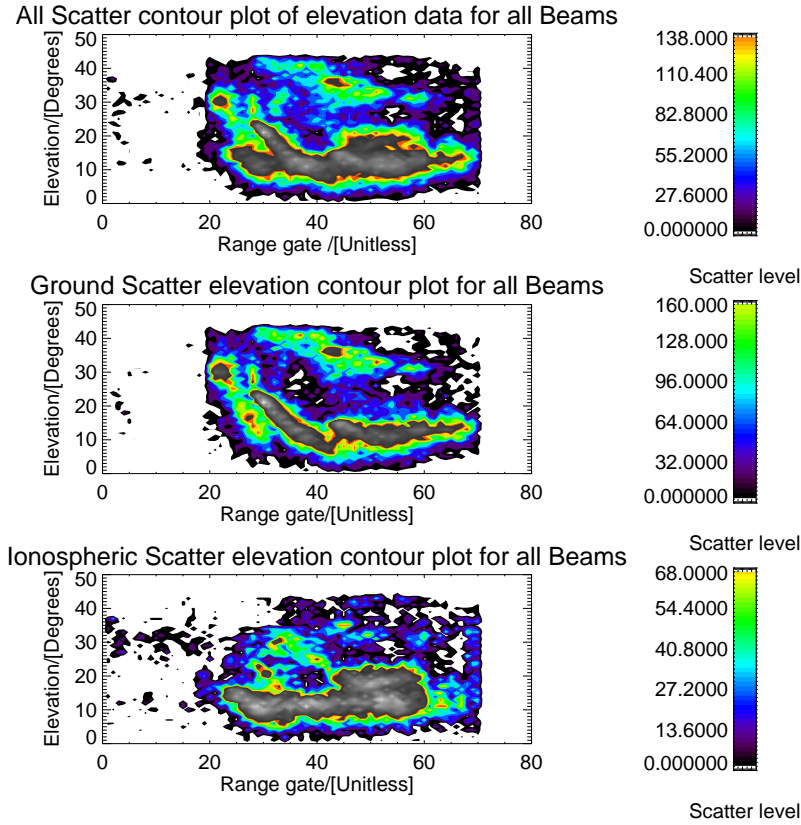


Figure 4.17: These scatter plots similar in nature to those of the figure just above except that they were generated for all the 16 Beams of radar's field of view. The top most panel shows all elevation scatter information plotted in one graph. The middle panel presents ground scatter data plot using the ground scatter flag embedded in the data 'fit' file. The bottom plot indicates the ionospheric scatter data produced by inverting the ground scatter flag and then masking it to the raw elevation data from the SuperDARN archive.

To get more information from Figure 4.16, Figure 4.17 was produced to check how data from all the Beams can aid in explaining the features observed in former-mentioned figure. Figure 4.17 illustrates the scatter patterns that were recovered from processing all the 16 Beams of the radar's field of view. In order to verify this phenomenon, ray tracing was performed on carefully picked out IRI Model Prince George ionospheres, according to the time periods of the day in Figure 4.15, to produce a picture of how ray tracing results relate to the SuperDARN community archived data resources.

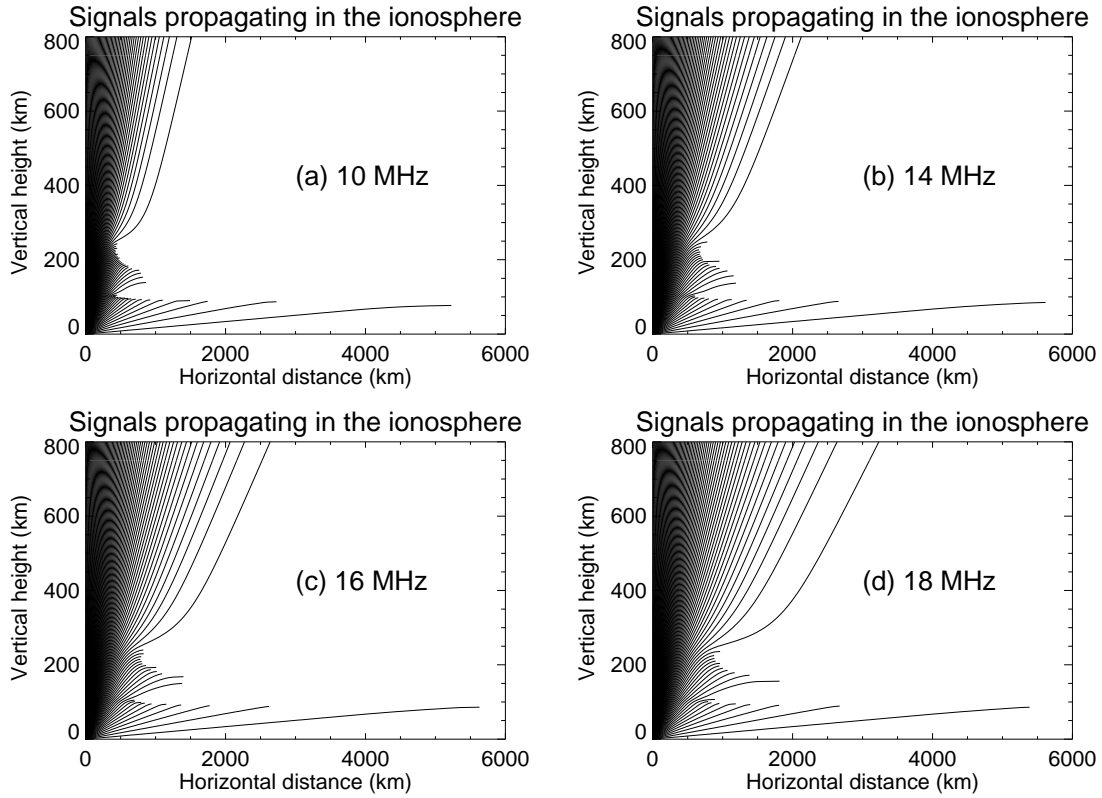


Figure 4.18: Ray traces through a Prince George ionosphere at about 00 : 30 hours UT with various transmission frequencies. The transmitted frequencies for the plots in Figure 4.15 are: 10 MHz for plot (a), 14 MHz for plot (b), 16 MHz for plot (c) and 18 MHz for plot (d).

Figure 4.18 shows ray traces of signals that were propagated through a constant Prince George IRI ionosphere at 00 : 30 UT of 5th April 2004 with different radio wave transmitted frequencies of 10, 14, 16 and 18 MHz respectively. In order to fully study the effect of changing ionospheres, similar experiments for IRI ionospheres at 01 : 30, 02 : 50, 03 : 30 and 03 : 50 UT were conducted for the said transmitted frequencies as evidenced in the plots indicated in figures 4.19, 4.20, 4.21 and 4.22 below respectively.

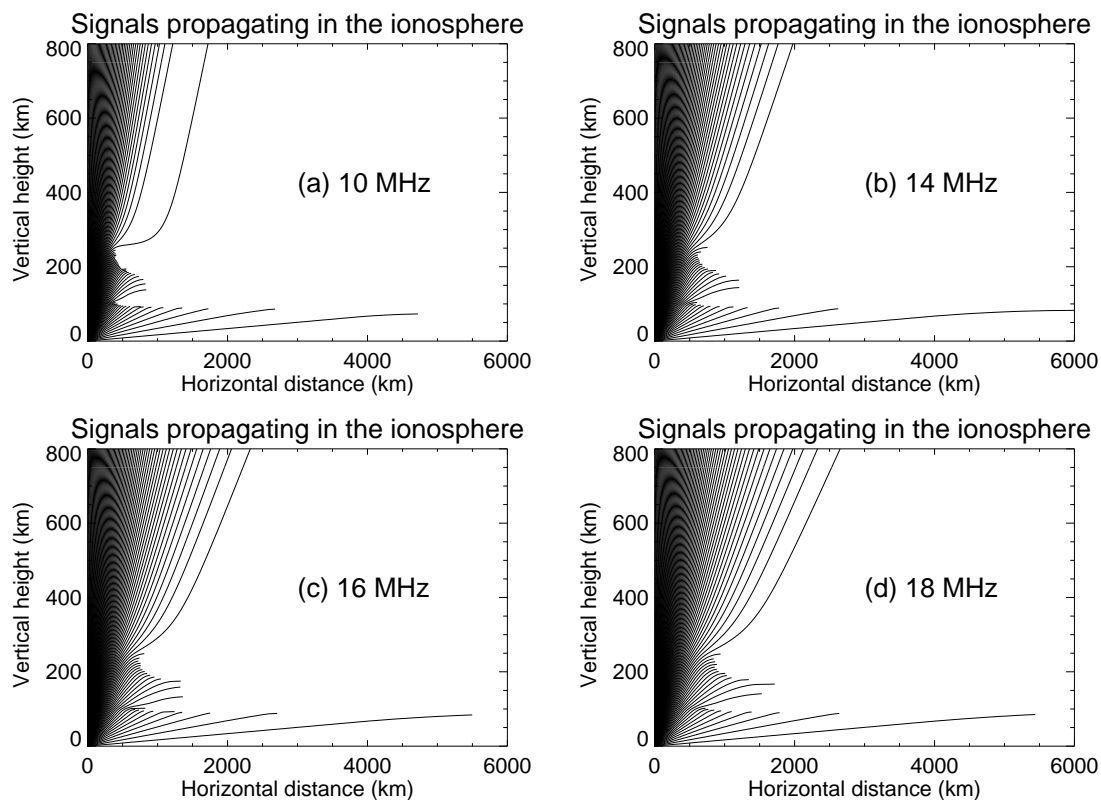


Figure 4.19: Ray traces through a Prince George ionosphere at about 01 : 30 hours UT with various transmission frequencies. The transmitted frequencies for the plots in Figure 4.15 are: 10 MHz for plot (a), 14 MHz for plot (b), 16 MHz for plot (c) and 18 MHz for plot (d).

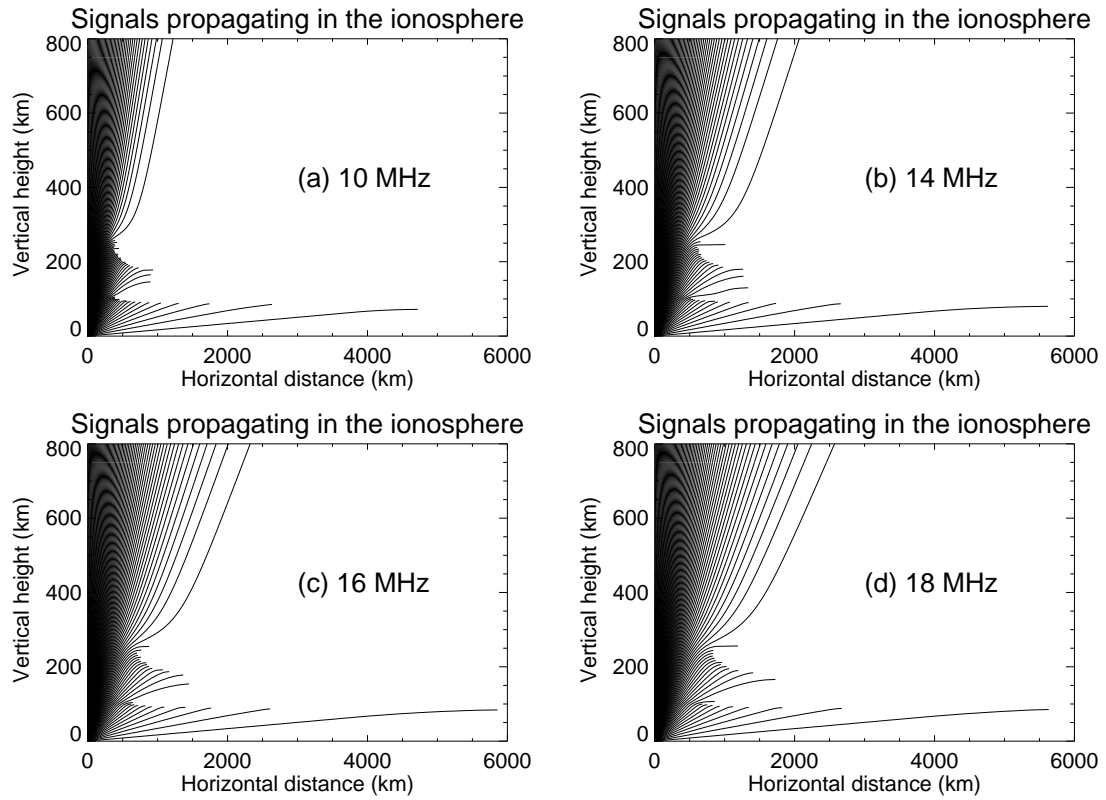


Figure 4.20: Ray traces through a Prince George ionosphere at approximately 02 : 50 hours UT with various transmission frequencies. The transmitted frequencies for the plots in figure 4.15 are: 10 MHz for plot (a), 14 MHz for plot (b), 16 MHz for plot (c) and 18 MHz for plot (d).

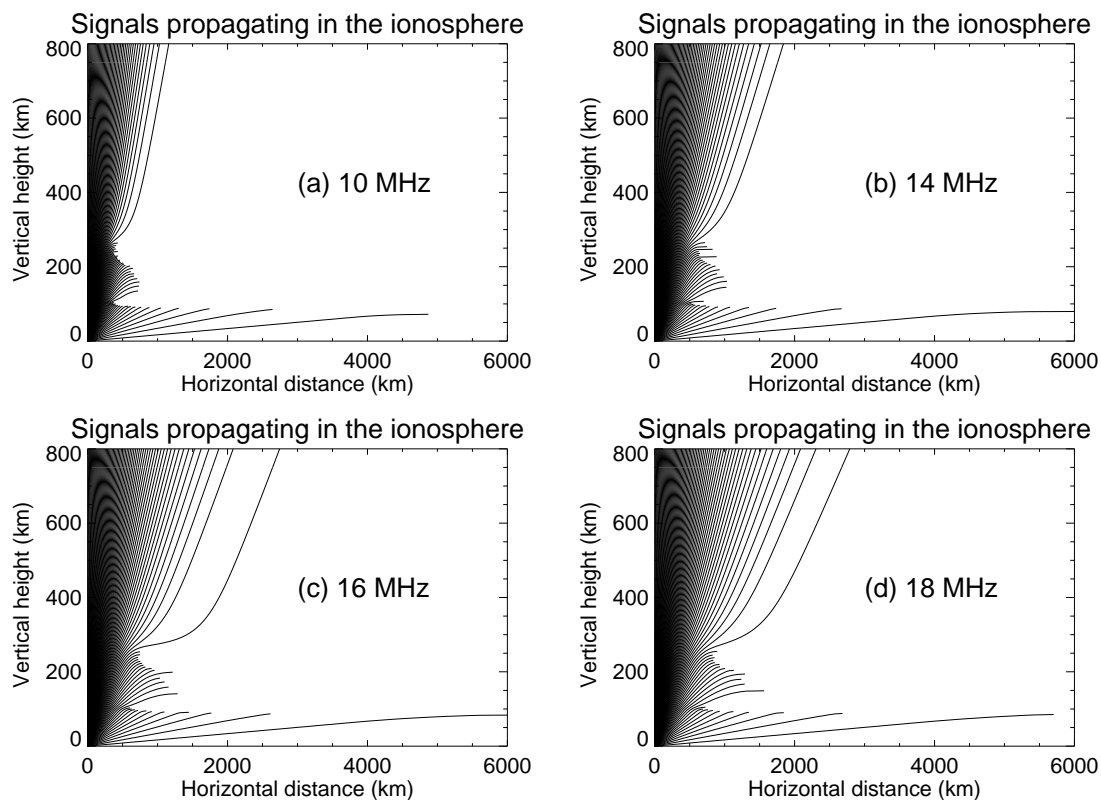


Figure 4.21: Ray traces through a Prince George ionosphere at approximately 03 : 30 hours UT with various transmission frequencies. The transmitted frequencies for the plots in Figure 4.15 are: 10 MHz for plot (a), 14 MHz for plot (b), 16 MHz for plot (c) and 18 MHz for plot (d).

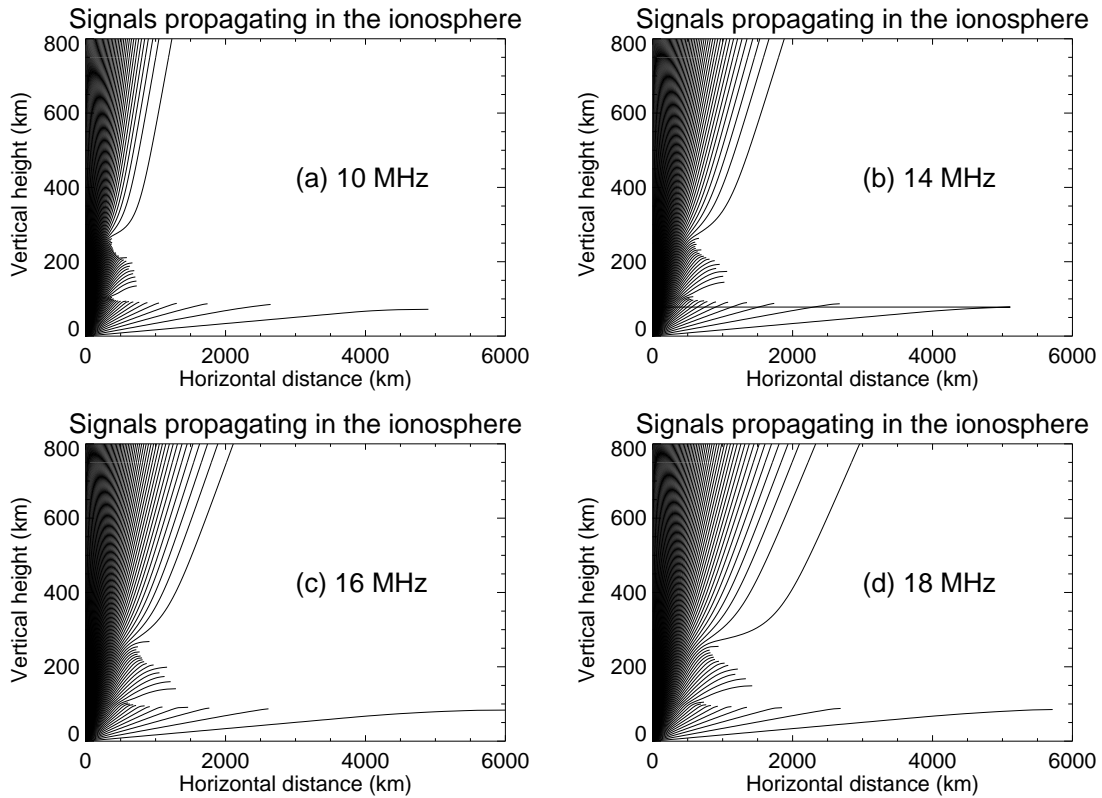


Figure 4.22: Ray traces through a Prince George ionosphere at approximately 03 : 50 hours UT with various transmission frequencies. The transmitted frequencies for the plots in Figure 4.15 are: 10 MHz for plot (a), 14 MHz for plot (b), 16 MHz for plot (c) and 18 MHz for plot (d).

The necessary information from the ray tracing program output on the various investigations mentioned above was then tabulated in Table 4.6 through to Table 4.10. Table 4.6 indicates the ray tracing program output values corresponding to Figure 4.18 for both a constant ionosphere and 20° elevation angle of the radio signal. In Chapter 5, mention is made regarding the use of 20° elevation here.

Table 4.6: Ionosphere at 00 : 30 UT and elevation with different backscattered ray transmitted frequencies

Freq. (MHz)	Elev. ($^\circ$)	Ray Path (km)	H-H H (km)
10	20	791	171
14	20	749	200
16	20	815	215
18	20	999	236

Also, the effect of how changing the ionosphere affects the ray propagation results on maintaining the same transmitted frequency and elevation angle was studied. Table 4.7 presents results for the radio wave transmitted frequency of 10 MHz at 20° take off angle for different ionospheres at the times of the day indicated.

Table 4.7: Constant backscattered ray transmitted at 10 MHz and elevation with different ionospheres

Freq. (MHz)	Elev. ($^{\circ}$)	Ray Path (km)	H-H H. (km)	Iono. (UT)
10	20	791	171	00:30
10	20	819	166	01:30
10	20	924	165	02:50
10	20	755	148	03:30
10	20	747	148	03:50

The just above procedure was repeated for a signal transmitted frequency of 14, 16 and 18 MHz respectively. The results from the program are given in Tables 4.8 for 14 MHz, 4.9 for 16 MHz and lastly 4.10 for 18 MHz below.

Table 4.8: Constant backscattered ray transmitted at 14 MHz and elevation with different ionospheres

Freq. (MHz)	Elev. ($^{\circ}$)	Ray Path (km)	H-H H. (km)	Iono. (UT)
14	20	749	200	00:30
14	20	746	198	01:30
14	20	771	203	02:50
14	20	827	206	03:30
14	20	842	207	03:50

Table 4.9: Constant backscattered ray transmitted at 16 MHz and elevation with different ionospheres

Freq. (MHz)	Elev. ($^{\circ}$)	Ray Path (km)	H-H H. (km)	Iono. (UT)
16	20	815	215	00:30
16	20	786	211	01:30
16	20	795	215	02:50
16	20	831	218	03:30
16	20	847	219	03:50

Table 4.10: Constant backscattered ray transmitted at 18 MHz and elevation with different ionospheres

Freq. (MHz)	Elev. ($^{\circ}$)	Ray Path (km)	H-H H. (km)	Iono. (UT)
18	20	999	172	00:30
18	20	897	227	01:30
18	20	866	229	02:50
18	20	872	231	03:30
18	20	892	232	03:50

After all that, the radio wave propagation of a 17 MHz transmitted frequency through a Prince George ionosphere at 00 : 30 MHz was simulated which was corresponding to scatter data shown in Figure 4.15 above. The ray plot results are given in both Figure 4.23 and Table 4.11 below.

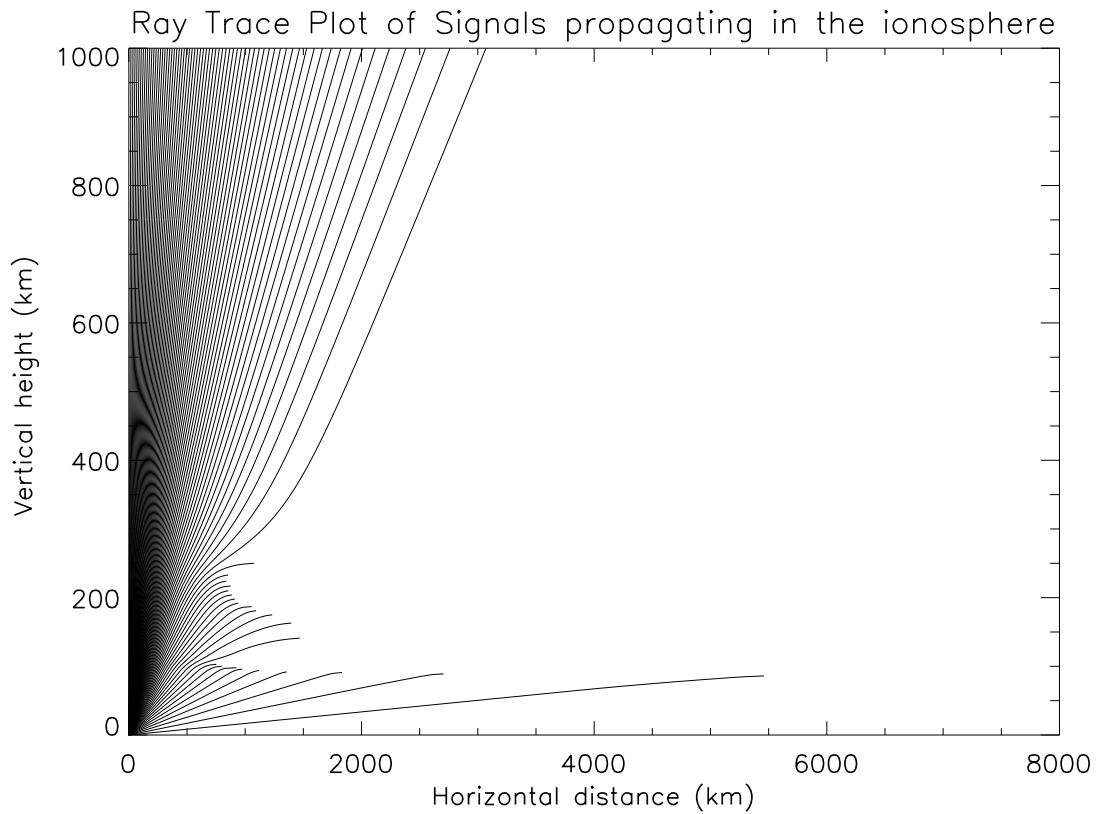


Figure 4.23: Ray Tracing of a 17 MHz signal propagating through Prince George IRI Model ionosphere at 00 : 30 hour UT.

Table 4.11: Constant rays transmitted at 17 MHz and an ionosphere at 00 : 30 UT with changing angles

Freq. (MHz)	Elev. ($^{\circ}$)	Ray Path (km)	H-H H. (km)	Iono. (UT)
17	0	0	65	00:30
17	10	1479	141	00:30
17	20	871	224	00:30
17	30	2160	N/A	00:30
17	40	1605	N/A	00:30
17	50	1325	N/A	00:30
17	60	1163	N/A	00:30
17	70	1067	N/A	00:30
17	80	1016	N/A	00:30
17	90	1	1	00:30

An analysis of all the procedures and results in this section is given in Chapter 5.

4.7 Averaging over One Month

In order to test the consistency of the data, or its variation, one full month's "fit" file data for the same time of the day, between 00 : 00 – 02 : 00 hours UT for Saskatoon (52.16° and 106.53° W geographical coordinate latitude and longitude respectively) December 2004 SuperDARN data was analysed. 31 ".fit" file filenames were written down into one '.txt' file. The data in this '.txt' file was then processed by a specially written IDL programming code. The program processed the data by reading the 2D (two dimensional) dataset, in range-gate and time-stamp, of elevation and power data and then added the following days' datasets successively forming a 3D (three dimensional) stack. The stack comprises of the 31 day length 2D Range-gate and time-stamp dataset of each particular day of the month. Each and every day's fit file had its elevation and power data scaled by resizing their time and Range-gate sizes to 60 and 75 array elements respectively. This was accomplished by using a `congrid` function, an IDL inbuilt procedure, in IDL programming language to do the scaling of each day's 2D datasets of elevation and power. Also, both 1D (one dimensional) datasets of the time axis and radar transmitted frequencies were scaled to the size of 60 elements to match the 2D datasets already mentioned above.

Each day's scaled data was then filtered through a range of radar transmitted frequencies from 8 – 20 MHz so that only the data for this window was processed further. The above mentioned stack was then formed by accumulating the 2D scaled data into a 3D one with day number of the month as the length component. The `moment` function (see Appendix A), another IDL inbuilt procedure, was then utilised to calculate the averaged 2D elevation and power data. The output of the data processing described in the above is given in Figure 4.24.

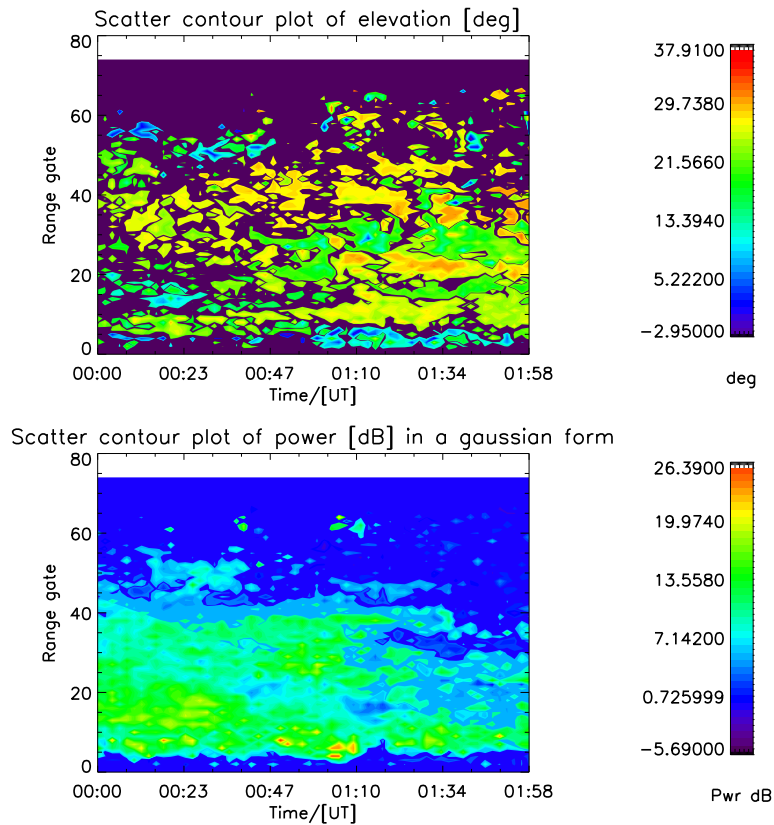


Figure 4.24: Scatter elevation and power plots for one full month of December 2004 recorded for 00 : 00 – 02 : 00 hours UT every day. The data used was from the Saskatoon SuperDARN radar. The transmitted frequency for the plots is all of those that the radar used within the range 8 – 20 MHz from which any SuperDARN radar can operate.

Since the scatter information is a composition of both ground and ionospheric scatter data, this 3D stack data was thus processed in its split two components independently. This was accomplished by using the procedure that has already been alluded to above in Section 4.1. The result of this operation on the data is Figure 4.25.

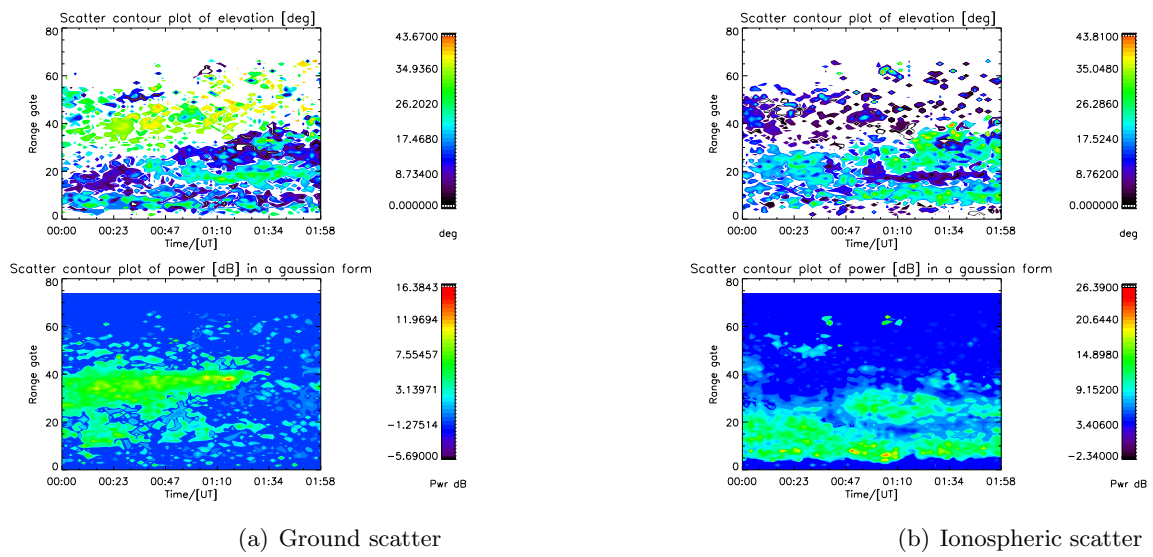


Figure 4.25: Both ground and ionospheric scatter plots for 8 – 20 MHz for one months Saskatoon data. The left hand plot shows the ground scatter while the rightmost one portrays the ionospheric scatter information.

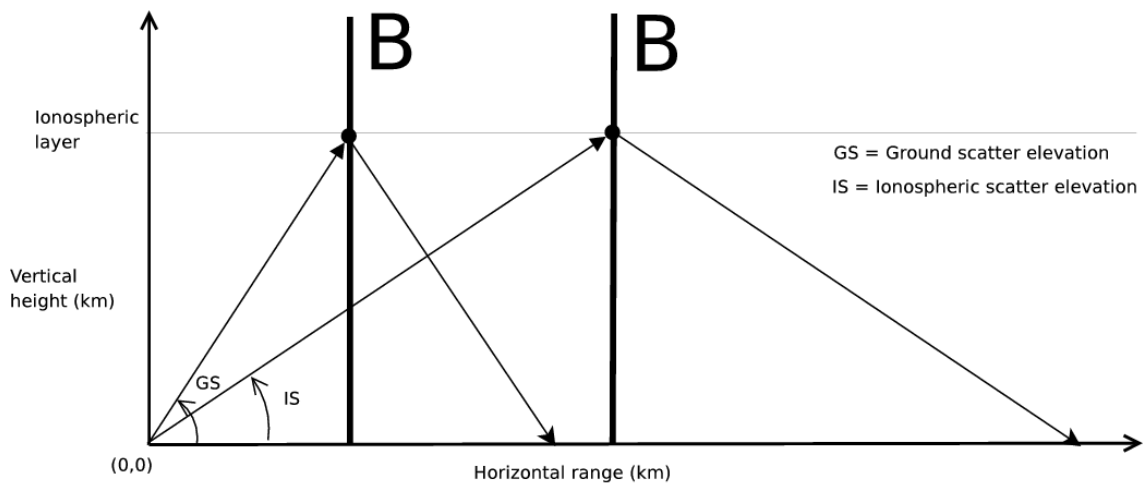


Figure 4.26: Ground and ionospheric scatter from higher and lower elevation angles respectively case as portrayed in Figure 4.25. **B** is the Earth's magnetic field.

In order to appreciate the various positions where backscatter emanates from in the Saskatoon ionosphere of December 2004, the behaviour of radio wave propagation was then studied by performing ray tracing. The resultant ray traces for a single elevation angle are shown in Figure 4.27.

Ray Trace Plot of Signals propagating in the ionosphere

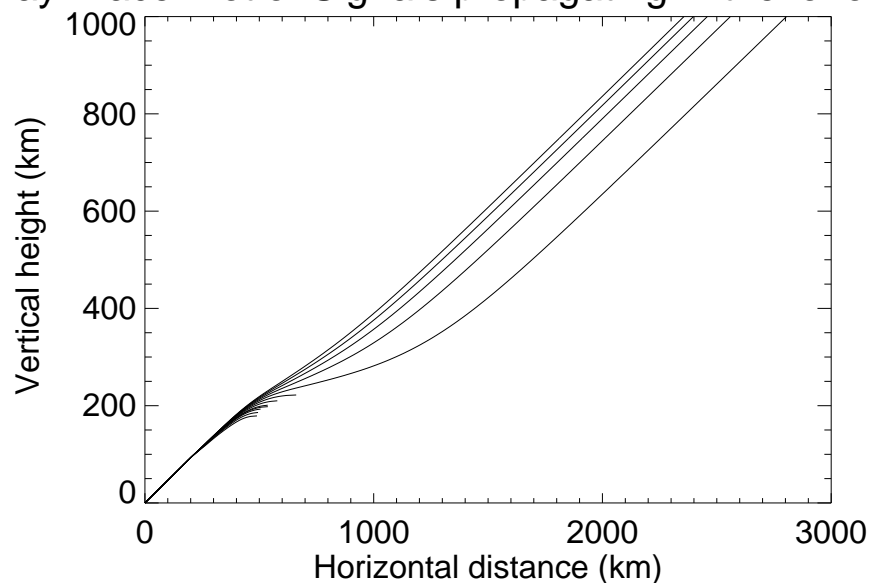


Figure 4.27: Ray traces through a Saskatoon IRI ionosphere for December 2004 with the radar transmitted frequency range of 8 – 18 MHz. The angle of elevation used in doing the necessary studies was 25° .

The following table (Table 4.12) shows some of the results that were generated by the ray tracing program for the Saskatoon IRI ionosphere.

Table 4.12: December 2004 IRI Saskatoon Ionosphere

Freq. (MHz)	Elev. ($^\circ$)	Ray Path (km)	H-H H. (km)	Iono. (UT)
8.000	25	525	179	00:00–02:00
9.000	25	531	186	00:00–02:00
10.000	25	544	193	00:00–02:00
10.590	25	576	198	00:00–02:00
11.000	25	577	201	00:00–02:00
12.000	25	620	210	00:00–02:00
13.000	25	704	222	00:00–02:00
14.000	25	2996	N/A	00:00–02:00
15.000	25	2756	N/A	00:00–02:00
16.000	25	2659	N/A	00:00–02:00
17.000	25	2601	N/A	00:00–02:00
18.000	25	2562	N/A	00:00–02:00

In looking at Section 4.6 and the resultant figures with their associated tables there-in, the effect of the radar transmitted frequency changes was taken into account so that only data for the frequency that was transmitted most throughout the 31 days could be studied carefully.

To this end, the above described computer program was modified to account for this effect. Thus, more computer code to calculate the most transmitted frequency and then picking

out only that frequency's scatter data was written. The way this was done was such that all transmitted frequencies data for the whole 31 days were placed into an accumulating array and then the mode of the data distribution was obtained.

Since it was established that scatter data is related to the signal transmitted frequency at an instance, the radio wave's frequency distribution over the one full month dataset was studied by plotting Figure 4.28 below. This was done to find reason as to why there was need to pick out scatter data for only the most transmitted frequency throughout the whole month.

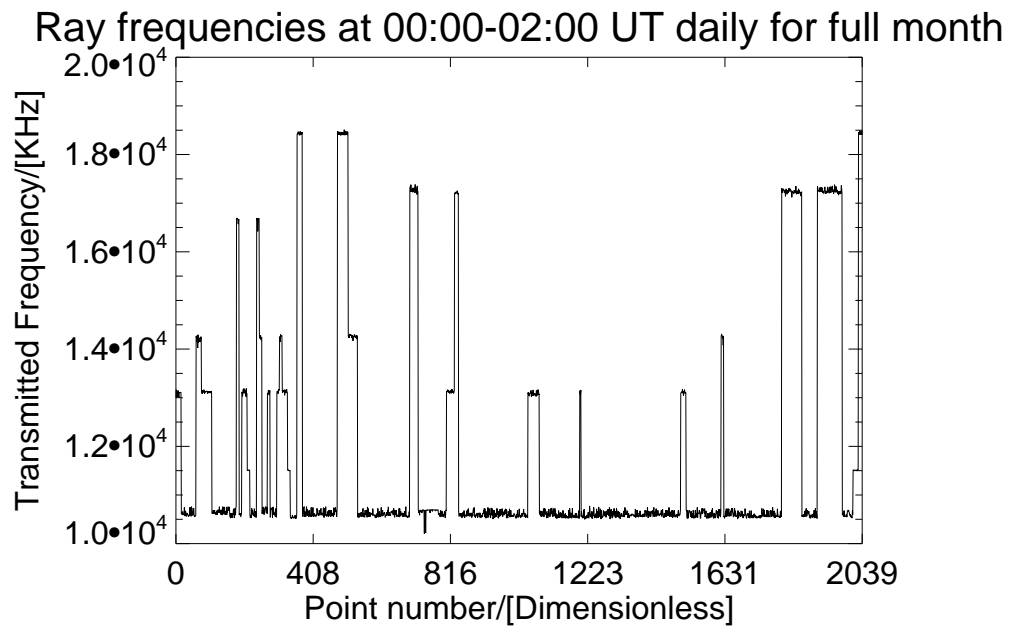


Figure 4.28: SuperDARN radar ray transmitted frequencies every day between 00 : 00 – 02 : 00 hours for the whole month of December 2004 for Saskatoon. 'Point number' is the number for the various 2 hour time length points when the radar transmission frequency at a specific time was recorded for each 2 hour data additively from 1st to the 31st day of the one full month between 00 : 00 – 02 : 00 hours.

The data for that most transmitted frequency was then filtered out from all the other data and a plot was generated (see Figure 4.29). The value of the most transmitted frequency for all the 31 days of December 2004 was computed as 10.59 MHz.

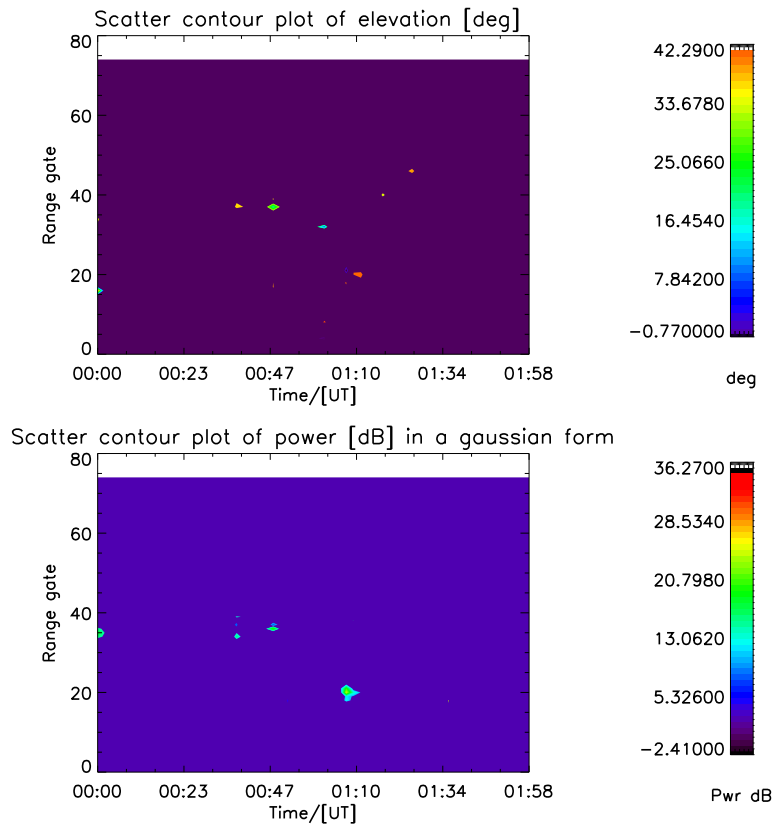


Figure 4.29: The plot was generated from SuperDARN data for a full month of December 2004 between 00 : 00 – 02 : 00 hours UT from the Saskatoon Radar. The most transmitted frequency, of 10.59 MHz, during the observation time was calculated and then only the (elevation and power) data for that particular frequency was plotted.

Table 4.13: Range results from the most-transmitted frequency plots of elevation and echo power

Range Gate	Elev. ($^{\circ}$)	Ground Range (km)	Vertical Height (km)	Ray Path (km)
20	42	1080	972	1453
37	25	1845	860	2036
37	35	1845	1292	2252

In order to do more analysis to compare the results with the ray tracing ones, both the ground and ionospheric scatter data was separated. The resultant ground and ionospheric backscatter data was then plotted in the manner that has already been discussed above. Figure 4.30 shows the plots for the two scatter data plots.

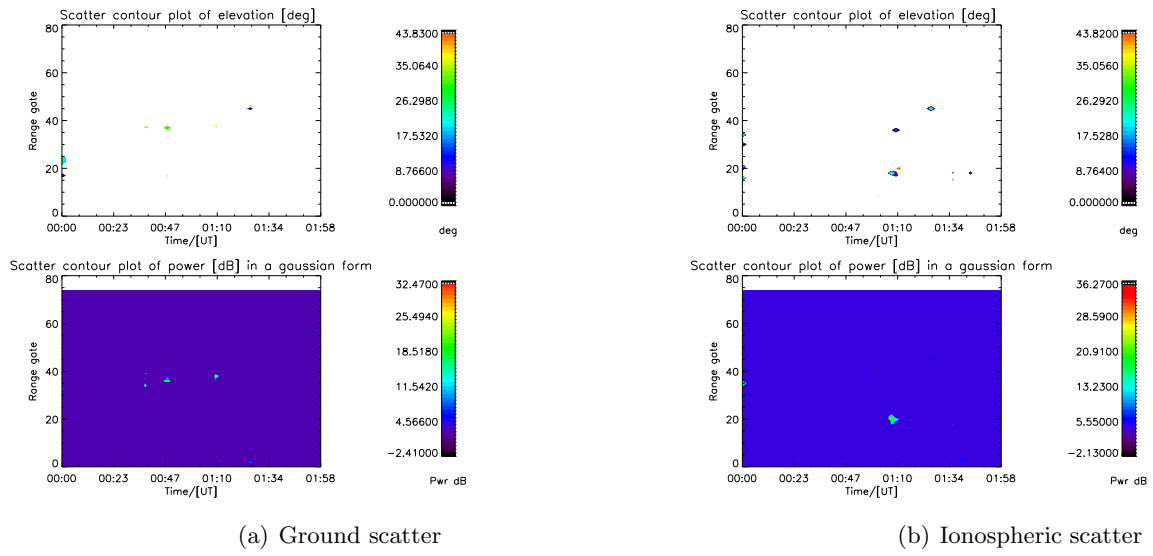


Figure 4.30: The plots were produced for the most transmitted frequency, 10.59 MHz. The ground scatter is illustrated in the leftmost plot and ionospheric one in the right placed plot for the Saskatoon radar elevation and power data respectively.

Then ray tracing was performed on the Saskatoon IRI ionosphere for the most transmitted frequency, i.e 10.59 MHz, only during the whole one month under study. Figure 4.31 below shows a ray traces which indicate how the 10.59 MHz radio signal was modelled as having propagated in that ionosphere.

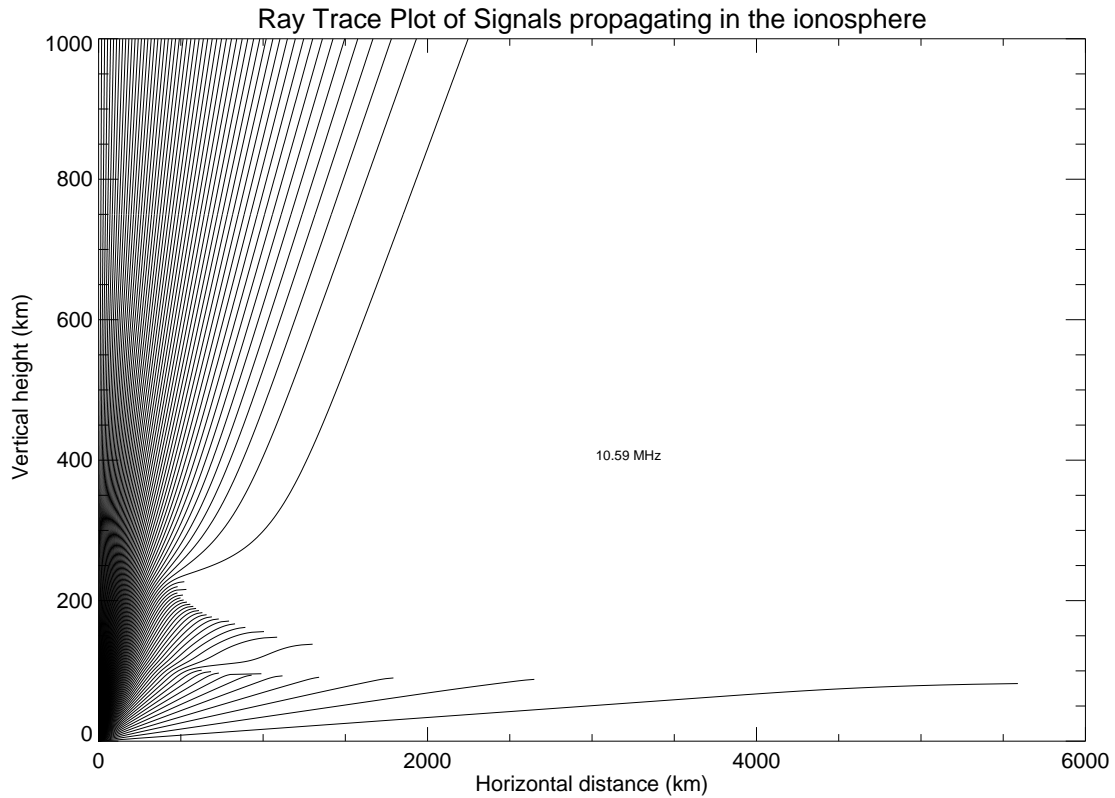


Figure 4.31: Ray traces at intervals of 1° corresponding to the December 2004 Saskatoon IRI Model ionosphere data that is portrayed in figure 4.29. The transmitted signal frequency was 10.59 MHz. This was calculated from the SuperDARN radar archived data by the ray tracing program as the most transmitted frequency through out the one month's 2 hour fit file data for each day between 00 : 00 – 02 : 00 hours UT.

On noting that very little information was gained from Figure 4.29, it was clear that sampling of the scatter data had to be expanded so as to increase on some useful information that would be learnt eventually. Therefore, ray tracing was conducted on a model Saskatoon ionosphere for December 2004 to observe which transmitted frequencies would be scattered by or propagated through the ionosphere in order that a range of frequencies which would show signal reflection back to the radar could be established.

Table 4.14: Most transmitted frequency, 10.59 MHz, ray tracing results for the Saskatoon IRI ionosphere.

Elev. ($^{\circ}$)	Ray Path (km)	H-H. H (km)	Iono. (UT)
0	0.000	65	01:00
10	635	101	01:00
20	660	183	01:00
30	585	216	01:00
40	1695	N/A	01:00
50	1352	N/A	01:00
60	1173	N/A	01:00
70	1071	N/A	01:00
80	1016	N/A	01:00
90	1	1	01:00

Once the frequency range of 10 – 11 MHz was established as the one which was close to 10.59 MHz, the most transmitted frequency, and signal backscatter from that (range of frequencies) was desirable, the scatter plots of elevation and power data were then generated for this frequency window. Figure 4.32 below is one such plot. It shows only the ground scatter information following the procedure that has already been discussed above. Also, the details of ionospheric scatter are illustrated in Figure 4.33 — whose production method has also been highlighted above.

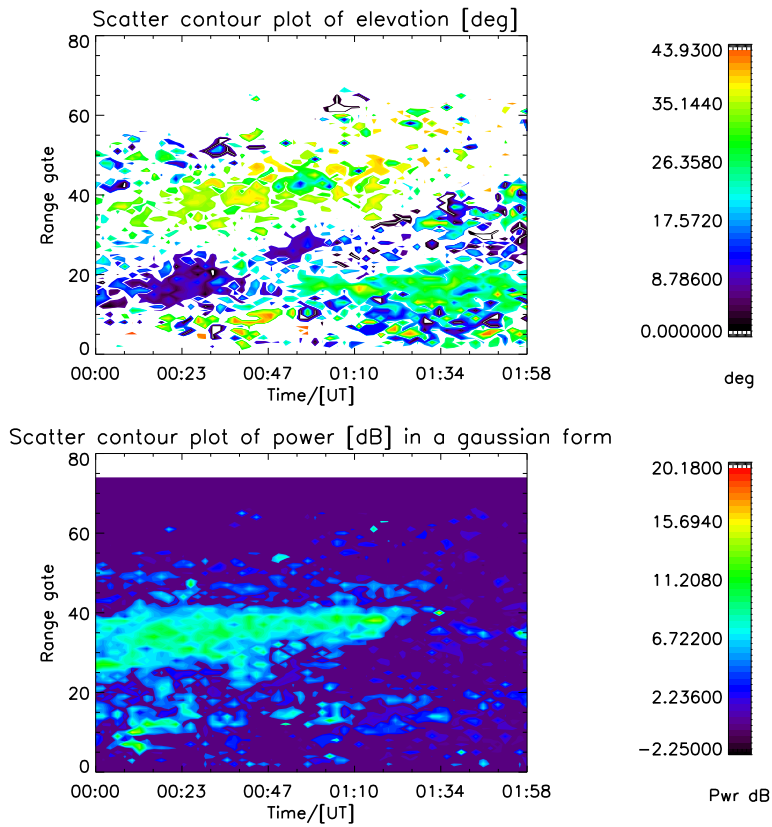


Figure 4.32: Ground scatter elevation and power plots for one full month of December 2004 recorded for 00 : 00 – 02 : 00 hours every day. The data used is from the Saskatoon SuperDARN radar. The transmitted frequency for the plots is range from 10.0 – 11.0 MHz.

The just above graphs (Figures 4.32 and 4.33) are given separately so that their scatter can be shown clearly.

Table 4.15: Ground scatter ray path results for 10 – 11 MHz transmitted frequencies

Range Gate	Elev. ($^{\circ}$)	Ground Range (km)	Vertical Height (km)	Ray Path (km)
5	43	405	378	554
10	43	630	587	861
32	37	1620	1221	2028
40	39	1980	1603	2548
50	39	2430	1968	3127

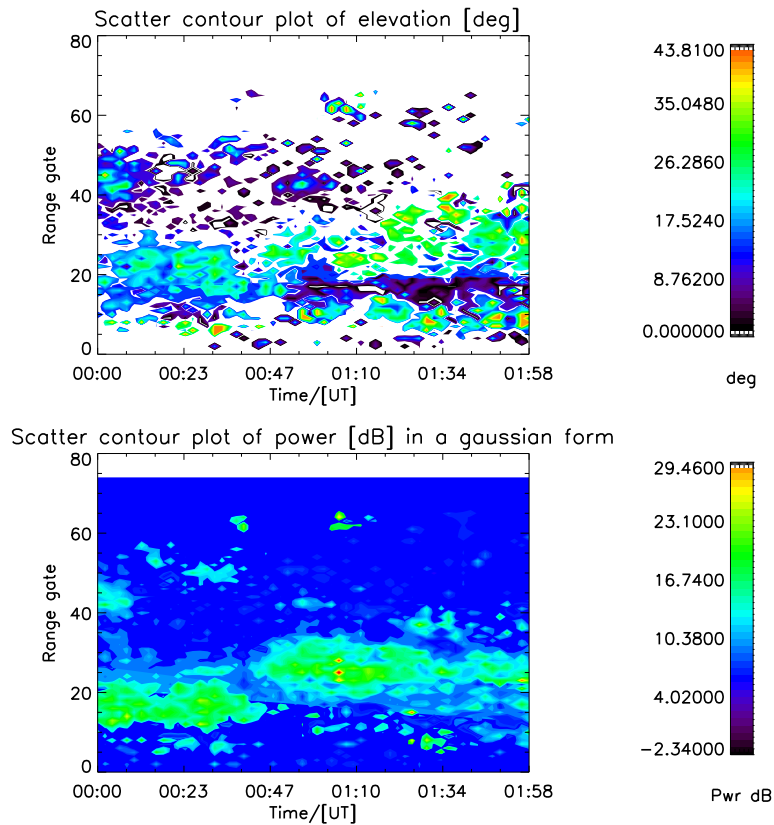


Figure 4.33: Ionospheric scatter elevation and power plots for one full month of December 2004 recorded for 00 : 00 – 02 : 00 hours every day. The data used is from the Saskatoon SuperDARN radar. The transmitted frequency for the plots is range from 10.0 – 11.0 MHz.

Table 4.16: Ionospheric scatter ray path results for 10 – 11 MHz transmitted frequencies

Range Gate	Elev. ($^{\circ}$)	Ground Range (km)	Vertical Height (km)	Ray Path (km)
6	43	450	420	615
25	43	1305	1217	1784
37	30	1845	1065	2130
40	12	1980	421	2024
62	43	2970	2770	4061

To complete the various arising arguments, the ray traces of transmitted frequencies of 10.0 – 11.0 MHz propagation are indicated in the plot below. The resultant propagation modes are indicated in Table 4.17 below.

Ray Trace Plot of Signals propagating in the ionosphere

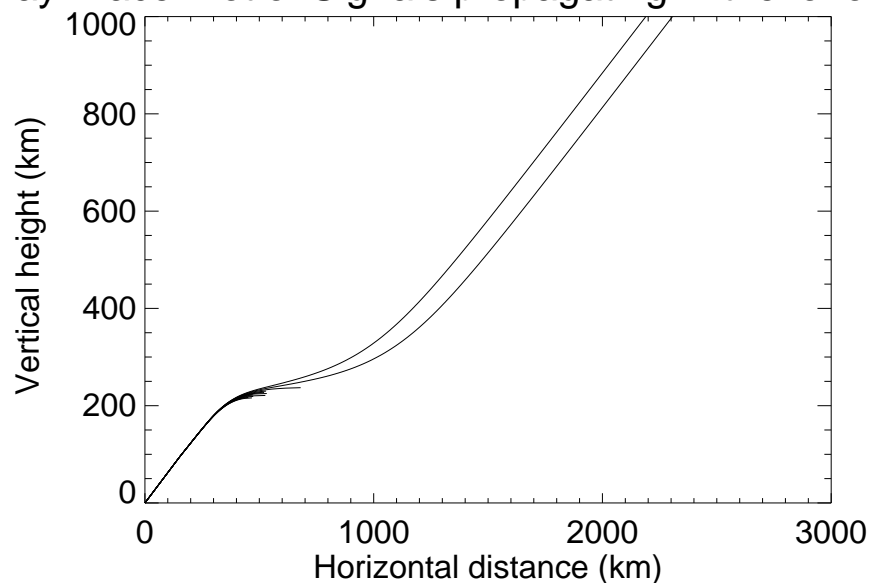


Figure 4.34: Ray traces of radar transmitted frequencies ranging from 10.0–11.0 MHz on 0.1 increments each successive time. The elevation angle of the signal is 32° .

Table 4.17: Results for 10.0 – 11.0 MHz transmitted frequencies through a Saskatoon IRI ionosphere

Freq.(MHz)	Elev.($^\circ$)	Ray Path (km)	H-H. H. (km)	Iono. (UT)
10.00	32	523	216	01:00
10.10	32	507	217	01:00
10.20	32	529	219	01:00
10.30	32	578	221	01:00
10.40	32	582	222	01:00
10.50	32	527	225	01:00
10.59	32	589	227	01:00
10.60	32	567	227	01:00
10.70	32	587	230	01:00
10.80	32	738	237	01:00
10.90	32	2551	N/A	01:00

Chapter 5

Discussion

This Chapter is dedicated to present the issues that have been learnt from the various analysis methods that were used to manipulate the data. The information that was gathered from the various plots and tables is explained to show sound lessons that come forth and how these compare with findings by others.

On the outset, it is cardinal to mention that all the IRI Model generated ionospheres in this thesis represent vertical heights from 60 – 1000 km with an interval of 1 km. However, the ray tracing program which uses these ionospheres was written in such a way that the height and electron density data is always re-worked thereby producing vertical heights that start from 0 km in increments of 1 km through to 1000 km before the ray traces through space can be calculated and then plotted. The 1 km interval between successive vertical heights allows for a better precision in determining the point where the HF wave vector is normal to the magnetic field.

In performing the ray tracings, consideration was made for the fact that radio signals slow down in the ionosphere as they move through a plasma, but propagate at c in free space. This behaviour is reflected in the way real and virtual vertical heights are portrayed in an ionogram (see Subsection 2.6.1). The ray paths give the route a signal takes. In radar terms, the actual interest is how far a target (such as an ionospheric irregularity) is, away from it (radar) in time. A ray whose path means it spends more time in the ionosphere will experience more of the retardation. This effect is taken care of in the group velocity calculation. All the ray paths of the ray traces were computed based on these premises.

It is worth indicating that the characteristics and position of the SuperDARN radar backscatter are dependent on factors like diurnal, seasonal and certainly solar activity (Chisham and Pinnock, 2002). In this dissertation, considerations of such have not been pursued since the primary goal is to learn how feasible it is to perform ionospheric tomography using an HF radar.

Having introduced issues relating to the data, analysis of the obtained project results proceeds from this point onwards. It is imperative to make mention that the SuperDARN

HF radar data of echo power, Doppler velocity, Doppler spectral width and elevation were plotted to take note of the events in them as portrayed in Figures 4.1 and 4.2 which includes a ray transmitted frequency plot. In Figure 4.1, the velocity panel plot shows much fluctuations from about 16 : 00–17 : 00 UT. Comparing the velocity data plot to the attendant spectral width and power plots indicates that not much information could be learnt from these plots except that certain data points will provide information regarding either ground or ionospheric scatter as evidenced by Figure 4.2. Also, the radio signal transmitted frequency at an instance throughout the 2 hours of the "fit" file causes scatter to originate from either the ground or ionosphere (see the lower panel plot of Figure 4.2).

5.1 Scatter Analysis

Figure 4.3 shows a situation where ground and ionospheric backscattered signals originate from varying angles for a particular beam and range-gate, e.g. beam 8 and range-gate 14. The ground scatter data is much more than that of ionospheric scatter. In fact, the elevation angles for the ground scatter data are very much spread ranging from $7^\circ - 24^\circ$ with a lot of wobbling. However, notable scatter is observable for times at about 16 : 50 UT and 17 : 25 UT where the elevation angle seems to vary significantly reaching values of 7° low from slightly above 20° over a short time range for the ground scatter elevation data plot (Figure 4.3 (a)). Perhaps, another striking result is that there is apparently few pockets of time ranges where ionospheric scatter appears while ground scatter data presents some continuous changes of elevation — as shown in Figure 4.3 for the 2 hours time range under consideration.

5.2 Elevation Scatter from all Beams and Range-gates Analysis

In looking at the elevation data from all 16 Beams and 75 Range-gates, the contour plot of elevation data in Figure 4.4 indicates that there is no scatter at elevation angles greater than 31 degrees approximately. Actually, scatter is notable over a fairly long distance, i.e., Range-gates 10 – 60. At approximately 20° and range-gate 18, high scatter was observed as evidenced by the yellow colour of the plot's associated colour-bar. All elevation angles where scatter comes back from are small. In looking at Table 4.1, the vertical distance and horizontal ground range are indicative of hop configurations of the sky wave propagation modes. This is deduced by critically taking note of the vertical heights, ground ranges and ray path distances provided in the above-mentioned table.

The current available theory explains that radio signals can only be reflected off the ionosphere in the E and F layers. Nonetheless, Table 4.1 presents backscatter coming from 790, 923 and 1637 km in vertical heights for 28° , 29° and 30° elevation angles respectively

which is practically not possible. However, rays backscattered from vertical heights of 214, 297 and 325 km can be viewed as having been 'reflected off' or scattered by the F2 layer in particular or F layer in general of the ionosphere. Thus, the 790 km vertical height scattered signal may be representing a one-hop signal backscattered from the ground; the 923 km one would represent a one-and-half hops ray scattered from the ionosphere's F layer; and the radio wave showing vertical height of 1637 km as having been scattered after two-and-half hops on taking the reflecting F maximum electron density height to be at roughly 300 km in height (see Figure 2.6). It is imperative to make mention that the ray hop configurations are sometimes complicated with combinations of reflections and thus backscatter originating from both the Earth's surface (ground), E (of which the reflecting E surface is somewhere at about 140 km in vertical height) and F layers. The possible propagation modes of one-full-hop F layer combined with half-hop E layer backscattered or reflected signals must not be ruled out as cases that are worthy considering for vertical height signal distances such as the above-mentioned 790 km one in table 4.1.

Such results are what prompted the masking of elevation data to either the 'ground scatter flag' data or its generated inverse (ionospheric scatter flagged data) as presented in Section 4.1.

Further details of the analysis of Figure 4.5 and comparisons with Table 4.1 results to those which are shown in Table 4.2 indicates that some of the scatter data is consistent with what is expected — following the discourse on signal hop propagation modes of sky waves above. This is clearly shown in the results for the transmitted radio signals with 8° , 10° and 19° elevation angles which have half-hop vertical height. It must be emphasised that the half-hop heights indicated in Table 4.2 are real vertical heights which are always lower than their corresponding virtual heights (Davies, 1990). This aids in understanding the differences inherent in the values for the same radio signals with 8° , 10° and 19° elevation angles portrayed in the two tables of which Table 4.1 results were read off from Figure 4.4 followed by the attendant use of elementary calculations using trigonometry. The angles with 'N/A' as the half-hop vertical heights indicate that the signals passed through the ionosphere unreflected to the maximum data point of 1000 km vertically upwards into space. Figures 4.4 and 4.6's power, velocity and high values of spectral width data together with Table 4.1 show that the SuperDARN data for the 2004030816*f.fit* file at Range-gates 17, 23, 29 and 33 presents ionospheric backscatter. This ionospheric scatter of signals information is confirmed by the Table 4.2 elevation angles of 19° and 10° which correspond to Range-gates 17 and 23 respectively in Table 4.1.

5.3 Ground and Ionospheric Scatter Analysis

In order to get a better understanding of the insights gathered thus far, it is necessary to study the individual ground and ionospheric scatter results shown in Figures 4.7 and 4.8 respectively. Some of the graphic information in the above-mentioned figures has

been outlined in tables 4.3 and 4.4. As a matter of fact, tables 4.3, 4.4 and 4.5 present very interesting results which confirm that the half-hop, one-hop and multi-hop sky wave configuration assertions alluded to in the above hold. Table 4.3 shows that most ground scatter portion, yellow colour, of Figure 4.7 comes back from a vertical height of about 300 km in space (around 275–307 km in the table). This clearly is not a correct vertical height representation because we know that 300 km represents the F layer reflection or scatter of rays. Hence, this only makes sense if it is one-hop scatter with the reflecting surface being the ionospheric E layer at about 150 km while the ground gives the shown backscatter at the surface of the Earth (i.e., 0 km sea level). Similarly, the about 600 km (i.e., 571–642 km) vertical height indicated in Table 4.4 for Figure 4.8’s most scatter point, again in yellow colour, tells us that this effect comes from a multi-hop signal configuration case as already discussed above. The backscattered signals could have a combination of both E and F layers’ full- and half-hop propagation arrangements with the reflecting surfaces at about 130 and 300 km respectively. To complete the signal hop analysis, ray tracing results for the elevation angles pertaining to the most scatter parts (yellow colour) of the two figures were studied. Table 4.5 illustrates that the half-hop vertical heights for the 17–18 degrees elevation falls in the range 223–226 km for an IRI Model ionosphere. Also, it shows that the half-hop vertical heights for the 26–27 degrees elevation falls around 266–278 km for the same IRI Model ionosphere.

This presents a problem since the elevation angle and range-gate analysis above, of the 17°–18° elevation signal, is supposed to show a one-hop ground backscatter off the E layer — as the reflecting surface. As for the 26°–27° elevation angle signal, this is consistent with what is expected as ionospheric scatter. The explanation of this disparity is that the IRI Model might not have calculated the real situation that occurred in the ionosphere at that particular moment in time since it is a simulation tool based on averages.

5.4 Other SuperDARN Radar Data Measurements Analysis

In order to be sure about the understanding gained thus far, Doppler characteristics were analysed to check the validity of the ground and ionospheric scatter plots information at Range-gates near 16–24 in figures 4.7 and 4.8 respectively. Figure 4.9 illustrates the scenario represented for the full 2 hour ‘fit’ file data. Clearly Doppler velocity of about 0–35 m/s representing ground scatter is observed for Range-gates 16–17 at about 16 : 50 UT. However, the spectral width for the same data and Range-gates indicates values that are greater than 66.400 m/s which shows that this information is not ground scatter data since it is a high value following the criterion in Section 2.10. Hence, separate ground and ionospheric Doppler characteristics were studied to ascertain the actual picture that transpired in the ionosphere for this dataset (see Section 2.10 for a recap on the ground scatter flag).

The ground scatter plots presented in Figure 4.10 do not show much useful information

around the Range-gates 16 – 17 to reflect the observed scatter in Figure 4.7 in the sense that the velocity data only presents a gray colour while the spectral width one indicates lots of values greater than 66.200 m/s in that data window. This could be due to the fact that only one beam, i.e., beam 8, was used to perform the operation that was implemented in generating the plots. On the other hand, ionospheric scatter data plots in Figure 4.11 illustrate a similar problem of affording little information to use in confirming the revelations of Figure 4.8 around Range-gates 22 – 24. In light of this, a comparison of the figures mentioned above and those archived by the SuperDARN community (Figures 4.12, 4.13 and 4.14) was carried out. The archived SuperDARN community data plots provided better information. It was observed that the gray colour shading that conceals most information in the generated plots — produced purely from the directly raw measured data from the radar(s) — suggests some effect which entails that the data and plots provided by the archiving SuperDARN group is further processed before such clear information is plotted.

Figure 4.12 appears to confirm that there is a lot of ground scatter around Range-gates 16 – 17 in the velocity plot panel and the low (blue colour) spectral width values. The combined ground and ionospheric scatter plots are indicated in Figure 4.13 with the colour bar showing the expected scenario for the Doppler velocity and spectral width. As for the ionospheric scatter, the 22 – 24 Range-gates velocity and spectral width data clearly shows that ionospheric backscatter is present around this data window in Figure 4.14. While the velocity values are low (red colour), some spectral width values are fairly well over the 35 m/s (light blue and green colours) threshold discussed in Section 2.10.

On the effects of the radar transmitted frequency changes and the scatter information recoverable from the data, Figures 4.15 and 4.16 are consistent in showing that backscatter was more prominent from Range-gates 20 – 70 for all three cases of both ground- and ionospheric-scatter; ground scatter alone; and lastly only ionospheric scatter data. Figure 4.17 affirms the issue of backscatter being more pronounced between ranges 20 – 70. Also, backscatter was only recorded for elevation angles at approximately 40° and below. This means that all rays transmitted at 10, 13, 16, 17 and 18 MHz with elevation angles greater than, say, 41° go through the ionosphere unreflected. This is in line with the fact that only lower elevation angles achieve perpendicularity to the magnetic field according to Walker *et al.* (1987). An analysis of Figure 4.15 indicates that ground scatter comes back from higher ranges (Range-gates 45 – 70) while the ionospheric scatter appears more prominent at ranges from about Range-gates 15 – 45 although it is noticeable even up to range-gate 70 in the background of the ionospheric information in the velocity and spectral width panel plots. Then middle panel plot in Figure 4.16 presents a situation which entails that the scatter changes observed in Figure 4.15 are pronounced from Range-gates 30 – 40. This effect is actually more clear in Figure 4.17's ground scatter (middle) panel plot. Hence as the transmitted frequency changes so does the range from which backscatter comes alters.

Thus, in looking at figures 4.15, 4.16 and the subsequent figures (i.e., figures 4.18, 4.19,

4.20, 4.21, 4.22) portraying ray traces, it is clear that the radar's signal transmitted frequency has a relationship with the ionosphere's change with time. Considering the attendant tables to the above-mentioned figures that were produced from the ray tracing program that generated the plots also, the above mentioned idea can be explained to greater details.

Table 4.6 shows that changing the signal transmitted frequency in a static ionosphere produces backscatter or the returned signal from different heights for elevation angle 20° . Also the distance travelled by the signal varies. The most interesting thing is that the half-hop propagation mode vertical height increases with increased transmitted frequency e.g. a 10 MHz signal has 171 km, 14 MHz one having 200 km while that of 16 MHz travelled 215 km and lastly 18 MHz moved 236 km vertically into the ionosphere for 20° take-off angle of flight. On the other hand, the ray path distances indicate that transmitted frequency increase does not necessarily entail that the ray traversed ranges also increase accordingly. This is clearly stipulated in the ray path of the signal for 10, 14, 16 and 18 MHz which are 791, 749, 815 and 999 km respectively. The range traversed for 14 MHz is less than those for all the other frequencies including 10 MHz which is lower in frequency. Hence, a change in transmission frequency of a radio wave for a static ionosphere and constant ray elevation angle produces significant changes in the backscattered signal's traversed range results.

Another effect of particular concern is the change of the ionosphere while the radar transmitted frequency is maintained constant together with the elevation angle of transmission. Using the elevation angle of the signal to be 20° once more, it was clearly noted that scatter comes back from various positions in the vertical height of the ionosphere for constant 10 MHz radio signals. An example of this is: on taking results from Table 4.7, the vertical half-hop heights for the backscattered signals at 00 : 30, 01 : 30, 02 : 50, 03 : 30 and 03 : 50 UT are 171, 166, 165, 148 and 148 km respectively. This behaviour is also observed in tables 4.8, 4.9 and 4.10. Relating these last 4 mentioned tables' results to Figure 4.15, it was observed that the scatter information is consistent with the ray tracing results. At most times, the higher the radio wave's transmitted frequency, the higher the vertical height from which backscatter originates. This is evidenced in values for the half-hop vertical height at say 00 : 30 UT of 171 km for 10 MHz, 200 km for 14 MHz, 215 km for 16 MHz and 172 km for 18 MHz transmitted frequencies and a constant 20° elevation angle in 4 tables. Notice also that the 172.000 km for 18 MHz is lower than the values for both 14 and 16 MHz transmitted frequencies. A similar comparison of values for 01 : 30, 02 : 50, 03 : 30 and 03 : 50 UT illustrates that all higher transmitted frequencies than the immediate lower one produces backscattered signals emanating from higher half-hop vertical heights e.g. 166 km for 10 MHz, 198 km for 14 MHz, 211 km for 16 MHz and 227 km for 18 MHz at 01 : 30 UT. This is in line with theory which outlines that the effect of the electron density on the ray path decreases appreciably with an increase in the radar's operating frequency (Villain *et al.*, 1984).

5.5 Radar Transmitted Frequency Change Effects Analysis

An analysis of Figure 4.15, which presents enough scatter information for the 17 MHz transmitted frequency of around 00 : 30 and 03 : 10 UT ionospheres, in relation to Figure 4.23's ray traces was conducted. It was gathered that scatter comes back from both the E and F layers. This was deduced after looking at a picture of how rays propagate through a modelled IRI ionosphere in Figure 4.23 which showed that the half-hop vertical heights of the tracings appear at about 100 km and 150 – 250 km in the plot. Table 4.11 provides more information on the ray traces which indicate that no backscatter is possible for rays having more than 30° or equal to it elevation angle. Also, radio waves propagating at exactly 90° elevation angle just go up to the next layer's starting point and then become evanescent.

5.6 Ray Tracing Analysis

After gaining many of the insights described above, attention was focused on determining the source of the backscattered rays. To start with, Figure 4.24 showed too much information which had to be unpacked in order to glean sound lessons from the echo elevation and power scatter data. To that end, an analysis of Figure 4.25 harbouring the separated ground and ionospheric scatter plots was done. The plots indicate that ground scatter comes back in cases where the elevation angles are much higher (yellow colour). In fact, the echo power panel plot of the ground scatter plots indicates that stronger backscatter originates from far away distances from the transmitting radar, i.e., Range-gates 20 – 40. On the other hand, ionospheric backscatter is prominent for lower elevation angles (green and blue colours) and hence nearer distances to the HF signals transmitting radar, e.g. Range-gates 5 – 20. This effect is noted from the ionospheric scatter plots of both elevation and power data. The ground scatter comes back with larger elevation compared to the ionospheric one probably because the lower elevation angles the larger the component of the ray perpendicular to the magnetic field line giving a greater chance of backscatter from the ionosphere (see Figure 4.26 for a graphical representation of this idea). Since the major interest of this dissertation is recovering the ionospheric structure, ray traces (that are shown in Figure 4.27 for a constant elevation angle of 25°) were studied. Table 4.12 shows a summary of the signal propagation that was recovered. Clearly, the half-hop vertical heights for the rays that were backscattered illustrate that the scatter comes from the F layer. Also, only rays propagated with transmitted frequencies of 13 MHz and less were returned back to the radar (transmitter).

This behaviour prompted the study of scatter that emanates from propagation of one transmitted frequency. This frequency had to be the radar's most transmitted frequency because backscatter data from it provides a larger dataset to look into. For the Saskatoon ionosphere's SuperDARN radar data that was experimented on, the most transmitted

frequency for the month of December 2004 was calculated as 10.59 MHz.

Elevation and echo power plots for this frequency produced very little information as portrayed in Figure 4.29. As a matter of fact, separated ground and ionospheric scatter plots shown in Figure 4.30 present too little data to use in making any meaningful analysis. The ray traces in Figure 4.31 and the results in Table 4.14 confirm that backscatter comes from both E (approximately 100 km) and F (about 180–220 km) layers. Thus, ray tracing was employed to find a range of transmission frequencies around the value of the most transmitted frequency that would provide just enough information to explain the situation regarding backscatter.

The range of frequencies that produces backscatter from the IRI Model Saskatoon ionosphere were 10.60 MHz and below. In light of this, Figures 4.32 and 4.33 were plotted to show the effects for a range of frequencies from 10 – 11 MHz. The ground scatter figure, Figure 4.32, shows that the Earth’s surface backscatter occurs for elevation angles less than about 40° . There is strong scatter between Range-gates 25 – 40. As for the ionospheric scatter, Figure 4.33 indicates that strong backscatter took place within the range 10 – 20 Range-gates between 00 : 00 – 00 : 50 UT while it continued for 20 – 30 Range-gates from about 00 : 50 – 01 : 58 UT. The elevation angles that provided most of this information are between approximately 20° – 35° . For both ground and ionospheric scatter, elevation angles of 43.81° also provided some backscatter.

Figure 4.34 and Table 4.17 revealed interesting information on radio waves propagating in the IRI Model Saskatoon ionosphere. Radio signals transmitted between 10 – 11 MHz at increments of 0.1 MHz through the ionosphere for the dataset under study show that all the scatter comes back from the F layer, i.e., 216 – 237 km vertically upwards from the Earth’s surface, for 32° elevation angle. Radio signal ray traces for these frequencies did not produce backscatter for angles greater than 33° .

It is worth mentioning that while most of the ray tracing results achieved in this dissertation appear somewhat consistent with what is expected, it is true that the actual radio signal paths through IRI Model ionospheres were not provided or produced in this work, since a disadvantage of refraction is that it is much more difficult to determine the exact path of any particular ray. The ionosphere may shield certain regions of irregular structures from being viewed (Villain *et al.*, 1984).

Chapter 6

Conclusion

The SuperDARN 'fit' file radar raw data is capable of being used to create a model which represents activities that arise in the polar ionosphere as radio waves propagate through it. Also, it was noted from the backscattered data that irregularities are present in the polar ionosphere. One important result that was obtained in this work is that ray tracing of radio signals traversing the polar ionosphere is able to provide us with answers to the many questions that come to mind upon viewing the generated figures from raw SuperDARN radar "fit" file data.

From figures, it was observed that the generated outputs in this study are similar in nature to those obtained from the SuperDARN online archived plotting resource, despite the fact that the plots sourced from there (online resource) appear to have data results that have been further processed probably by having noise removed. Hence, the data presented here-in is unmodified.

In looking at the ray tracing operations, recovering the accurate horizontal, vertical and ray path distance values from the scatter plots' Range-gate numbers remained a challenge. The most that has been done is to single handedly pick out areas of significant scatter from the plots by sight. It is possible, nonetheless, to look into the use of a computer program to perform this, seemingly enormous task.

It has been observed also that multi-hop configurations provide answers to complications that were encountered in utilising simple elevation angle and Range-gate calculations to produce vertical heights while analysing ground and ionospheric backscatter information.

The results from the Doppler characteristics of the generated plots compared to the online archived SuperDARN community ones tells us that some work has to be done to remove (certain) noise that is still inherent in the raw radar data, so that the plots can show much more useful information than what has been observed in this dissertation.

6.1 Possible Future Work

In terms of the future work regarding improvements to the results obtained in this work, the curvature of the Earth must be considered in the ray tracing programs so that more precise ray traces can be modelled for the ionosphere(s) being studied. Another possible future work area of study to improve on the concerns learnt herein is to investigate an implementation of carrying out real time 3D tomography using the SuperDARN HF radar.

Also, using a ray tracing program that uses differential equations (see Terry, 1971 and Coleman, 1998) to solve the ray path(s) in space will certainly offer better results than the Pythagorean method of point-to-point triangular calculations used in this work that only uses simple Snell's law which requires that the horizontal component of the refractive index vector remains constant (Walker *et al.*, 1987) and trigonometry.

6.2 Inference

In a nutshell, it was discovered that with more effort in analysing the (SuperDARN) HF radar data, it may be possible to perform Ionospheric Tomography using an HF radar. However, there is a lot of work that needs to be done to make sure the SuperDARN HF radar data is processed into a format that will allow such a task to be achieved properly.

References

- Baker K.B., Greenwald R.A., Ruohoniemi J.M., Dudeney J.R., Pinnock M. and Mattin N., "Space Physics in Antarctica: An Adventure on the Ice," *Johns Hopkins APL Technical Digest*, **11**: pp. 228 – 238, 1990.
- Baker K.B., Greenwald R.A., Ruohoniemi J.M., Dudeney J.R., Pinnock M., Mattin N. and Leonard J.M., "PACE Polar Anglo-America Conjugate Experiment," *EOS, Transactions of the American Geophysical Union*, **70**: pp. 785 – 799, 1989.
- Bennett J.A., Dyson P.L. and Norman R.J., "Progress in radio ray tracing in the Ionosphere," *Radio Science Bulletin*, **310**, 2004.
- Blewitt G., "An automatic editing algorithm for GPS data," *Geophysical Research Letters*, **17**: pp. 199 – 202, 1990.
- Carlson H.C.J., "The dark polar ionosphere: Progress and future challenges," *Radio Science*, **29**: pp. 157 – 166, 1994.
- Chapman S., "The atmospheric height distribution of band absorbed solar radiation," *Proceedings of the Physical Society*, **51**: pp. 93 – 109, 1939.
- Chen F.F., *Introduction to Plasma Physics and Controlled Fusion*, volume 1: Plasma Physics, second edition, Plenum Press, New York and London, 1983.
- Chisham G., Lester M., Milan S.E., Freeman M.P., Bristow W.A., Grocott A., McWilliams K.A., Ruohoniemi J. M. Y.T.K., Dyson P.L., Kikuchi T., Pinnock M. R.J.P.S., Sato N., Sofko G.J., Villain J.P. and Walker A.D.M., "A decade of the Super Dual Auroral Radar Network (SuperDARN): scientific achievements, new techniques and future directions," *Surveys of Geophysics*, **28**: pp. 33 – 109, 2007.
- Chisham G. and Pinnock M., "Assessing the contamination of the SuperDARN global convection maps by non-F-region backscatter," *Annales Geophysicae*, **20**: pp. 13 – 28, 2002.
- Coleman C.J., "A ray tracing formulation and its application to some problems in over-the-horizon radar," *Radio Science*, **33**: pp. 1187 – 1197, 1998.
- Davies K., *Ionospheric Radio*, ISBN 0 86341 186 X, Peter Peregrinus Ltd, 1990.

- Gauld J.K., Yeoman T.K., Davies J.A., Milan S.E. and Honary F., "SuperDARN radar HF propagation and absorption response to the substorm expansion phase," *Annales Geophysicae*, **20**: pp. 1631–1645, 2002.
- Greenwald R.A., Baker K.B., Dudeney J.R., Pinnock M., Jones T.B., Thomas E.C., Villain J.P., Cerisier J.C., Senior C., Hanuise C., Hunsucker R.D., Sofko G., Koehler J., Nielsen E., Pellinen R., Walker A.D.M., Sato N. and Yamagishi H., "DARN/SuperDARN A Global View of the Dynamics of High-Latitude Convection," *Space Science Reviews*, **71**: pp. 761–796, 1995.
- Greenwald R.A., Baker K.B., Hutchins R.A. and Hanuise C., "An HF phased-array radar for studying small-scale structure in the high-latitude ionosphere," *Radio Science*, **20**: pp. 63–79, 1985.
- Haselgrove J., *Ray theory and a new method for ray tracing in Physics of the Ionosphere*, Physical Society, London, 1955.
- Hathaway D.H., Wilson R.M. and Reichmann E.J., "The Shape of the Sunspot Cycle," *Solar Physics*, **151**: p. 179, 1994.
- Hunsucker R.D. and Hargreaves J.K., *The High-latitude Ionosphere and its Effects on Radio Propagation*, Cambridge University Press, 2003.
- Katamzi Z.T., *Verification of Ionospheric Tomography using MIDAS over Grahamstown, South Africa*, Master's thesis, Rhodes University, 2007.
- Kunitsyn V.E. and Tereshchenko E.D., *Ionospheric Tomography*, Springer-Verlag Berlin Heidelberg, 2003.
- Liu C.T., Tsai L.C. and Tsai W.H., "Computerized Ionospheric Tomography Using the GPS/MET and NNSS Data," in "GIS development, Asian Association for Remote Sensing (AARS), Asian Conference in Remote Sensing (ACRS2000), Taipei, Taiwan," 2000.
- Ma G. and Marunyama T., "Derivation of TEC and estimation of instrumental biases from GEONET in Japan," *Annales Geophysicae*, **21**: pp. 2083 – 2093, 2003.
- McKinnell L., "The Ionosphere," A lecture presentation at the HMO Summer School on Space Physics, Hermanus Magnetic Observatory Space Physics Summer School, February 2006, 2006.
- McKinnell L.A., Opperman B. and Cilliers P., "GPS TEC and ionosonde TEC over Grahamstown, South Africa: First comparisons," *Advances in Space Research*, **39**: pp. 816 – 820, 2007.
- McNamara L.F., *The Ionosphere: Communications, Surveillance, and Direction Finding*, Krieger Publishing Company, 1991.

- Milan S.E., Yeoman T.K., Lester M., Thomas E.C. and Jones T.B., "Initial backscatter occurrence statistics from the CUTLASS HF radars," *Annales Geophysicae*, **15**: pp. 703 – 718, 1997.
- Mitchell C.N. and Spencer P.S.J., "A three-dimensional time-dependent algorithm for imaging using GPS," *Annales Geophysicae*, **46**: pp. 687 – 696, 2003.
- Mthembu S.H., *An investigation of Ultra Low Frequency (ULF) pulsations using radar data and solar wind data*, Master's thesis, University of Kwazulu-Natal, Durban, 2006.
- Munsami V., Pinnock M. and Roger A.S., "HF radar observation of field-aligned currents associated with quiet time transient flow bursts in the magnetosphere," *Journal of Geophysical Research*, **107 (A9)**: pp. 1232 – 1241, 2002.
- Nambala F., "Scale Height Analysis for Grahamstown," Bachelor of Science Honours with Specialisation in Astrophysics and Space Science Degree Project Report to the University of Cape Town, 2006.
- Nambala F.J., McKinnell L.A. and Oyeyemi E., "Variations in the ionospheric scale height parameter at the F2 peak over Grahamstown, South Africa," *Advances in Space Research*, **42, Issue 4**: pp. 707 – 711, 2008.
- Norman R.J., Parkinson M.L. and Dyson P., "Comparing HF radar backscatter from the Southern Ocean with ray-tracing results using the IRI Model," Proceedings of the Workshop on the Applications of Radio Science (WARS2004), Hobart, Tasmania, paper G-8, pp 1 - 10, 2004., 2004.
- Rash J.P.S., Walker A.D.M., Scourfield M.W.J., Stoker P.H. and Moraal H., "SHARE - An HF radar system for Sanae," *South African Journal of Antarctic Research*, **21**: pp. 185– 186, 1991.
- Ratcliffe J., *An Introduction to the Ionosphere and Magnetosphere*, Cambridge University Press, 1972.
- Senior A., Kosch M.J., Yeoman T.K., Rietveld M. and McCrea I., "Effects of the high-latitude atmospheric gravity wave disturbances on artificial HF radar backscatter," *Annales Geophysicae*, **24**: pp. 2347–2361, 2006.
- Tate B.S. and Essex E.A., "Investigation of Irregularities in the Southern High Latitude ionosphere," *Advances Space Science*, **27**: pp. 1385 – 1389, 2001.
- Terry P.D., *Complex Ray Tracing in Ionospheric Radio Propagation*, Ph.D. thesis, University of Cambridge, UK., 1971.
- Tucker A., "Computerised Ionospheric Tomography," *John Hopkins APL Technical Digest*, **19**: pp. 66 – 71, 1998.

- Vastberg A., "RaTS, A System for Ionospheric Ray Tracing," *IEE Conference Publication*, **392**: pp. 371 – 375, 1994.
- Villain J.P., Greenwald R.A. and Vickey J.F., "HF ray tracing at high latitudes using measured meridional electron density distributions," *Radio Science*, **19**: pp. 359 – 374, 1984.
- Walker A., "The SHARE Radar at SANAE, Antarctica," *South African Journal of Science*, **98**: pp. 257–263, 2002.
- Walker A.D.M., Greenwald R.A. and Baker. K.B., "Determination of the fluctuation level of ionospheric irregularities from radar backscatter measurements," *Radio Science*, **22**: pp. 689 – 705, 1987.

Appendix A

IDL Moment Function

The MOMENT function is designed to compute the mean, variance, skewness, and kurtosis of a sample population contained in an n-element vector e.g. X . Consider the vector X as

$$X = (x_0, x_1, x_2, \dots, x_{n-1})$$

, the moments are then defined as

$$Mean, \bar{x} = \frac{1}{n} \sum_{j=0}^{n-1} x_j$$

$$Variance = \frac{1}{n-1} \sum_{j=0}^{n-1} (x_j - \bar{x})^2$$

$$Skewness = \frac{1}{n} \sum_{j=0}^{n-1} \left(\frac{x_j - \bar{x}}{\sqrt{Variance}} \right)^3$$

$$Kurtosis = \frac{1}{n-1} \sum_{j=0}^{n-1} \left(\frac{x_j - \bar{x}}{\sqrt{Variance}} \right)^4 - 3$$

$$MeanAbsoluteDeviation = \frac{1}{n} \sum_{j=0}^{n-1} |x_j - \bar{x}|$$

$$StandardDeviation = \sqrt{Variance}$$

For the purpose of this thesis work, only the Mean moment is used to calculate the average of the 31 days' elevation and power datasets for a specific range-gate and time. More details can be obtained from the IDL documentation in its Online Help part.